# Use of A Hill-based Muscle Model in the Fast Orthogonal Search Method to Estimate Wrist Force and Upper Arm Physiological Parameters

by

Katherine Mountjoy

A thesis submitted to the
Department of Electrical and Computer Engineering
in conformity with the requirements for
the degree of Master of Science (Engineering)

Queen's University
Kingston, Ontario, Canada
October 2008

# Abstract

Modelling of human motion is used in a wide range of applications. An important aspect of accurate representation of human movement is the ability to customize models to account for individual differences. The following work proposes a methodology using Hill-based candidate functions in the Fast Orthogonal Search (FOS) method to predict translational force at the wrist from flexion and extension torque at the elbow. Within this force estimation framework, it is possible to implicitly estimate subject-specific physiological parameters of Hill-based models of upper arm muscles. Surface EMG data from three muscles of the upper arm (biceps brachii, brachioradialis and triceps brachii) were recorded from 10 subjects as they performed isometric contractions at varying elbow joint angles. Estimated muscle activation level and joint kinematic data (joint angle and angular velocity) were utilized as inputs to the FOS model. The resulting wrist force estimations were found to be more accurate for models utilizing Hill-based candidate functions, than models utilizing candidate functions that were not physiologically relevant. Subject-specific estimates of optimal joint angle were determined via frequency analysis of the selected FOS candidate functions. Subject-specific optimal joint angle estimates demonstrated low variability and fell within the range of angles presented in the literature.

# Acknowledgments

Firstly, I would like to thank my supervisors Dr. Keyvan Hashtrudi-Zaad and Dr. Evelyn Morin for their patience and guidance through this project. Thank you especially for all of your comments and feedback offered during the writing of this thesis. I appreciate this incredible opportunity to pursue research in a field that combines my love of physiology and human movement with technology that could one day help improve quality of life.

I would also like to thank my labmates Behzad Khademian and Amir Haddadi for their friendship and support, for introducing me to the wonderful Persian cuisine, for putting up with the noisy robot during those weeks of constant data collection, and for their never-ending willingness to answer my questions. Also thanks to previous labmates Corina Leung and Maryam Moradi for your friendship and for making me feel welcome at Queen's when I first arrived. A special thanks to Maryam for all of the work you did with the QARM system during your time here. Without your expertise I would have spent a lot more time getting set-up before I could begin my project. Also thanks for always being willing to answer my emails and questions, even after you had moved on from the lab and were working full-time, you were a huge help and I really appreciated it.

A huge thanks goes out to everyone in the PEARL crew for welcoming me to their

biology family and for making it so easy to feel part of the group. A special thanks to Melissa and Brian for your friendship.

None of this would have been possible without the tremendous help from all of the test subjects. Thank you all for volunteering your time so willingly and being so patient during the long sessions.

Finally, I would not have been able to make it through these two years without the support from my family. You always pushed me to try new things, encouraged me when I thought I had taken on too much, and taught me to never give up. Thanks to Mum for the pep-talks and for being such a great role model, to Dad for being my engineering inspiration and for your willingness to chat and give advice, and to Meg for being there when I needed some sisterly support or understanding. Thanks also to the Jeziorskis; Liz, George and James, for welcoming me into your family and always offering your support and encouragement. And most importantly, thank you from the bottom of my heart to Adam for all of your love and support, for always being there, for your abilities to make me smile, for being my rock. I love you.

I would like to acknowledge financial support for this project from the Natural Sciences and Engineering Research Council of Canada (NSERC) and the Queen's Advisory Research Committee (ARC).

Katherine C. Mountjoy

October, 2008

# Contents

# List of Tables

# List of Figures

# List of Abbreviations

| | |
|---|---|
| $\alpha$ | Pennation angle. |
| $\varphi_m$ | Gaussian shape parameter describing the centre of the Gaussian function. |
| $\varphi_v$ | Gaussian shape parameter describing the variance of the Gaussian function. |
| $\varphi_{vT}$ | Modified Gaussian shape parameter describing the variance of the Gaussian function. Applies to force-angle curves rather than force-length curves. |
| $\theta$ | Elbow joint angle. Defined as external elbow angle, where zero degrees occurs at full extension. |
| $\theta_0$ | Optimal joint angle. Joint angle in which a muscle can develop maximal isometric force. |
| $\theta_{0w}$ | Weighted optimal joint angle. Average joint angle found through frequency analysis of candidate functions selected in FOS models. |
| $\sigma$ | Maximum muscle stress/specific tension. The maximum force developed per unit of cross-sectional area. |
| $\Delta Li$ | Change in length for muscle *i*. |
| $\Delta L_{PE}$ | Change in length of the PE beyond the tendon slack length |
| $\Delta L_{PEmax}$ | Maximium change in length of the PE. |

| | |
|---|---|
| ANN | Artificial neural network. |
| a(t) | Muscle activation. |
| Bi | Biceps brachii. |
| Brd | Brachioradialis. |
| CE | Contractile Element. |
| CMA | Constant Moment Arm. One method used in the calculation of muscle moment arm used in FOS candidate functions. |
| CNS | Central Nervous System. |
| DOF | Degree-of-Freedom. |
| EMG | Electromyography. |
| e(t) | Processed EMG signal. |
| FOS | Fast Orthogonal Search. |
| $F_0$ | Maximal isometric force. |
| $F^{CE}$ | Force generated by the contractile element. |
| $F_i$ | Force generated by muscle $i$. |
| $f_l$ | Force-length relationship. |
| $F^{PE}$ | Force generated by the parallel elastic element. |
| $F_{max}^{PE}$ | Maximum force exerted by the PE for a maximum change in length of the PE |
| $f_v$ | Force-velocity relationship. |
| $F_w$ | Force measured at the wrist. |
| $L_0$ | Muscle length in which a muscle can develop maximal isometric force. |

| | |
|---|---|
| $L_F$ | Muscle fibre length. |
| $L_m$ | Muscle length. |
| $L_{MTmax}$ | Maximum musculotendon length. |
| $L_S$ | Sarcomere length. |
| $L_{S0}$ | Optimal sarcomere length. |
| $L_{Ts}$ | Tendon slack length. |
| $MA_i$ | Moment arm for muscle $i$. |
| $MA_{forearm}$ | Forearm length. |
| $M_{elbow}$ | Net moment about the elbow. |
| MVC | Maximal voluntary contraction. |
| PCSA | Physiological Cross-Sectional Area. Total muscle area normal to the longitudinal axis of the muscle fibres. |
| PE | Parallel Elastic Element. |
| PMA | Polynomial Moment Arm. One method used in the calculation of muscle moment arm in FOS candidate functions. |
| %RMSE | Percent Relative Mean Square Error. |
| $RMSE_{AVE}$ | Average Relative Mean Square Error. Calculated using %RMSE found for each FOS model developed with data from one session. |
| $RMSE_{MIN}$ | Minimum Relative Mean Square Error. Minimum %RMSE calculated for each FOS model developed with data from one session. |
| S | Shape factor used in the $F^{PE}$ equation. |
| SE | Series Elastic Element. |
| sEMG | Surface Electromyography. |

| | |
|---|---|
| $SD_{AVE}$ | Standard deviation of all %RMSE calculated for FOS models developed with data from one session. |
| $SD_{MIN}$ | Minimum standard deviation of all %RMSE calculated for FOS models with data from one session. |
| Tri | Triceps brachii. |
| u(t) | Neural activation signal. |
| $v_{ce}$ | Contraction velocity. |
| $v_{max}$ | Maximal contraction velocity. |

# Chapter 1

# Introduction

Modelling of human motion is used in a wide range of applications such as assessment of athletic performance, diagnosis of pathogenic motion, assessing rehabilitation from traumatic events such as spinal cord injury or stroke and control of prosthetic devices [17, 47, 71, 85]. Therefore, it is important to achieve an accurate representation of human movement and be able to customize models to account for individual differences. Such modelling is often performed using biomechanical methods, where information on joint position is obtained using kinematic methods, net joint reaction forces are measured and individual muscle forces are estimated through calculation or using measurements of muscle activity via surface electromyography (sEMG). Isometric muscle contractions which are performed at a constant joint angle have often been used for the development of biomechanical models, because joint position remains fixed, and the interaction between muscle activity and resulting force output can be observed more easily. Assessment of dynamic motion such as in gait analysis introduces more variables and thus may be more difficult to accurately model.

Models to estimate joint torque can be developed using non-linear identification

methods such as neural networks [87], second-order dynamic models [34] and other methods [14, 5, 96]. However, these are "black box" models where inputs are mapped to outputs, but the internal structure of the model may not be known. Building upon the classic work of A.V. Hill [38], Hill-based models [8, 30, 47, 100] reflect the neuromuscular behaviour of individual muscles and are commonly used for skeletal muscle modelling. Hill-based muscle models describe muscle behaviour as three elements arranged in series and in parallel and estimate the forces generated by individual muscles. These force estimates depend on accurate representation of physiological parameters to ensure reliable results [48]. Therefore, accurate estimation of these parameters from individuals using non-invasive techniques is critical.

## 1.1 Estimation of Physiological Parameters

The number of physiological parameters included in a Hill-based muscle model depends on the complexity of the model, however a few key parameters are almost always used. These include the optimal muscle length, tendon slack length, maximum isometric force, physiological cross-sectional area and muscle specific tension. The optimal muscle length ($L_0$) is the muscle length ($L_m$) at which a muscle can generate a maximum isometric force ($F_0$). $L_0$ and the associated joint angle (optimal joint angle $\theta_0$) are also often inferred as the length or joint angle where maximal torque about a joint is measured [6, 10, 45, 81]. However, this may not be a valid assumption, as torque measured at a joint is *net* torque, and is the result of multiple muscles acting simultaneously on the joint. Tendon slack length ($L_{Ts}$) is tendon length when the tendon becomes taught and tension begins to develop [100]. $L_{Ts}$ has been measured in some cadaver studies [53, 74], however it is generally estimated as the

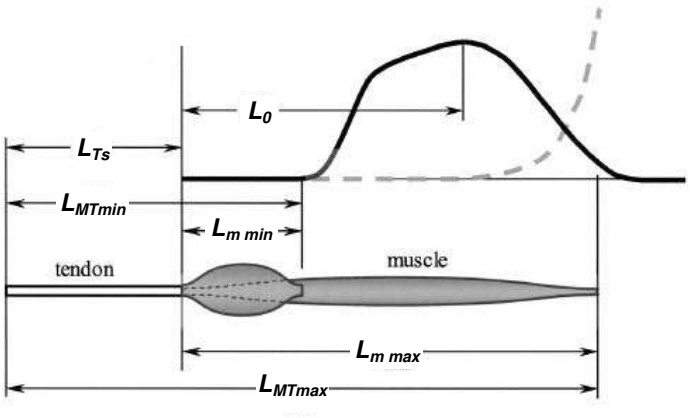


Figure 1.1: Relationship between optimal muscle length $L_0$, tendon slack length $L_{Ts}$, and the minimum and maximum lengths of a muscle $L_{mmax}$ and $L_{mmin}$ and musculotendon unit $L_{MTmax}$ and $L_{MTmin}$ adapted from [31]

difference between maximal musculotendon length ($L_{MTmax}$) and $L_0$ [7]. Figure 1.1 illustrates the interaction between $L_0$, $L_{Ts}$ and $L_{MTmax}$. Physiological cross-sectional area (PCSA) is defined as the total cross-sectional area normal to the longitudinal axis of the muscle fibres [46] and muscle specific tension $\sigma$ is defined as the maximum force that is developed per unit of cross-sectional area [6]. Further information on these parameters including a summary of values provided in the literature can be found in Appendix A.

Due to the challenges associated with measuring muscle physiological parameters *in-vivo*, values presented in the literature are compiled from a range of sources including measurements from cadaver studies [1, 2, 53, 74, 91], imaging techniques such as ultrasound and MRI [64] or estimations through optimization procedures using musculoskeletal models [31, 48]. Computer models of the musculoskeletal system are available [17], however subject-specific scaling is required to represent differences in subject physiology from the generalized model [27]. A wide range of parameter values

are available in the literature, however it has been shown that neuromusculoskeletal models in which these parameters are used may be sensitive to errors in these values [78, 86]. Obtaining accurate measurements *in vivo* for subject-specific applications can be difficult, but is necessary to ensure accuracy and reliability of subject-specific neuromusculoskeletal models.

## 1.2 Proposed Fast Orthogonal Search (FOS) Model

The methods used in this study build upon the techniques of biomechanical modelling, using surface EMG to estimate muscle activation, and measuring joint position and velocity. Rather than using forward or inverse dynamics with a traditional Hill-based model, or an optimization routine to determine individual muscle forces and moment contributions about the joint of interest, this work proposes the use of a non-linear identification method called Fast Orthogonal Search (FOS) to map the relationship between muscle activation, joint kinematics and the resulting net moment for the muscles about the elbow, expressed as force at the wrist. The method will be based on equations describing the Hill-based model parameters.

The FOS method was first developed by Korenberg [49, 51] as an efficient, non-parametric model-based identification method. The method selects terms from a pool of candidate functions to build a model in which the error between the predicted and measured output is minimized.

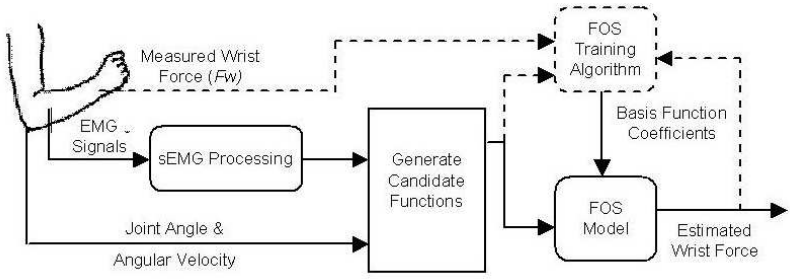


Figure 1.2: Proposed force observer. Dashed lines represent signals used for training.

## 1.3 Thesis Objectives

The aim of this research is to use a FOS-based identification method that utilizes muscle activation information from sEMG measurements and joint kinematic data to develop a model that accurately maps these inputs to the net force generated at the wrist. A schematic of the proposed system is provided in Figure 1.2. FOS candidate functions will be tailored to reflect the neuromuscular behaviour of the muscles using the Hill-muscle model. The objectives of this work are to:

- develop a Hill-based muscle model to describe the force generated by various components of muscle for isometric contractions.
- utilize the FOS method to more accurately predict the force induced at the wrist from flexion and extension torque at the elbow using physiologically relevant model components.
- utilize the FOS method to obtain subject-specific Hill-based muscle model parameters.
- lay groundwork for more comprehensive candidate function development.

## 1.4 Organization of Thesis

The thesis is divided into six chapters that are organized as follows:

**Chapter 2:** provides a description of the Hill-muscle model and an overview of some examples of Hill-based muscle models provided in the literature. This chapter also includes a detailed review of methods used to estimate muscle activation using surface electromyography, musculoskeletal geometry *in vivo*, and an overview of the relationship between EMG and muscle force.

**Chapter 3:** provides an overview of the methods used to develop the Hill-based muscle model candidate functions for the (FOS) method.

**Chapter 4:** provides details about the experimental set-up and the procedures used to collect and process sEMG and kinematic data from human subjects. Experimental results for both isometric and dynamic studies are presented, including values for subject-specific Hill-muscle-model parameters.

**Chapter 5:** includes an assessment of the results and how these may have been affected by some simplifying assumptions used in the model development. A description of the method used to validate results for one muscle of the upper arm is provided as well as suggestions for additional methods, which can be used to validate results in the future.

**Chapter 6:** A summary of the work concludes this thesis and suggestions for future research are provided.

# Chapter 2

# Background

## 2.1 Elbow Joint Dynamics

Flexion and extension of the elbow results from muscles acting across the elbow joint. These are classified into two categories: flexors (i.e. biceps brachii, brachioradialis and brachialis) which generate a moment about the elbow, causing the arm to bend, and extensors (i.e. triceps brachii and anconeous) which generate a moment in the opposite direction, causing the arm to straighten. An illustration of the key muscles acting on the elbow is provided in Figure 2.1.

Elbow joint motion is a result of the contraction of multiple muscles working together to create smooth and controlled joint rotation. The moment generated by each muscle is a function of the force produced by each muscle, and the moment arm of the muscle, which is defined as the minimum distance perpendicular to the line-of-action of the muscle, and the centre of the elbow joint [74] and is shown in Figure 2.2. The net moment about the elbow, $M_{elbow}$ can be calculated as the sum

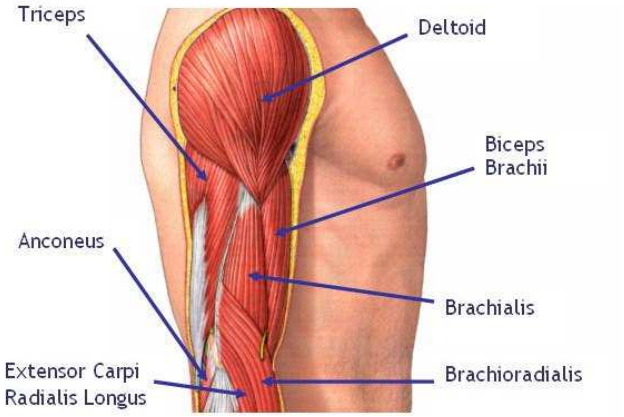


Figure 2.1: Muscles of the upper arm [37]

of individual moments generated by each muscle, that is

$$M_{elbow} = \sum_{i=1}^{I} F_i \cdot MA_i \tag{2.1}$$

where $i$ represents an individual muscle, $I$ is the number of muscles considered to be acting on the joint, $F_i$ is the force generated by muscle $i$, and $MA_i$ is the moment arm of muscle $i$.

Force at the wrist induced by a moment about the elbow can be measured using a force transducer positioned at the wrist, with the shoulder and wrist held in a fixed position. It is then possible to quantitatively determine the net moment about the elbow from the force measured at the wrist and using the length of the forearm as the moment arm as follows:

$$M_{elbow} = F_w \cdot MA_{forearm} \tag{2.2}$$

where $F_w$ is the measured wrist force and $MA_{forearm}$ is the forearm moment arm, as illustrated in Figure 2.3.

The challenge is to separate the calculated net moment into individual muscle

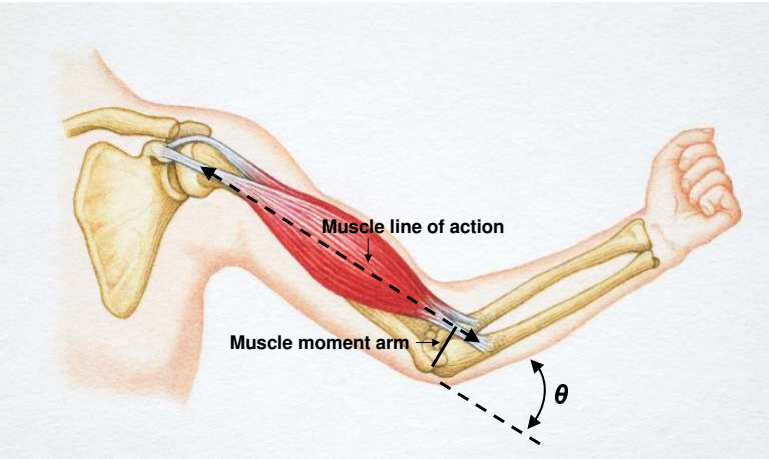


Figure 2.2: Example of the line of action and moment arm for the biceps brachii (adapted from [61]). Elbow joint angle $\theta$ is defined as the external elbow angle, where zero degrees occurs when the arm is at full extension.

forces for each muscle acting on the elbow. Muscle force can be described as the result of "activation dynamics" and "contraction dynamics" as illustrated in Figure 2.4. "Activation dynamics" refers to the activation of the contractile components of muscle tissue in response to neural signals from the Central Nervous System (CNS) and will be discussed in Section 2.5. "Contraction dynamics" describes the process of force generation in the contractile component of the muscle [100]. Many models exist to estimate the force produced in muscles, including the Hill-muscle model.

## 2.2 Modeling Hill-Muscle Model Components

Hill-based muscle models are often used to estimate of the magnitude of force generated in individual muscles. As shown in Figure 2.5, the classic Hill model is composed of a contractile element (CE), a series elastic element (SE), and a parallel elastic element (PE) [94].

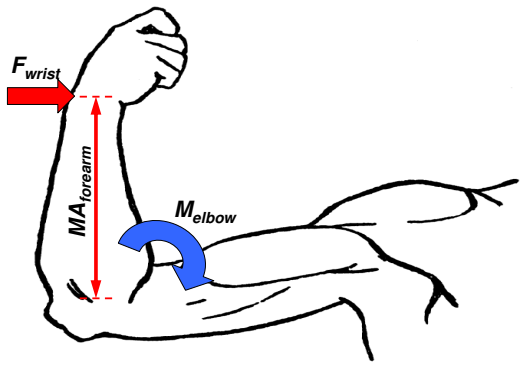


Figure 2.3: Calculation of the net elbow moment $M_{elbow}$ using the force measured at the wrist $F_{wrist}$ and the length of the forearm $l_{forearm}$ [29]

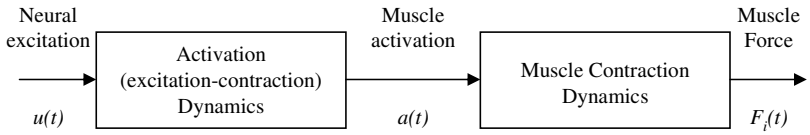


Figure 2.4: Block diagram of process of muscle activation and contraction [100]

The force generated by the CE ($F^{CE}$) is equal to that in the SE ($F^{SE}$), and the total muscle force $F_{muscle}$ is equal to the sum of the forces in each of the two parallel sections of the model, that is

$$F^{CE} = F^{SE} \tag{2.3}$$

$$F_{muscle} = F^{CE} + F^{PE} \tag{2.4}$$

### 2.2.1 Contractile Element

Force generated by the CE ($F^{CE}$) can be interpreted as the activity of the contractile units within the muscle fibre, called sarcomeres, which contract and generate tension

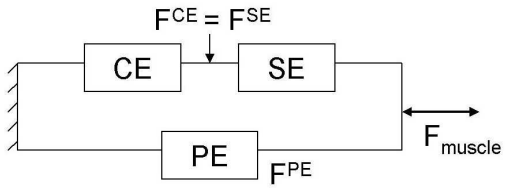


Figure 2.5: Structure of the Hill muscle model adapted from [94]

following stimulation from a motor nerve. The amount of tension that can be developed depends on the muscle length, and the maximum amount of tension that the muscle generates ($F_0$) when it is maximally activated at its optimal length $L_0$.

The muscle force-length relationship describes the force that a muscle generates as a function of the length of the muscle. As shown in Figure 2.6, the peak contractile force that can be generated by a muscle occurs at the $L_0$ and this force is reduced to zero at lengths of approximately $0.5L_0$ and $1.5L_0$, respectively [100].

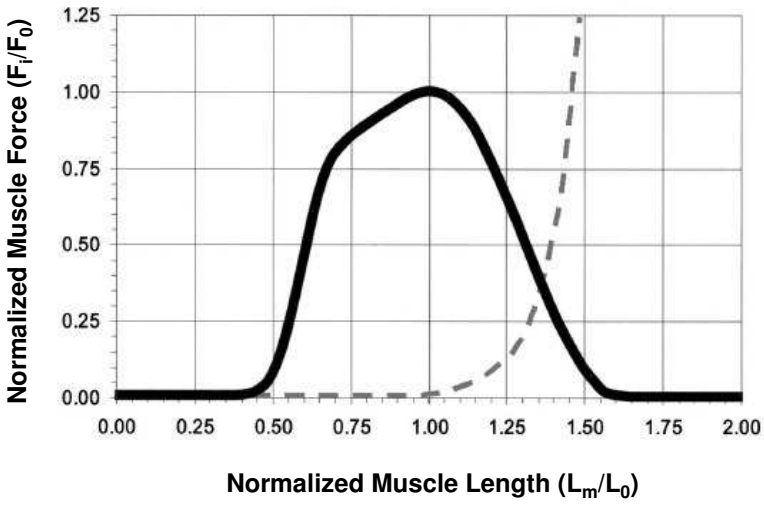


Figure 2.6: Isometric contractile element force $F^{CE}$ curve (solid line) and the parallel elastic force $F^{PE}$ (dashed line) extracted from [31]

The muscle contractile force also depends on the speed at which a contraction

takes place. The force-velocity relationship only applies to dynamic contraction of muscle, and represents the ability of the muscle fibres to generate force when the muscle is actively shortening (i.e. during a concentric contraction). During isometric contractions, the shortening velocity is zero and the maximum force achieved by a muscle will equal $F_0$. As shown in Figure 2.7, the force generation capabilities of muscle diminish with the contraction velocity ($v_{ce}$). In contrast, muscle force can exceed the isometric force during eccentric (lengthening) contractions. A lengthening contraction occurs when the load that the muscle is acting against is heavier than the muscle can actively support. The muscle fibres will lengthen and the tension in the fibres will help support the extra weight. This behaviour is illustrated in Figure 2.7.

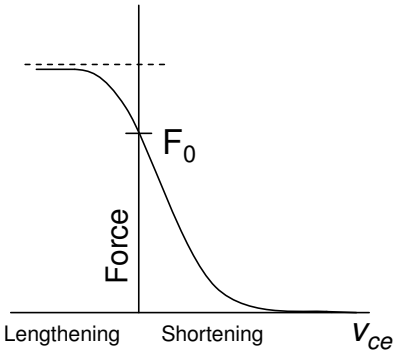


Figure 2.7: General shape of the force-velocity relationship. The vertical axis represents zero velocity or an isometric contraction

$F^{CE}$ can therefore be expressed as the product of $F_0$, the force-length ($f_l$) and force-velocity ($f_v$) relationships and muscle activation $a(t)$ [100], that is

$$F^{CE} = F_0 \cdot f_l \cdot f_v \cdot a(t) \tag{2.5}$$

Muscle activation is commonly estimated using EMG signals recorded from the

active muscle. Since $F_0$ is a constant value for each muscle, and assuming that muscle activation can be estimated from EMG measurements, approximations of the force-length and force-velocity relationships are required in order to calculate $F^{CE}$.

### 2.2.2 Parallel Elastic Component

The force generated by the PE component ($F^{PE}$) is attributed to the stretch resistance in inactive muscle. Behaving similarly to an elastic band, the PE only exerts tension when it is stretched beyond its resting length, which is equivalent to the optimal muscle length $L_0$. As the muscle lengthens beyond $L_0$, tension builds up slowly at first, and then increases quickly. The general shape of the $F^{PE}$ is illustrated in Figure 2.6.

### 2.2.3 Series Elastic Component

The SE component represents elastic material connected in series with the contractile component and refers to elastic energy that is stored within the individual sarcomeres, [100] as well as inherent elasticity in the tendon. An isometric contraction is defined as the development of muscle tension with no visible muscle shortening [24, 28]. This is accomplished via active shortening of the CE to generate active muscle force, which is offset by an extension of the series elastic element. The SE component is often neglected in Hill-based models by assuming that the tendon is infinitely stiff [80].

## 2.3 Determining the Relationship between Muscle Length and Isometric Force

Early investigations into the force generated by muscle fibres were performed on single *in-vitro* fibres and muscles from amphibians (*i.e.* frogs) and small animals [56]. The classic work of Gordon *et al.* [33] presented the traditional shape of the force-length curve for frog muscle fibres, while later studies identified optimal sarcomere lengths for human tissue [92]. Identifying the *in-vivo* force-length characteristics is important to describe, understand and predict human motion.

Early studies looking at individual sarcomeres of *in-vitro* muscle tissue identified an optimal sarcomere length ($L_{S0}$) as the length at which maximal overlap of actin and myosin myofiliments occurred. Suggested values for $L_{S0}$ for human skeletal muscle range between $\sim 2.0 - 2.8\mu m$ [33, 84, 92]. Optimal length of whole muscle can be represented as muscle fibre length ($L_F$) normalized to the optimal sarcomere length using measured sarcomere lengths ($L_S$), and assuming a value of $2.8\mu m$ for $L_{S0}$ as follows:

$$L_{0i} = L_F \frac{2.8}{L_S} \tag{2.6}$$

Several researchers have described the force-length relationship in human muscles for maximal voluntary contraction and /or artificially evoked contractions. In general, evoked contractions involve injecting low frequency current via surface stimulating electrodes to activate skeletal muscle and mimic voluntary contraction. The use of electrical stimulation to isolate specific muscles removes the problems associated with several muscles contributing to net joint torque, as the measured torque or force

is a result of activation of only the stimulated muscle fibres. In addition, subject motivation and the associated variation in maximal voluntary contraction are not factors and researchers are able to maintain a constant level of activation between trials [56].

Leedham and Dowling [56] used electrical stimulation to isolate the contribution of the biceps brachii to elbow joint torque. They also examined joint torque at various joint angles for maximum voluntary contraction of the biceps brachii. The resulting joint angle curves are shown in Figure 2.8.

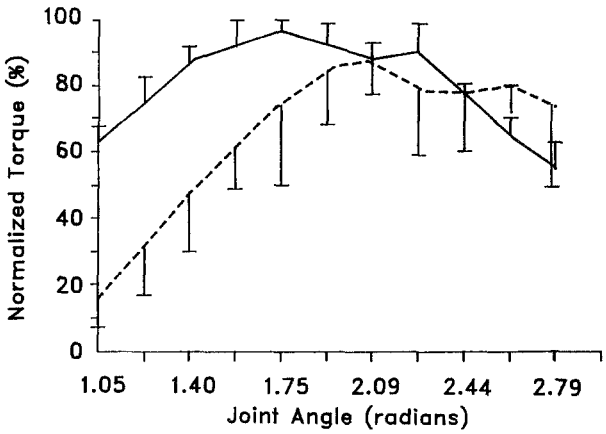


Figure 2.8: Torque-length curves for the biceps brachii obtained from maximal voluntary contractions (solid line) and electrical stimulation (dashed line) [56]. In this study, full elbow extension was defined as a joint angle of $3.14rad$ or 180°

.

Koo *et al.* [48] used electrical stimulation to determine torque-angle curves for the biceps brachii and brachioradialis at stimulation parameters of 20mA of current, pulse width of $0.3ms$ and at a frequency of $30Hz$ [48]. Elbow torque was measured over a range of joint angles and individual muscle force was calculated using an optimization solution procedure of a Hill-based model. The joint angle where the maximum muscle

force was achieved was used as the optimal joint angle as shown in Figure 2.9.

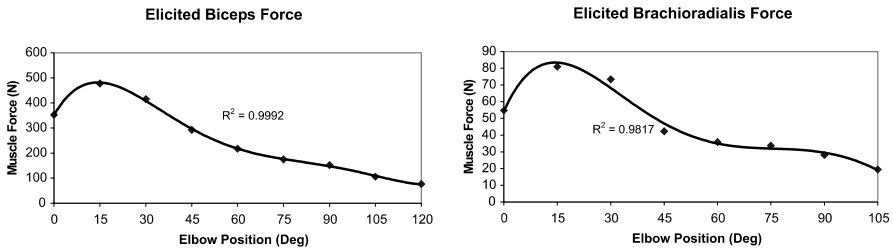


Figure 2.9: Examples of torque-angle and force-angle curves obtained through submaximal electrical stimulation of the biceps brachii and brachioradialis [48]. Full extension is defined as 0°

.

Some studies have investigated the effect of contractions at a percentage of maximum on the shape of the force-length curve and suggest that the maximal force output of the force-length relationship is shifted towards longer lengths for submaximal muscle activation [35, 84] as well as following eccentric exercise [81].

## 2.4 Muskuloskeletal Geometry

### 2.4.1 Optimal Joint Angle

A key parameter for upper arm muscles that has not been widely reported in the literature is the optimal joint angle associated with optimal muscle length. Many researchers provide muscle optimal length measurements from cadaver studies [1, 2, 53, 74], or estimates from biomechanical models [9, 31, 32, 40, 48]. Some researchers have provided relationships between muscle length and joint angle [57, 83], but only three studies were found that provided estimates of both the optimal muscle length and joint angle for the same subjects [9, 48, 74]. In many studies the optimal joint

angle is inferred as the angle where maximal torque about a joint is measured [6, 10, 45, 81]. Table 2.1 provides a summary of optimal joint angle values for upper arm muscles presented in the literature. An elbow angle of 0° represents full extension. In the majority of studies, optimal joint angles were reported for the biceps brachii and brachioradialis, or were grouped giving one optimal flexion angle.

Table 2.1: Optimal Joint Angle for muscles about the elbow as presented in the literature

| **Reference** | **Optimal Joint Angle (deg)** | | | |
|---|---|---|---|---|
| | **Study Size (n)** | **Biceps** | **Brachioradialis** | **Triceps** |
| An *et al.*, 1981 [2] | 6 | 75 | 80 | – |
| Buchanan, 1995 [6] | 11 | 90 | 90 | 108 |
| Chang *et al.*, 1999 [9] | 7 | 110 | 50 | – |
| Jaskolska *et al.*, 2006 [45] | 22 | – | – | 83-90 |
| Koo *et al.*, 2002 [48] | 4 | 20 | 17 | – |
| Lieber *et al.*, 2005 [60] | 8 | – | 94 | – |
| Murray *et al.*, 2000 [74] | 10 | 20 | 20 | ∼70-90 |
| Philippou *et al.*, 2004 [81] | 14 | 67 | 67 | – |
| Van Zuylen *et al.*, 1988 [90] | 4 | ∼90 | – | – |
| **Average** | | **67.4** | **59.7** | **88.2** |

### 2.4.2 Estimating Muscle Moment Arms

In order to translate the force generated in a muscle, into torque about a joint, the moment arm of the muscle is required. As previously described, the moment arm is the minimum distance perpendicular to the line-of-action of the muscle, and the centre of the elbow joint [74]. A number of estimations of how this value changes with respect to joint angle are available in the literature [3, 57, 83], and a few key methods are summarized below.

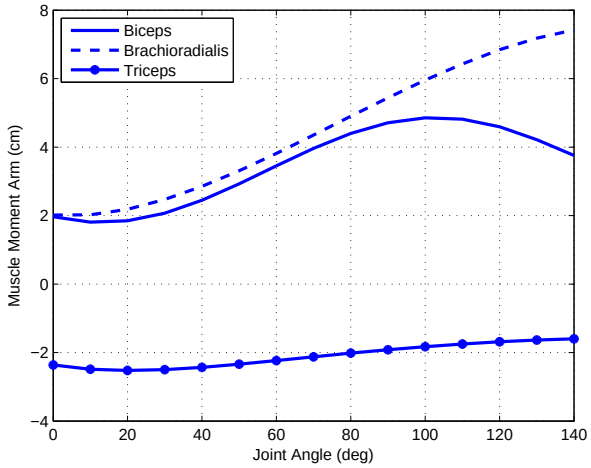


Figure 2.10: Muscle moment arm ($cm$) for the biceps brachii, brachioradialis and triceps brachii estimated as a function of joint angle [57]

Lemay and Crago [57] presented a polynomial model of the moment arm (in $cm$) for muscles of the arm as a function of elbow joint angle (in radians). Polynomial approximations of the moment arm models were estimated from moment arm curves presented by Amis *et al.* [1]. These polynomial relationships are provided below, where $MA_{bi,brd,tri}$ refer to the moment arm of the biceps brachii, brachioradialis and triceps brachii, respectively. The shapes of the resulting curves are presented in Figure 2.10.

$$MA_{bi} = 1.963 - 1.440\theta + 3.031\theta^2 + 0.887\theta^3 - 1.418\theta^4 + 0.285\theta^5 \quad (2.7)$$

$$MA_{brd} = 2.015 - 0.458\theta + 3.058\theta^2 - 1.081\theta^3 + 0.159\theta^4 - 0.0187\theta^5 \quad (2.8)$$

$$MA_{tri} = -2.363 - 1.015\theta + 1.920\theta^2 - 1.035\theta^3 + 0.257\theta^4 - 0.0262\theta^5 \quad (2.9)$$

Murray *et al.* (1995) [76] looked at 2 cadaver specimens to generate a model of moment arm for muscles of the upper arm. Moment arms were calculated as the

partial derivative of the muscle-tendon length $\partial l$, with respect to joint angle $\partial\theta$ as per the "tendon excursion" method outlined in [3]. The tendon excursion method can also be used with imaging techniques such as ultrasound or MRI to determine muscle moment arm for subjects *in-vivo*. A point on a tendon is marked on an ulrasound image, and as the joint rotates, the distance that this point moves is quantified. The muscle moment arm is approximated by taking the derivative of the tendon displacement over joint rotation. Figure 2.11 presents an example from Ito *et al.* [44] where an ultrasound image was captured for each 5° of joint rotation, and the moment arm $MA = \Delta x/\Delta a$, was found where $\Delta x$ is the distance travelled by point $x$ in each image and $\Delta a$ is 5°.

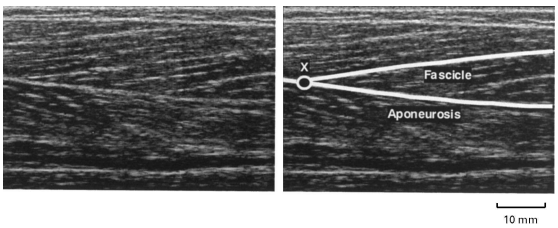


Figure 2.11: Longitudinal ultrasound image of the Tibialis Anterior (TA) [44]. The point $X$ represents the selected point of attachment between the muscle fascicle and aponeurosis. The distance travelled by $X$ over a range of images taken every 5° was measured with a ruler

In a subsequent study, Murray *et al.* (2002) [75] examined 10 cadaver specimens (5 male, 5 female) and quantified the moment arm for muscles of the upper arm with respect to joint angle. Their moment arm measurements are shown in Figure 2.12. It is clear that the range of moment arm for brachioradialis and biceps is variable between the cadaver specimens especially around 90-100° of flexion. This variability corresponds to approximately $2cm$ or 33% of the peak moment arm length.

An additional method used to determine muscle moment arm is the "muscle line

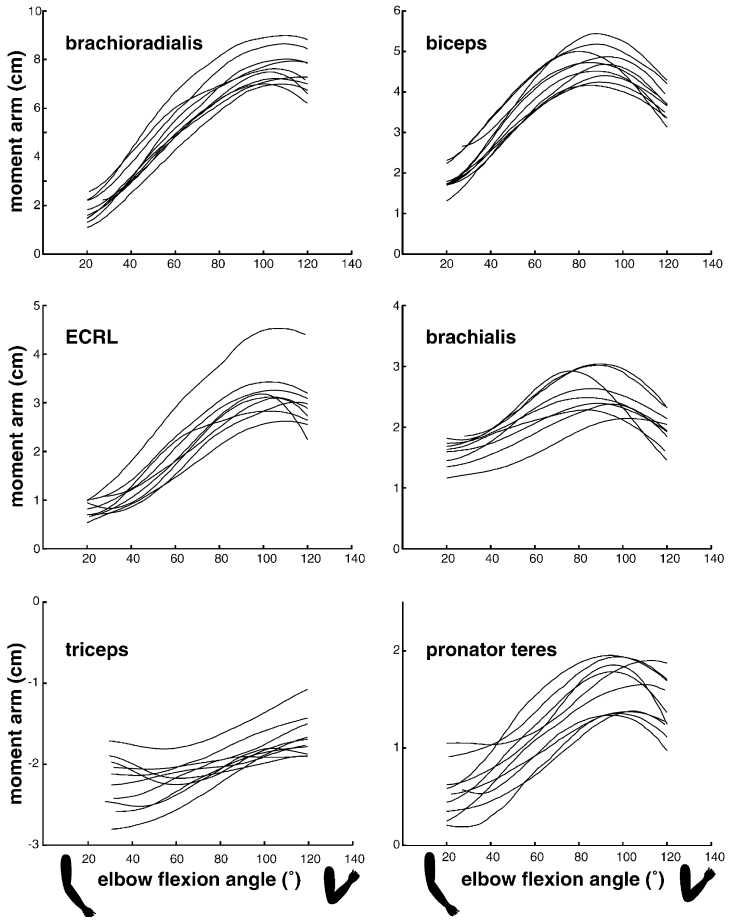


Figure 2.12: Elbow muscle moment arms vs. elbow angle (deg) for 10 cadaver specimens [75]

of action" method. Images of a joint centre of rotation as well as the action line of a tendon are obtained using X-rays or MRI [65]. The perpendicular distance from the joint centre to the action line of the tendon is measured directly from the images taken in the plane in which the joint operates.

### 2.4.3 Computer Models

Computational models of the human neuromuscular system have become commonly used by researchers for simulating the control of movement, athletic performance and medical treatments such as surgical tendon transfer [17, 30, 40, 60]. A widely used commercially available system called Software for Interactive Musculoskeletal Modelling (SIMM) is a software platform that enables researchers to build models of musculoskeletal structures in the body [17]. It is based upon rigid segments (bones) connected by joints and surrounded by muscles and ligaments. Users can alter the line of action of a muscle and properties associated with force generation, measure muscle length and moment arm for various positions, or input muscle activation data and receive the resulting muscle forces and/or joint moments. The system incorporates traditional Hill-based model components such as force-length and force velocity relationships for muscle and tendon and muscle parameters such as maximal isometric force ($F_0$), optimal muscle length ($L_0$), tendon slack length ($L_{Ts}$), pennation angle ($\alpha$) and maximal contraction velocity ($V_{max}$).

## 2.5 Measurement of Muscle Activation

Muscle activation $a(t)$ is defined as the neural input for a desired muscle force and is commonly estimated from recorded EMG. The EMG is a recording of the electrical signals known as action potentials, that are generated in muscle fibres when they are instructed to contract, and can be influenced by many factors.

### 2.5.1 Generation of the Action Potential

A muscle is comprised of many motor units, where a motor unit is a group of muscle fibres, all of which are directly innervated by a single motor neuron. Thus the motor unit is the smallest functional unit in a muscle. The location at which the motor neuron branches terminate on the muscle fibres is called the motor end plate, or neuromuscular junction [59].

When an action potential arrives at the motor end plate from the motor nerve, action potentials are, in turn, generated in the muscle fibres. These action potentials travel away from the end plate in both directions as shown in Figure 2.13. These travelling electromagnetic waves can be detected using appropriate sensors called electrodes.

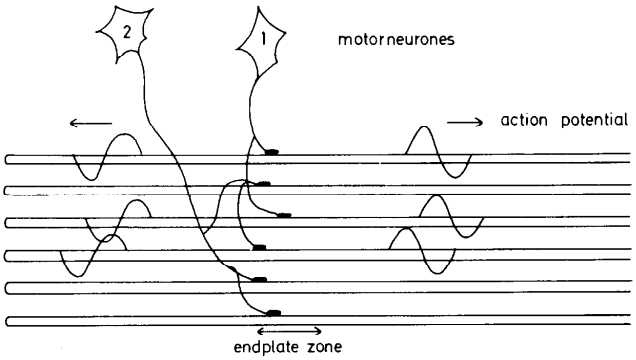


Figure 2.13: Example configuration of two motor units; Number 1 of which has just been excited [52]

Electrodes placed within this electromagnetic field will be able to detect a potential difference between the muscle tissue and ground. Figure 2.14 illustrates an example of this process for $n$ muscle fibres of one motor unit. The spatio-temporal sum of the individual action potentials for all muscle fibres in one motor unit form the motor unit action potential (MUAP), given in Figure 2.14 as $h(t)$ [4].

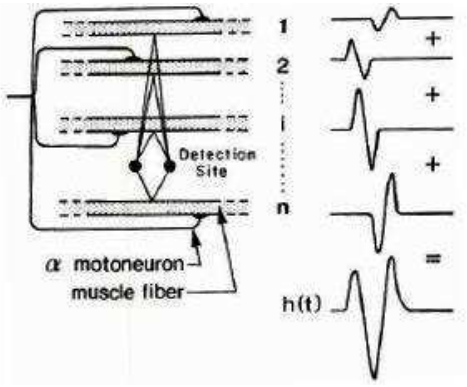


Figure 2.14: The contribution of individual muscle cell action potentials to the measured motor unit action potential (MUAP) [4]

### 2.5.2 Surface Electromyography

Metal electrodes that are placed on the surface of the skin over a particular muscle can be used to detect the sEMG signal. Electrodes are primarily arranged in monopolar or bipolar configurations. As the names suggest, monopolar signal recording uses one recording electrode placed over a muscle with a reference electrode located elsewhere on the body. In bipolar signal recording, two recording electrodes with a relatively small inter-electrode distance are attached on the skin surface, with the electrode axis parallel to the underlying muscle fibres. Electrodes are generally placed between the innervation zone and terminal tendon of the muscle [73]. The configuration and an example of the resulting raw EMG signal are illustrated in Figure 2.15.

The use of bipolar electrodes have the advantage of good signal-to-noise-ratio (SNR) through a process called differential amplification. A differential amplifier (shown in Figure 2.16) subtracts the signals from each terminal of the bipolar electrode, effectively removing the noise signal that is common to both terminals of the surface EMG electrode. The resulting signal is then amplified by gain $A$ [93]. The

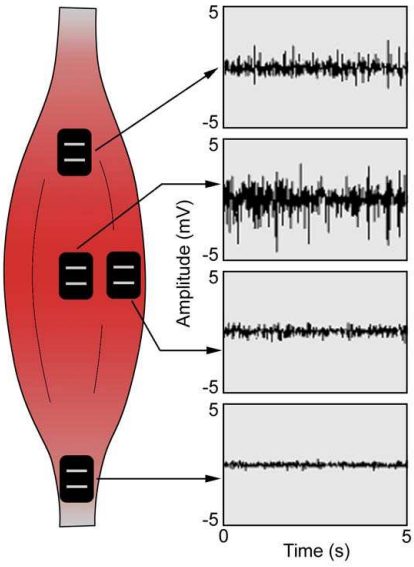


Figure 2.15: Conceptual placement of EMG electrodes with respect to innervation zone (top electrode) and tendon (bottom electrode) [16]

benefits associated with active electrodes are based on the fact that the differential amplification of the signal takes place onboard the EMG sensor, rather than carrying the signal through wires and differentially amplifying the signal at a computer. This effectively eliminates the amplification of any noise signals that may be caused by high skin impedance or cable motion artifact.

Prior to sampling, EMG signals are filtered. A high pass filter with corner frequency $\sim 20Hz$ removes low frequency motion artifact, and a low pass filter with a cutoff frequency of just less than half the sampling frequency prevents aliasing effects [15]. Cross-talk, or signal contamination from nearby contracting muscles can also affect EMG signal measurement. Unfortunately, it is difficult to identify and remove cross-talk from EMG signals, due to the fact that cross-talk signals exist in a similar frequency range as the desired muscle signal, therefore removal of extraneous signals by traditional filtering methods is not an option. A variety of methods for reducing

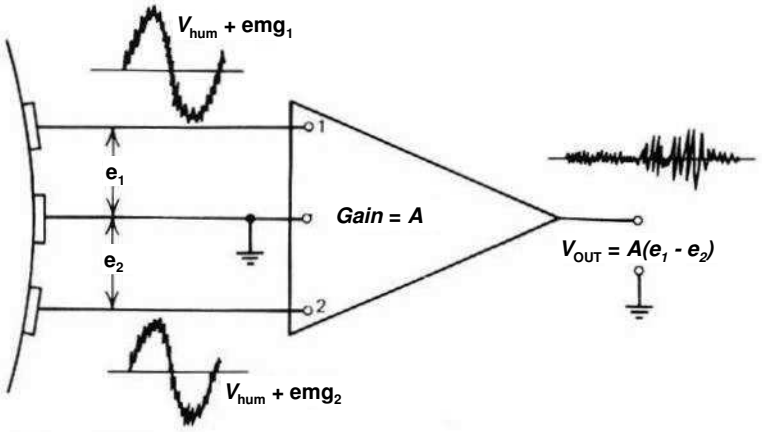


Figure 2.16: Differential amplifier subtracts the signals from each terminal of the EMG electrode to eliminate the noise common to both signals [93]

the effects of cross-talk are reviewed in [23].

### 2.5.3 Amplitude Estimation

EMG is a stochastic signal that varies about a zero-mean value [73]. The signal amplitude is generally considered to provide an estimate of the level of muscle activation $a(t)$. Two common methods used to estimate EMG amplitude are the smoothed, rectified EMG (also referred to as the linear envelope) and the root mean square (RMS) value of the EMG which are computed as:

$$LE = \frac{1}{N+1} \sum_{i=-N/2}^{N/2} |u_i(t)| \tag{2.10}$$

$$RMS = \left( \frac{1}{N+1} \sum_{i=-N/2}^{N/2} |u_i^2(t)| \right)^{0.5} \tag{2.11}$$

where $u_i(t)$ are the EMG samples and $N+1$ is the window length [73].

## 2.6 Methods used to Relate EMG to Muscle Force

EMG amplitude is observed to increase when an individual generates more force in a muscle. The magnitude of force generated by a particular muscle is modified by varying the number of motor units which are instructed to contract (recruitment), or by adjusting the frequency at which the motor units fire (rate coding) [52]. Many researchers have attempted to define a relationship that describes the dependence of force on EMG, however this has proved to be a difficult task [16]. A brief overview of methods used in the past to estimate muscle force or joint torque from EMG signals follows.

### 2.6.1 Linear and Non-linear Approximations

Early studies attempting to compare processed EMG signals from a variety of muscles suggested that the relationship between normalized muscle force and EMG was quasi-linear for small muscles of uniform muscle fibre composition, and non-linear for larger muscles of mixed fibre composition [4, 55, 99]. It has come to be understood, however that these simple relationships are not entirely accurate, as many factors can influence the relationship between measured joint torque or muscle force and EMG signals, including co-contraction of agonist-antagonist muscles and signal cross-talk, especially for small muscles.

Additional work by Clancy *et al.* [14, 13] provided a model to estimate joint torque about the elbow as a function of EMG contribution from two inputs (an elbow flexor and extensor). Using a least-squares method they determined fit parameters to accompany processed EMG amplitude in order to estimate torque contribution from the elbow flexor and extensor. Problems with this method however are due to

the fact that the model assumes contribution from only one muscle in flexion (biceps brachii) and one muscle in extension (triceps brachii). This simplification neglects contribution to elbow torque from additional muscles such as the brachioradialis and brachialis.

### 2.6.2 EMG-Driven Models

EMG-driven or Hill-based muscle models have been used for muscle force or joint torque prediction in a wide range of applications. Langenderfer *et al.* [54] utilized an EMG-based upper-arm model to predict the force in the long head of the biceps to aid in clinical assessment of superior labrum anterior posterior (SLAP) lesions. Other researchers have developed their own Hill-based models to describe motion of specific joints [39, 95], regions of the body [30, 40, 43] or to assess pathologic movement [25, 47]. Often an optimization procedure is implemented within the model to further refine internal parameters and achieve more accurate force prediction [31, 48, 54], however it has been demonstrated that these types of models may have trouble predicting co-contraction in antagonist muscles [11].

### 2.6.3 Artificial Neural Networks

To take into account the non-linearities between EMG and joint torque or muscle force, artificial neural networks (ANN) have become a common method to predict joint torque based on muscle activity and joint kinematics. Neural networks are composed of many small neurons, which are connected together and arranged in layers. Weighting factors are assigned to each connection and modified during training procedures, where inputs are mapped to a desired output. Sepulveda *et al.* [87]

successfully used an ANN with a back-propagation algorithm to map EMG signals from muscles in the leg to joint torques at the hip, knee and ankle during human gait. Liu *et al.* [63] utilized a 3-layer ANN to predict tendon force in the cat soleus from measured EMG measurements and achieved an estimation accuracy with root-mean-square-error less than 15%. Figure 2.17 provides an example of the ANN structure from [63].

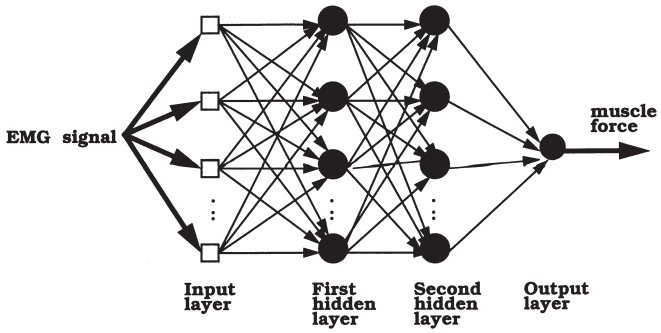


Figure 2.17: An ANN configuration for predicting force from EMG [63]

Rosen *et al.* [85] compared the use of ANN to Hill-based models for predicting joint torques and concluded that while the ANN was slightly more accurate in its ability to predict joint torque, the method is hampered by its high computational demand and reliance on specific training data. For applications where force or torque prediction is required in real-time, Hill-based models may be more desirable because they are more computationally efficient during model training, especially compared to neural networks with many hidden layers and a large number of nodes. As well, Hill-based models are more widely applicable for different individuals and generalizable across varying movement conditions.

### 2.6.4 Fast Orthogonal Search (FOS)

First developed by Korenberg in [49] and further described in [50, 51], the Fast Orthogonal Search (FOS) method is a nonlinear identification method that forms a sum of $M$ linear or nonlinear basis functions $p_m(n)$ and coefficient terms $a_m$ and aims to minimize the mean square error between the estimate and the system output. The FOS model takes the form:

$$y(n) = \sum_{m=1}^{M} a_m p_m(n) + e(n) \tag{2.12}$$

where *y(n)* is the actual system output, *e(n)* is the estimation error and $n$ is the discrete time sample index. The FOS method searches through a number, $N$, of available candidate basis functions, where $N >> M$ and iteratively selects those functions which contribute the most reduction in mean square error (MSE) between the model estimate and the actual system output. Complete details about the FOS method including the algorithm used to generate the FOS models are provided in Appendix B.

In previous research [70], a set of candidate functions composed of common mathematical terms were identified to predict force at the wrist during flexion and extension of the elbow. The resulting candidate functions are summarized in Table 2.2. The resulting FOS models were able to predict force at the wrist and demonstrated equivalent estimation error to models generated with multi-layer perceptron neural networks. Evaluation error for models trained and evaluated with isometric data was given in terms of percent mean square error (%MSE) and ranged from 6% to 19% across 5 subjects. Neural network models trained and evaluated with the same data resulted in an evaluation %MSE ranging from 5-17%.

FOS has been used in a wide variety of applications including nonlinear system

Table 2.2: Candidate functions suggested for use in Mobasser *et al.* (2007) [70], where $e_{Bi,Brd,Tri}$ refer to the processed EMG signals for the biceps brachii, brachioradialis and triceps brachii respectively

| **Common Functions** | |
|---|---|
| offset | $\dot{\theta}$ |
| $e_{Brd}$ | $e_{Tri}$ |
| $e_{Bi}$ | |
| $\cos\theta \cdot e_{Bi}$ | $\sin\theta \cdot e_{Bi}$ |
| $\cos\theta \cdot e_{Tri}$ | $\sin\theta \cdot e_{Tri}$ |
| $\cos\theta \cdot e_{Brd}$ | $\sin\theta \cdot e_{Brd}$ |
| $\cos\theta \cdot e_{Brd} \cdot e_{Tri}$ | $\sin\theta \cdot e_{Brd} \cdot e_{Tri}$ |
| $\cos\theta \cdot e_{Bi} \cdot e_{Brd}$ | $\sin\theta \cdot e_{Bi} \cdot e_{Brd}$ |
| $\cos\theta \cdot e_{Bi} \cdot e_{Tri}$ | $\sin\theta \cdot e_{Bi} \cdot e_{Tri}$ |
| (c) **Square Root Functions** | |
| $\cos\theta \cdot \sqrt{e_{Brd}}$ | $\sin\theta \cdot \sqrt{e_{Brd}}$ |
| $\cos\theta \cdot \sqrt{e_{Bi}}$ | $\sin\theta \cdot \sqrt{e_{Bi}}$ |
| $\cos\theta \cdot \sqrt{e_{Tri}}$ | $\sin\theta \cdot \sqrt{e_{Tri}}$ |
| $\cos\theta \cdot \sqrt{e_{Brd} \cdot e_{Tri}}$ | $\sin\theta \cdot \sqrt{e_{Brd} \cdot e_{Tri}}$ |
| $\cos\theta \cdot \sqrt{e_{Bi} \cdot e_{Tri}}$ | $\sin\theta \cdot \sqrt{e_{Bi} \cdot e_{Tri}}$ |
| $\cos\theta \cdot \sqrt{e_{Bi} \cdot e_{Brd}}$ | $\sin\theta \cdot \sqrt{e_{Bi} \cdot e_{Brd}}$ |

identification and process control [20] spectral analysis [12, 67], predicting response to drug treatment [88] and estimating the speed of AC induction motors [68], to name a few. Many aspects of FOS make it a desirable method for estimating time series data, especially compared to neural networks. The FOS method develops models extremely quickly because the orthogonal candidate functions do not need to be computed directly. The method circumvents these costly calculations by finding only the coefficients of the orthogonal functions. Therefore, the computational time required to develop models is significantly faster than the time required for neural networks, especially for complex networks with many hidden layers and a large number of nodes. As well, compared to least-squares methods, FOS is able to generate a model solution with fewer terms. This means that estimates of the system will be less likely to fit noise, and will be more generalizable to system inputs [70].

# Chapter 3

# Hill-Based FOS Model Design

## 3.1 Hill-Based Muscle Model Design

The Hill-based model used in this study includes estimates for the force generated in the contractile element and in the parallel elastic element. Descriptions of the methods used to estimate these force components are provided in the following sections.

### 3.1.1 Contractile Element

#### Force-Length Relationship

Models of the force-length relationship typically relate output force to the muscle length. However, since accurate measurements of muscle length are difficult to obtain, we wish to use a model relating output force to joint angle, $\theta$. Lemay and Crago [57] derived a polynomial relationship between elbow joint angle and change in muscle length ($\Delta L_i$) from a position of full extension, for muscles of the upper arm. Estimates of the relationship between muscle length and elbow joint angle from Amis *et al.* [1]

were integrated to obtain the change in muscle length with respect to joint angle. Polynomial fits of these curves were found and are provided in the following equations:

$$\Delta L_{bi} = 0.145 + 0.307\theta + 2.460\theta^2 - 0.472\theta^3 \tag{3.1}$$

$$\Delta L_{brd} = 0.107 + 0.946\theta + 1.798\theta^2 - 0.127\theta^3 \tag{3.2}$$

$$\Delta L_{tri} = 0.0299 - 2.775\theta + 0.352\theta^2 - 0.0312\theta^3 \tag{3.3}$$

where $\theta$ is the external elbow joint angle in radians and the change in muscle length $\Delta L_{i=Bi,Brd,Tri}$ for muscle $i$ is given in *cm*. According to equations 3.1 to 3.3, a positive change in muscle length occurs for muscles which shorten as joint angle increases, *i.e.* as the elbow is flexed. However, for the purposes of this research, the sign convention was reversed and the equations modified such that a positive change in muscle length denotes muscle lengthening, while a negative change denotes muscle shortening. This modified relationship is shown in Figure 3.1 with joint angle converted from radians to degrees. Full extension of the arm is given as an angle of 0°, while full flexion occurs between 120° and 140° depending on the individual and the testing apparatus.

It is assumed that at maximal extension of the elbow, $L_{MTmax}$ of the arm flexors (biceps brachii and brachioradialis) is attained, while at full flexion of the elbow, $L_{MTmax}$ for the extensors (triceps brachii) is reached. Therefore, if the maximal musculotendon length for the relevant muscles is known, it is possible to use the relations in 3.1 to 3.3 to estimate the length of the muscles over a range of elbow joint angles. Lemay and Crago [57] provided estimates from their upper arm model of $L_{MTmax}$ for the biceps brachii and brachioradialis in positions of full elbow extension and pronation, while $L_{MTmax}$ for the triceps brachii was estimated at full elbow

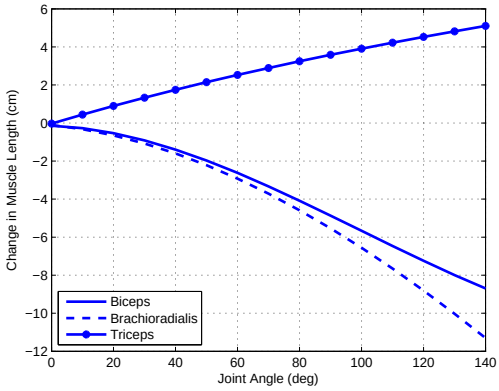


Figure 3.1: Change in muscle length ($cm$) for the biceps brachii, brachioradialis and triceps brachii estimated as a function of joint angle [57]

flexion. Values for $L_{MTmax}$ from a second source [8] were used to calculate an average $L_{MTmax}$ for each of the muscles. A summary of these values are provided in Table A.1 in Appendix A.

Muscle lengths $L_m$ for the biceps brachii and brachioradialis were determined by subtracting the value of $\Delta L_{bi,brd}$ from $L_{MTmax_{bi,brd}}$ from $\theta = 0°$ to $\theta = 140°$ in $10°$ intervals. $L_m$ for the triceps brachii was calculated by subtracting the value of $\Delta L_{tri}$ from $L_{MTmax_{tri}}$ starting at $\theta = 140°$ to full extension at $\theta = 0°$. Calculated muscle lengths are plotted in Figure 3.2 and given in Table 3.1.

Values reported in the literature for optimal muscle length $L_0$ for each of the muscles across the elbow vary substantially [1, 2, 31, 40, 48, 53, 74]. A summary of values for the biceps brachii, brachioradialis and triceps brachii is provided in Table A.3 in Appendix A. Weighted average values for each muscle (averaging across multiple muscle heads) were calculated to estimate the optimal muscle lengths. Values from studies with larger sample sizes were weighted more heavily than studies with only a few specimens or subjects. Translating the weighted average $L_{0i}$ found for each

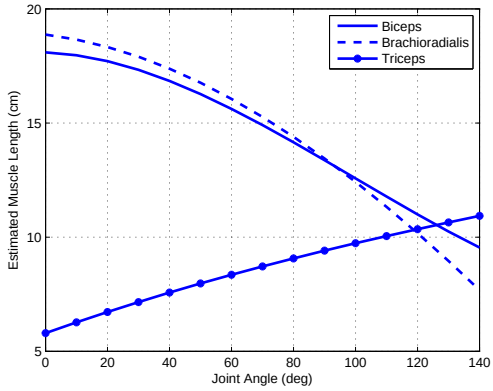


Figure 3.2: Estimated muscle length ($cm$) for the biceps brachii, brachioradialis and triceps brachii as a function of joint angle

muscle in Table A.3 using the muscle-length-to-joint-angle relationship presented in Figure 3.2, the optimal lengths would correspond to optimal joint angles ($\theta_0$) of 73.3°, 37.5° and 98.0° for the biceps brachii, brachioradialis and triceps brachii respectively. However, considering the range of $L_0$ values in Table A.3, the extreme minimum and maximum values of $L_0$ for each muscle give optimal joint angles ranging from 40° to 101° for the biceps brachii, 0° to 92° for the brachioradialis and 40° to 140° for the triceps brachii. To address the variability in values of $L_0$, we chose to calculate and test a wide range of potential $L_0$ representing a range of joint angles from 20° to 120° for each muscle. This range represents the range of comfortable functional range of motion for subjects positioned in the data collection apparatus.

The force-length relationship was previously introduced in Section 2.2.1 and an example is illustrated in Figure 2.6. The force-length curve is commonly depicted as a normalized force-length curve, where muscle force is normalized to the maximal isometric force and is therefore presented on a scale of 0-1. If muscle length is normalized with respect to $L_0$, the peak force will be achieved at a normalized muscle

Table 3.1: Estimated muscle length for the biceps brachii, brachioradialis and triceps brachii as a function of joint angle

| | **Muscle Length (*cm*)** | | |
|---|---|---|---|
| **Angle (deg)** | **Biceps** | **Brachioradialis** | **Triceps** |
| 0 | 18.1 | 18.9 | 5.8 |
| 10 | 18.0 | 18.7 | 6.1 |
| 20 | 17.7 | 18.3 | 6.4 |
| 30 | 17.3 | 17.9 | 6.7 |
| 40 | 16.8 | 17.4 | 7.0 |
| 50 | 16.3 | 16.8 | 7.3 |
| 60 | 15.6 | 16.1 | 7.7 |
| 70 | 14.9 | 15.3 | 8.0 |
| 80 | 14.2 | 14.4 | 8.4 |
| 90 | 13.4 | 13.4 | 8.8 |
| 100 | 12.6 | 12.4 | 9.2 |
| 110 | 11.8 | 11.3 | 9.6 |
| 120 | 11.0 | 10.2 | 10.0 |
| 130 | 10.2 | 9.0 | 10.5 |
| 140 | 9.5 | 7.7 | 11.0 |

length of 1. The normalized muscle length can also be given in terms of the difference in muscle length ($\Delta L_m$) from $L_0$, in which case the peak force will be achieved at a difference in muscle length of zero.

Here, we have adopted a force-length model presented in Cavallaro *et al.* [8] for the biceps brachii, brachioradialis and triceps brachii, where the normalized force-length curve is given with respect to $\Delta L_m$. The force-length curve is modeled as a Gaussian function as in equation 3.4:

$$f_{l_i} = \exp\left(-0.5\left(\frac{\frac{\Delta L_{mi}}{L_{0i}} - \varphi_m}{\varphi_v}\right)^2\right) \tag{3.4}$$

where the Gaussian fit parameters $\varphi_m$ and $\varphi_v$ represent the the mean and variance of the Gaussian distribution respectively. The choice of $\varphi_m$ is such that the force-length

model will have a maximum value at $\Delta L_m$=0. Values for $\varphi_v$ were optimized in [8] within the range $[0.1, 0.8]$.

The force-length relationship in equation 3.4 was modified so that the curve is a function of normalized muscle length by changing the numerator $(\Delta L_m/L_0)$ to $(L_m/L_0)$ and setting the value of $\varphi_m$ to 1. With respect to the value of $\varphi_v$, the range provided in [8] was quite wide. An example of the force-length curves generated using the entire range of $\varphi_v = [0.1 - 0.8]$ for the biceps brachii is presented in Figure 3.3.

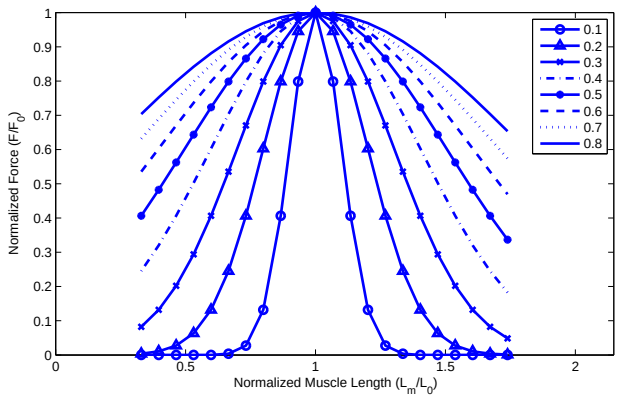


Figure 3.3: Example force-length curves from [8] for the biceps brachii for the full range of $\varphi_v = [0.1 - 0.8]$

Zajac [100] suggested that the magnitude of the force-length curve should be zero at muscle lengths of $0.5L_0$ and $1.5L_0$. Looking at the shape of the curves in 3.3, values of $\varphi_v = 0.1 - 0.3$ were selected visually as most compliant with this requirement. In addition, a value of $\varphi_v$=0.19 was given in a study by Rosen *et al.* [85], using the same model as presented in [8].

Force-length curves were generated using the relationship in Figure 3.1 for a range of optimal muscle lengths equivalent to joint angles of 20°-120° for each of the three muscles. Example curves generated for the biceps brachii with $L_0 = 17.7cm$ and

$11.0cm$ (equivalent to $\theta_0 = 20°$ and $120°$) are presented in Figure 3.4.

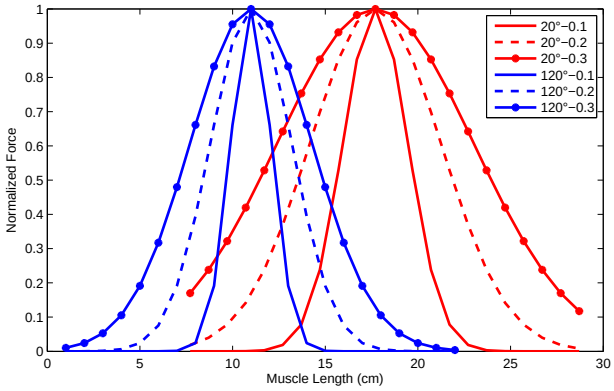


Figure 3.4: Example force-length curves for the biceps brachii with $L_{0i} = 17.7cm$ and $11.0cm$ or $\theta_{0i} = 20°$ and $120°$ and $\varphi_v = [0.1 - 0.3]$

The force-length curve is shifted along the x-axis for different $L_0$. Figure 3.4 shows complete curves over a total muscle length of $30cm$, depending on which muscle length was chosen as $L_0$. However, the length values for the biceps brachii calculated in Table 3.1 corresponding to a functional range of motion of $\theta = 0° - 140°$ suggested that the muscle length is a minimum at $9.5cm$ and a maximum at $18.1cm$. Therefore, we are forced to focus on a limited region of the force-length curve because of the limits on the functional range of motion. The left-side of Figure 3.5 provides example force-length curves for the biceps brachii, brachioradialis and triceps brachii with $L_{0i}$ which are equivalent to $\theta_{0i} = 20°$ and $120°$, over muscle lengths limited by the functional range of motion, $0° - 140°$.

While it is difficult to measure the length of a muscle *in vivo*, obtaining a direct measurement of elbow joint angle is very easy. Therefore, it is in our interest to re-define the force-length model from [8] in terms of joint angle rather than muscle length. By changing the force-length relationship in [8] into a function of $\theta$, the shape

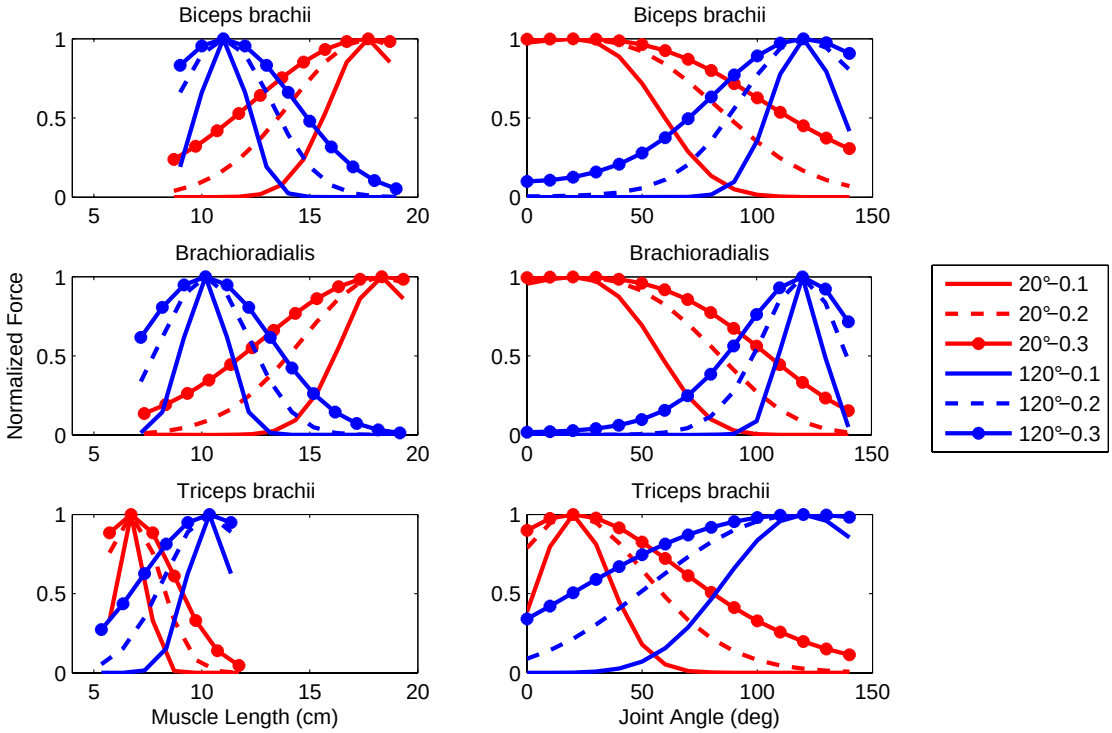


Figure 3.5: Example force-length and force-angle curves for the biceps brachii, brachioradialis and triceps brachii over the functional range of motion with $\theta_{0i} = 20°$ and $120°$ and $\varphi_v = [0.1 - 0.3]$. Figures on the left are given as a function of muscle length while figures on the right are given as a function of joint angle.

of the force-angle relationship can be defined as:

$$f_{l_i} = \exp\left(-0.5\left(\frac{\frac{\theta}{\theta_0} - \varphi_{mT}}{\varphi_{vT}}\right)^2\right) \tag{3.5}$$

The shape of the force-length curve changes when it is represented as a function of joint angle rather than as a function of muscle length, because the relationship between joint angle and muscle is non-linear. New values of the Gaussian fit parameter representing the width of the force-angle curve $\varphi_{vT}\ \epsilon\ [0.07 - 4.08]$ were required

to adequately represent the force-angle relationship. These values were calculated by minimizing the MSE between the new force-angle curves and original force-length curves expressed as a function of joint angle. Table 3.2 provides a summary of $\varphi_{vT}$. Example force-angle curves calculated using equation 3.5 for the biceps brachii, brachioradialis and triceps brachii with $\theta_{0i} = 20°$ and $120°$ are presented in the right-side of Figure 3.5. It should be noted that since $0°$ represents full extension, the biceps brachii and brachioradialis shorten with increasing joint angle.

Table 3.2: Values for $\varphi_{vT}$ calculated to estimate force-length curves as a function of joint angle to correspond with values of $\varphi_v = 0.1, 0.2, 0.3$ for the biceps brachii, brachioradialis and triceps brachii

| $\theta_0$ | $\varphi_{vT}$ | | | | | | | | |
|---|---|---|---|---|---|---|---|---|---|
| | **Biceps** $\varphi_v$ | | | **Brachioradialis** $\varphi_v$ | | | **Triceps** $\varphi_v$ | | |
| | **0.1** | **0.2** | **0.3** | **0.1** | **0.2** | **0.3** | **0.1** | **0.2** | **0.3** |
| 20 | 1.65 | 2.82 | 4.08 | 1.58 | 2.59 | 3.56 | 0.77 | 1.67 | 2.67 |
| 30 | 1.05 | 1.74 | 2.5 | 1.00 | 1.58 | 2.18 | 0.57 | 1.24 | 1.96 |
| 40 | 0.77 | 1.24 | 1.78 | 0.72 | 1.12 | 1.52 | 0.47 | 1.01 | 1.60 |
| 50 | 0.58 | 0.97 | 1.38 | 0.53 | 0.87 | 1.16 | 0.41 | 0.87 | 1.37 |
| 60 | 0.42 | 0.80 | 1.15 | 0.38 | 0.70 | 0.96 | 0.37 | 0.77 | 1.18 |
| 70 | 0.31 | 0.66 | 0.99 | 0.27 | 0.56 | 0.82 | 0.35 | 0.69 | 1.02 |
| 80 | 0.24 | 0.54 | 0.86 | 0.20 | 0.44 | 0.70 | 0.33 | 0.62 | 0.91 |
| 90 | 0.19 | 0.43 | 0.71 | 0.15 | 0.33 | 0.57 | 0.31 | 0.57 | 0.83 |
| 100 | 0.16 | 0.34 | 0.57 | 0.12 | 0.25 | 0.44 | 0.29 | 0.53 | 0.78 |
| 110 | 0.14 | 0.28 | 0.46 | 0.09 | 0.19 | 0.32 | 0.28 | 0.51 | 0.74 |
| 120 | 0.12 | 0.24 | 0.37 | 0.07 | 0.15 | 0.24 | 0.30 | 0.49 | 0.72 |

### Force-Velocity Relationship

The force-velocity relationship was assumed to be negligible in this study as all experiments were performed with isometric contractions. Therefore, the value of the force-velocity component of $F^{CE}$ was set equal to 1.

### 3.1.2 Parallel Elastic Element

The non-linear behaviour of $F^{PE}$ is often modeled as an exponential relationship. The following model for $F^{PE}$ was introduced in Cavallaro *et al.* [8]:

$$F^{PE} = \left(\frac{F^{PE}_{max}}{e^{s}-1}\right)\left(e^{((S/\Delta L_{PEmax})\Delta L_{PE})} - 1\right) \tag{3.6}$$

where $F^{PE}_{max}$ is the maximum force exerted by the PE for a maximum change in length $\Delta L_{PEmax}$, $S$ is a shape parameter defined in [8] that is related to the stiffness of the PE and $\Delta L_{PE}$ is the change in length of the PE as it is stretched beyond the tendon slack length.

Using this model, $F^{PE}$ curves were generated for the biceps brachii, brachioradialis and triceps brachii using values of $S = 0.9$ for each muscle [8]. $F^{PE}_{max}$ and $\Delta L_{PE}$ were defined in Cavallaro *et al.* [8] for each muscle as:

$$F^{PE}_{max} = 0.5F_0 \tag{3.7}$$

$$\Delta L_{PE} = L_{MTmax} - (L_0 + L_{Ts}) \tag{3.8}$$

where $L_{Ts}$ and $F_{0i}$ were approximated from literature values as reported in Tables A.2 and A.6 respectively, in Appendix A.

Each of the resulting $F^{PE}$ curves was approximated using a 2nd-order polynomial for computational simplicity, over a range of $L_{0i}$ equivalent to values of $\theta_{0i}$ spanning 20°-120° of flexion in 10 degree intervals, that is

$$F^{PE} = \begin{cases} A_i\theta_i^2 + B_i\theta_i + C_i & \forall \begin{cases} \theta_i < \theta_{0i} \;\; i{=}bi,\; brd \\ \theta_i > \theta_{0i} \;\; i{=}tri \end{cases} \\ 0 & \text{Otherwise} \end{cases}$$

The coefficients for each polynomial approximation were found using the polyfit function in MATLAB. The shapes of the parallel elastic curves for each of the muscles is provided in Figure 3.6.

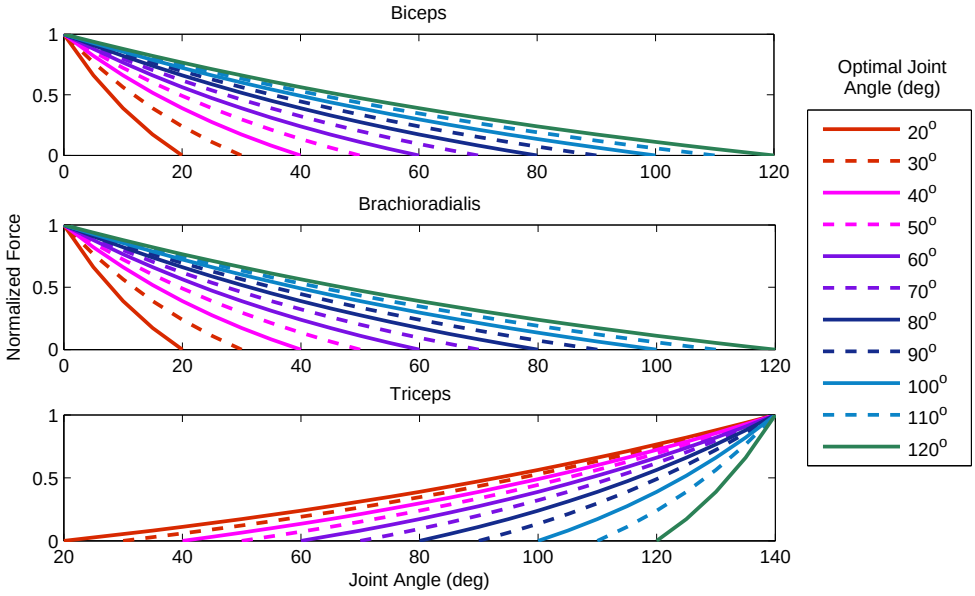


Figure 3.6: Example parallel elastic force curves as a function of joint angle for the biceps brachii, brachioradialis and triceps brachii calculated using varying $\theta_{0i}$

## 3.2 Model Generation using Fast Orthogonal Search (FOS) Method

As previously described, FOS is a nonlinear identification method that aims to generate the a sum of $M$ functions that are selected from a large pool of $N$ potential candidate functions ($N >> M$), to minimize the mean square error between the system output and the measured value. In this work, the set of candidate functions was based on the Hill muscle model in an attempt to create a more physiologically relevant FOS model representation. The new pool of $N$ candidate functions incorporates the Hill-based muscle model estimates for $F^{CE}$ and $F^{PE}$ previously described for the biceps brachii, brachioradialis and triceps brachii, into functions which represent the expression of each muscle's contribution to elbow moment at the wrist, that is

$$Candidate\ Functions = \begin{cases} F^{CE}(\theta_{0i}, \varphi_{vTi}) \cdot \frac{MA_i}{MA_{forearm}} = \frac{F_{0i} \cdot f_{li}(\theta_{0i}, \varphi_{vTi}) \cdot f_{vi}(\theta_{0i}) \cdot a_i(t) \cdot MA_i}{MA_{forearm}} \\ F^{PE}(\theta_{0i}) \cdot \frac{MA_i}{MA_{forearm}} = \frac{F^{PE}(\theta_{0i}) \cdot MA_i}{MA_{forearm}} \end{cases} \tag{3.9}$$

where $i$ represents the specific muscle, $MA_{forearm}$ is the measured length of the subject's forearm and $MA_i$ is the moment arm of muscle $i$. The parameter arguments in the parentheses denote the dependency of the corresponding function. For candidate functions used with isometric data, $f_{vi}$ is set equal to 1.

To take advantage of the ability of FOS to generate coefficients for each candidate function, constant terms in the $F^{CE}$ equations, $F_{0i}$ and $MA_{forearm}$, and in the $F^{PE}$ equations, $MA_{forearm}$, were set equal to 1. This allows FOS to choose values

which best represent the physiology of the specific subject. Values for the muscle moment arm $MA_i$ were calculated in two ways. As previously described in Section 2.4.2 a polynomial approximation from [57] can be used to represent the change in $MA_i$ (known as the Polynomial moment arm method or PMA). In addition, models were also developed for the case where muscle moment arms $MA_i$ in the $F^{CE}$ and $F^{PE}$ equations were set equal to 1 (known as the Constant moment arm method or CMA). While a polynomial moment arm is expected to better reflect the physiological nature of the muscle moment arm as it changes with joint angle, the applicability of the relationship to subjects with varying physiological make-up has not been tested. Therefore, using the CMA and allowing the FOS coefficient terms to adjust for this value may lead to more accurate force prediction.

In order to generate the $F^{CE}$ candidate functions for each muscle, nine optimal joint angles ($\theta_{0i} = 20°, 30°, \ldots, 120°$) were identified based on the range of values for $L_{0i}$ reported in the literature. The force-length component of the $F^{CE}$ equation depends on the value chosen for $\theta_{0i}$ as well as one of three Gaussian shape parameters ($\varphi_v = \varphi_{0.1}, \varphi_{0.2}, \varphi_{0.3}$). Therefore, 33 $F^{CE}$ functions were created for each of the three muscles, resulting in a total of 99 $F^{CE}$ functions included in the candidate pool. Similarly, $F^{PE}$ equations were generated for each of the 11 chosen values of $\theta_{0i}$, resulting in a total of 33 $F^{PE}$ equations. Therefore, the candidate pool included a total of $N$=132 functions. A summary of all candidate functions included in this pool is provided in Table C.1 in Appendix C.

Examples of candidate $F^{CE}$ and $F^{PE}$ equations for the biceps brachii, with an optimal joint angle of 60° and using a force-length curve with a Gaussian fit parameter $\varphi_v = \varphi_{0.1}$ are provided below:

$$F_{bi}^{CE}(\theta_0, \varphi_{vT}) = (f_{li}(60°, 0.42) \cdot a_{bi}(t)) \cdot MA_i \tag{3.10}$$

$$F_{bi}^{PE}(\theta_0) = \begin{cases} F^{PE}(60°) \cdot MA_i & \forall \theta_i < 60° \\ 0 & \text{Otherwise} \end{cases} \tag{3.11}$$

Models were generated with a pre-determined model size of 7 candidate functions for data from each subject based on findings from Mobasser *et al.* [70]. The FOS method is structured such that the first function selected by any model is assigned a value of 1, with a coefficient term to account for bias in the system. Following this first iteration, all subsequent functions are tested from the candidate pool, and the one which contributes the most error reduction to the model is selected. When a function is selected, it is removed from the candidate pool so that it will not be selected again for that particular model. In addition, the first function selected for a particular muscle is classified based on the value of $\theta_0$ used in its calculations. The optimal angle in that function is then defined as $\theta_0$ for that muscle for the entire model and the remaining pool of functions for that muscle is limited to only those functions with the same $\theta_0 \pm 10°$. For example, looking at the list of candidate functions in Table C.1, if a function from grouping "BI-5" (corresponding to an optimal joint angle of 60°) is the first candidate function selected for the biceps brachii, then for the remainder the model, only candidate functions from groupings "BI-4", "BI-5" and "BI-6" will be considered for selection. Since $F^{CE}$ is a function of the shape parameter of the force-length curve, $\varphi_{vT}$, more than one $F^{CE}$ function for each muscle (all with the limited range of $\theta_0$ and different values of $\varphi_{vT}$) may be included in each model.

# Chapter 4

# EMG Data Collection and Model Identification

## 4.1 Experiment Setup

### 4.1.1 1-DOF Experimental Testbed

Experiments were conducted on a 1-Degree-of-freedom (DOF) exoskeleton testbed that holds the shoulder and wrist of each subject in a fixed position, and constrains flexion and extension of the right arm to the horizontal plane as shown in Figure 4.1. The apparatus is composed of a platform supporting a Maxon DC motor, an 8:1 cable driven power system, and a pivoting aluminum bar to support the subject's forearm. Force at the wrist ($F_w$) is measured using an ATI 6-DOF Gamma force/torque sensor secured on the aluminum bar.

A subject's arm is positioned in the testbed such that the axis of rotation of the elbow is aligned with the pivot point of the aluminum bar. Therefore, the elbow

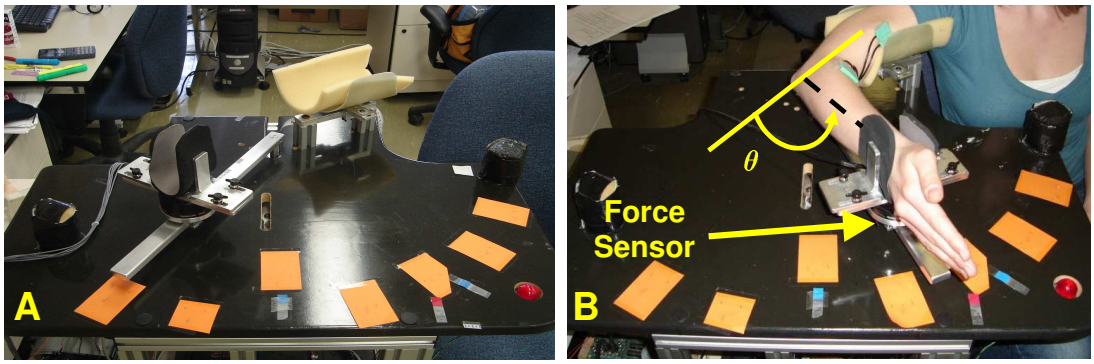


Figure 4.1: A: QARM (1-DOF Queen's University Arm) B: Subject positioned in the QARM

angle is equivalent to 1/8 of the motor angular position and can be measured using a resolver with a resolution of 0.0027°. Elbow angular velocity can be calculated by taking the derivative of the angle measurements within the data collection software. The subject is positioned such that the shoulder is stabilized at approximately 90° abduction, 15° horizontal adduction and full supination.

The computer used for data collection is equipped with a Quanser Wincon/ Venturcom RTX real-time control system. All programming is performed in MATLAB (v. R2006a) and system models are developed using Simulink. Data are collected at a sampling rate of 1kHz and saved individually as MATLAB files for offline processing and analysis.

### 4.1.2 EMG Collection and Processing

Surface EMG data from the biceps brachii, brachioradialis and triceps brachii muscles were collected from the right arm of 10 subjects (4 male, 6 female) with a mean age of 25. Subjects had no known neuromuscular deficits of the right arm. The experimental protocol has been approved by the Health Sciences Research Ethics Board, Queen's

University and subjects gave informed consent prior to participating in the study. Two Invenium Technologies active bipolar sEMG electrode units were placed adjacent to each other and secured over the belly of each of the three muscles. Electrode locations were measured with respect to anatomical landmarks such as the cubital fossa (on the anterior of the elbow joint of the arm) and the olecranon (bony structure located at the proximal end of the ulna) and recorded for each subject. These measurements were used to locate the EMG electrode placement over multiple sessions for 4 subjects (M2, M3, F1 and F2) in an attempt to minimize placement variability between sessions. An alternate method was used for the remaining 6 subjects (M1, M4, F3, F4, F5 and F6). In the alternate procedure, data were collected in either 2 or 3 sessions over a short time period (maximum 3 consecutive days) and the location of the electrode units were marked on the subject's skin with a pen after each session so that the electrode position was easily visible at the start of the next data collection session and placement was consistent across sessions. Average electrode positions across all 10 subjects were found to be $8cm$ proximal to the cubital fossa for the biceps brachii electrodes, $10cm$ proximal to the olecranon for the triceps brachii electrodes and $3.2cm$ distal to the cubital fossa and shifted $3cm$ in a lateral direction for the brachioradialis electrodes.

Recorded sEMG data were processed to obtain the linear envelope $e_i(t)$, for each muscle [70]. Specifically, the DC bias was measured and subtracted from the raw EMG data, and the resulting EMG data were rectified and smoothed using a moving average window with a window size of 400. This process is illustrated in Figure 4.2.

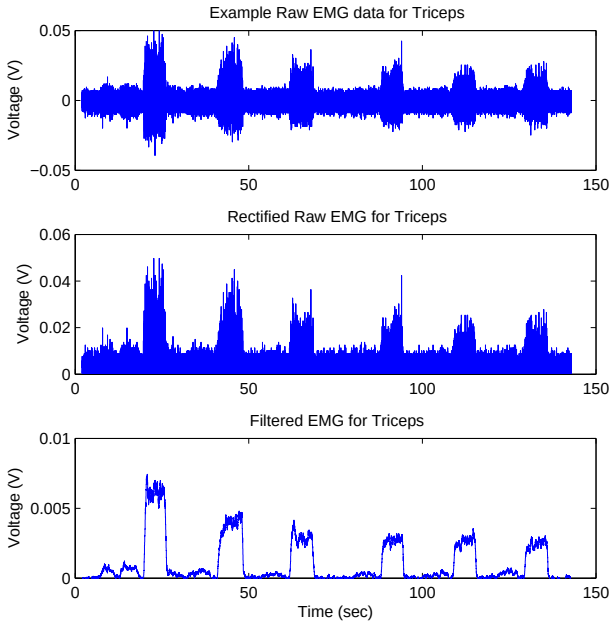


Figure 4.2: Stages of processing of EMG signal. Top: Raw EMG signal collected for the triceps brachii. Middle: Rectified raw EMG signal for the triceps brachii. Bottom: Filtered EMG for the triceps brachii

### 4.1.3 EMG Normalization

Many factors can influence the magnitude of a recorded EMG signal between subjects and data collection sessions. The purpose of normalizing the EMG is so that comparisons across data collection sessions and subjects can be made. Typically, normalization is performed using a maximum voluntary contraction (MVC), where the subject is asked to contract the relevant muscle isometrically as strongly as possible. The resulting recorded EMG signal level normalized to the MCV will lie between values of 0 and 1, where 1 represents MVC. This method has however been subject to scrutiny as it is difficult for individuals to actually achieve a maximum contraction level [18, 62, 89]. Thus, an alternate method was used in this study [21, 70].

With the subject positioned in the QARM experimental testbed, the motor generated a specific torque pattern at the elbow. The subject was instructed to resist the torque to maintain a constant position (isometric) contraction. This was done for both flexion and extension at the beginning of each experimental session. The torque applied by the motor was approximately $5Nm$, depending on the length of the subject's forearm, and the subject was positioned at 75° of elbow flexion. An example of the force pattern recorded during the normalization experiment is provided in Figure 4.3, where negative force measurement indicates extension and positive force indicates flexion. The normalization procedure included a step input from the motor with an elbow-applied torque of $2.5Nm$, followed by two ramped elbow-applied torque patterns with sustained torque of $2.5Nm$ and $5Nm$. The plateau region of the third ramp pattern ($5Nm$) was the segment of data that was ultimately used to normalize all corresponding EMG data, as the higher torque value was sufficient to recruit all muscles of interest, and the ramp pattern enabled the subject to steadily resist the torque with minimal reactive arm motion. An average of this EMG amplitude was calculated for each muscle and all subsequent processed EMG recordings collected in that session were divided by the average amplitude for each muscle.

The resulting normalized EMG signals for the two electrode units over the biceps brachii and triceps brachii were each averaged to obtain the mean normalized EMG signal for each muscle, and were used as the muscle activation term $a_i(t)$ in the $F^{CE}$ function equations (equation 2.5) for the biceps brachii and triceps brachii, respectively. The normalized EMG signal from only the medial of the two sensors placed over the brachioradialis was used as muscle activation $a_i(t)$ for the brachioradialis, because it was observed that the lateral brachioradialis sensor was recording EMG

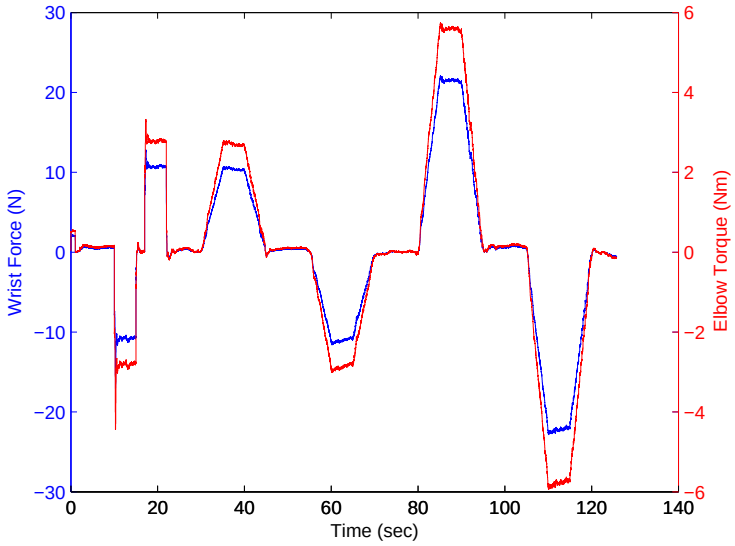


Figure 4.3: Wrist force pattern (solid) resulting from motor-applied torque signal (dashed) used to collect normalization data for the EMG signals

signals from an adjacent wrist extensor muscle (extensor carpi radialis). Further discussion of these observations is provided in Section 5.2.4.

### 4.1.4 Experiment Procedure

Ten subjects (4 males, 6 females) performed a series of twelve isometric contractions (six in flexion and six in extension) at six joint angles ranging from 30° to 105° of flexion in 15° intervals, taking full arm extension as an angle of 0°. This series of contractions was classified as one trial. During each contraction, the end of the rotating aluminum bar on the QARM was held in position by the experimenter, and the subject flexed or extended his/her arm against the wrist brace on the apparatus. Each session was comprised of 8 trials, with a target wrist force level of 10N in the first four trials and a target wrist force level of 20N for the remaining four trials.

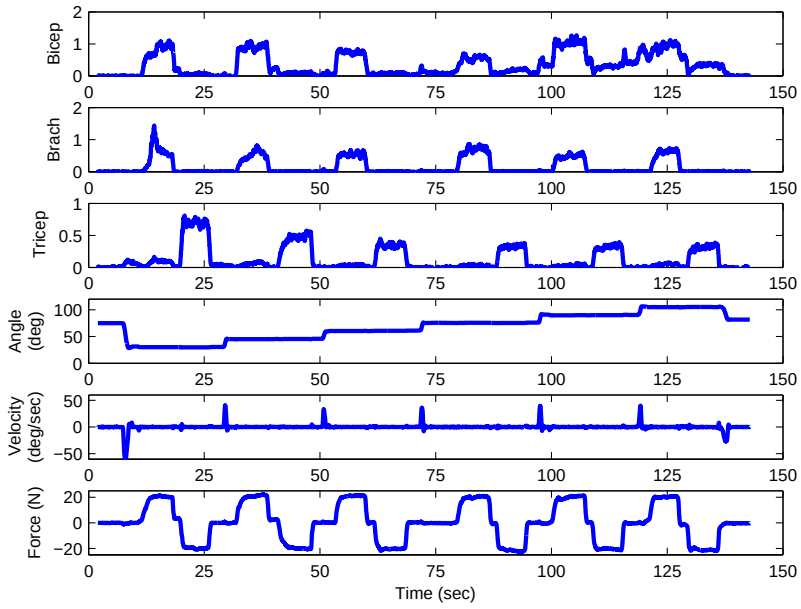


Figure 4.4: Typical isometric data collected during a 20N target force trial, with shoulder at 90° abduction and 15° horizontal adduction and the forearm in maximum supination

Visual wrist force feedback was provided to the subjects so they could generate the desired target wrist force. Two minutes of rest was enforced between trials to prevent muscle fatigue. Data were collected in two or three separate sessions on different days. An example of typical data collected from one subject (M3) with mean EMG signal amplitudes for each muscle at a target force level of 20N is shown in Figure 4.4.

Data were separated into two or three groups, depending on the number of sessions in which data were collected. A FOS model was generated for each of the 8 data sets in the session using the pool of candidate functions ($N = 132$) previously described. Models were evaluated using percent relative mean square error (%RMSE):

$$\%RMSE = \frac{\sum_{i=1}^{n}(F_{wi} - \hat{F_{wi}})^2}{\sum_{i=1}^{n} F_{wi}^2} \times 100 \tag{4.1}$$

where $F_{wi}$ is the measured force at the wrist and $\hat{F_{wi}}$ is the FOS model estimate of wrist force. Each model was then evaluated using the remaining 7 data sets collected in the same session. The estimation error associated with each of the 7 data sets as they were evaluated with a model was calculated using the equation above for %RMSE, and a mean evaluation %RMSE was found. This mean evaluation %RMSE value was used as an indication of the success of the model in its ability to predict $F_w$. For the 8 models generated from the 8 datasets collected in one session, an average of the mean evaluation %RMSE values ($RMSE_{AVE}$) for each of the 8 models in the session grouping was calculated and used as the primary value from which to evaluate the success of the models from that session. This procedure was repeated for each subject over 2 or 3 data collection sessions, resulting in up to 24 FOS models. An example of the models generated for data from one subject is provided in Appendix D.

### 4.1.5 Modifications to Experimental Procedure through Testing and Evaluation

The experimental procedure presented above was the result of changes and modifications made to testing conditions and analysis procedures throughout the course of this project. For justification of the main decisions that were made with respect to testing and analysis procedures see Appendix E.

Table 4.1: Evaluation %RMSE (Average) for models developed using one session of data for each subject, and with varying model sizes ranging from $M = 4$ to $M = 10$. A PMA was used in the candidate function equations.

| **Subject** | **Session** | **Evaluation %RMSE for Varying Model Size** | | | | | | |
|---|---|---|---|---|---|---|---|---|
| | | **M** | | | | | | |
| | | 4 | 5 | 6 | 7 | 8 | 9 | 10 |
| M1 | 4 | 11.26 | 10.72 | 9.63 | 8.88 | 8.66 | 8.53 | **8.31** |
| M2 | 2 | 13.83 | 11.38 | 11.38 | **11.05** | 11.14 | 11.21 | 11.19 |
| M3 | 2 | 8.72 | 8.45 | 7.00 | 6.40 | 6.09 | 5.62 | **5.46** |
| M4 | 1 | 12.87 | 12.25 | 10.86 | **10.51** | 10.61 | 11.06 | 11.73 |
| F1 | 1 | 11.50 | 10.72 | 11.09 | 11.34 | 11.28 | 10.99 | **10.65** |
| F2 | 2 | 13.14 | 11.44 | 11.02 | 10.62 | 10.17 | 9.69 | **9.57** |
| F3 | 1 | 8.35 | 8.04 | 7.45 | 7.33 | 7.30 | **7.08** | 7.15 |
| F4 | 3 | 8.64 | 8.54 | 8.53 | 8.62 | **8.52** | 8.60 | 8.65 |
| F5 | 2 | 4.48 | 4.53 | 4.43 | **4.40** | 4.55 | 4.67 | 4.73 |
| F6 | 3 | **8.01** | 8.73 | 8.73 | 8.77 | 8.55 | 8.73 | 8.85 |
| **Average** | | **10.08** | **9.48** | **9.12** | **8.79** | **8.69** | **8.62** | **8.63** |

### 4.1.6 Optimal Model Size

For this study, the number of functions to include in each FOS model was chosen to be 7. A preliminary analysis was performed on the evaluation %RMSE for models generated with varying models sizes from $M = 4$ to $M = 10$ to justify this decision. One session of data was selected for this analysis for each subject which demonstrated the low evaluation %RMSE. Results are summarized in Table 4.1, with the lowest %RMSE for each subject presented in bold. It appears that the optimal model size does change from subject to subject. Previous work by Mobasser *et al.* [70] stated that an optimal model size should be selected at either 7 or 10 functions, however on average, the difference in evaluation error observed in Table 4.1 between model sizes of 7 and 10 functions is small ($\sim 6\%$). However, there is a possibility that larger model sizes may cause the models to overfit the data.

Figure 4.5 provides an illustration of the evaluation %RMSE for all 10 subjects, with varying model size ranging from $M = 4$ to $M = 10$. Average %RMSE values

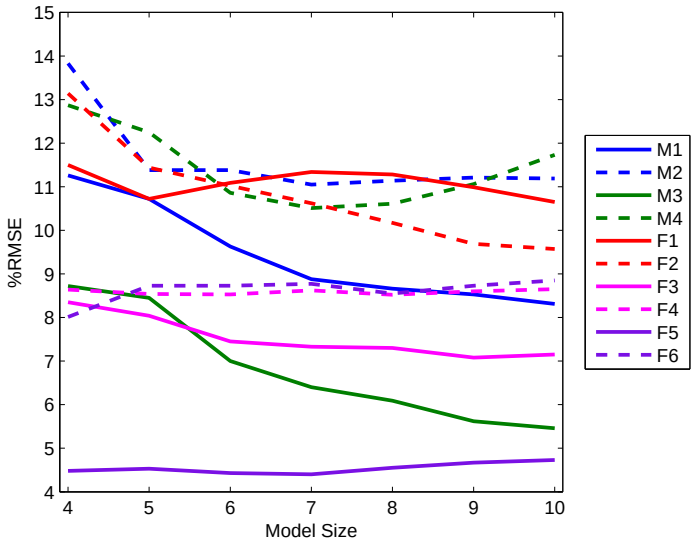


Figure 4.5: Evaluation %RMSE associated with varying model sizes for data from each subject

across all subjects for each model size are clearly higher for low model sizes, however average %RMSE values are quite consistent for models with size ranging from 7-10. Therefore, all models used for the following work were developed using 7 candidate functions to maintain consistency with [70].

## 4.2 Repeatability of Surface EMG

In order to evaluate the repeatability of EMG data collected for each subject across data collection sessions, statistical analysis of the variance in EMG amplitude was performed using a 2-way ANOVA. Mean normalized EMG amplitudes were calculated for each subject, during isometric contractions at each of the six joint angles measured in each trial. Mean normalized EMG amplitudes were grouped by the joint angle at which they were recorded. A 2-way ANOVA was performed on the normalized mean

EMG data at each angle for each muscle, with *data collection session* and *subject* as the two independent factors. A significance level of 0.05 was used. A summary of the results are provided in Table 4.2.

Table 4.2: Results of 2-way ANOVA examining the effect of subject and session on normalized EMG amplitudes recorded at specific joint angles

| **Muscle** | **Joint Angle (deg)** | **Force Level** (N) | **P-value** | | |
|---|---|---|---|---|---|
| | | | **Subject** | **Session** | **Interaction** |
| Biceps | 30 | 10 | $< 0.05$ | 0.947 | $< 0.05$ |
| | | 20 | $< 0.05$ | $< 0.05$ | $< 0.05$ |
| | 45 | 10 | $< 0.05$ | $< 0.05$ | $< 0.05$ |
| | | 20 | $< 0.05$ | $< 0.05$ | $< 0.05$ |
| | 60 | 10 | $< 0.05$ | 0.226 | $< 0.05$ |
| | | 20 | $< 0.05$ | $< 0.05$ | $< 0.05$ |
| | 75 | 10 | $< 0.05$ | 0.871 | $< 0.05$ |
| | | 20 | $< 0.05$ | 0.422 | $< 0.05$ |
| | 90 | 10 | $< 0.05$ | $< 0.05$ | $< 0.05$ |
| | | 20 | $< 0.05$ | 0.134 | $< 0.05$ |
| | 105 | 10 | $< 0.05$ | $< 0.05$ | $< 0.05$ |
| | | 20 | $< 0.05$ | $< 0.05$ | $< 0.05$ |
| Brachioradialis | 30 | 10 | $< 0.05$ | $< 0.05$ | $< 0.05$ |
| | | 20 | $< 0.05$ | 0.156 | 0.096 |
| | 45 | 10 | $< 0.05$ | $< 0.05$ | $< 0.05$ |
| | | 20 | $< 0.05$ | 0.097 | $< 0.05$ |
| | 60 | 10 | $< 0.05$ | $< 0.05$ | $< 0.05$ |
| | | 20 | 0.345 | 0.482 | $< 0.05$ |
| | 75 | 10 | $< 0.05$ | $< 0.05$ | $< 0.05$ |
| | | 20 | $< 0.05$ | 0.172 | $< 0.05$ |
| | 90 | 10 | $< 0.05$ | $< 0.05$ | $< 0.05$ |
| | | 20 | $< 0.05$ | 0.656 | 0.064 |
| | 105 | 10 | $< 0.05$ | $< 0.05$ | $< 0.05$ |
| | | 20 | $< 0.05$ | $< 0.05$ | $< 0.05$ |
| Triceps | 30 | 10 | $< 0.05$ | $< 0.05$ | $< 0.05$ |
| | | 20 | $< 0.05$ | $< 0.05$ | $< 0.05$ |
| | 45 | 10 | $< 0.05$ | $< 0.05$ | $< 0.05$ |
| | | 20 | $< 0.05$ | $< 0.05$ | $< 0.05$ |
| | 60 | 10 | $< 0.05$ | $< 0.05$ | $< 0.05$ |
| | | 20 | $< 0.05$ | $< 0.05$ | $< 0.05$ |
| | 75 | 10 | $< 0.05$ | $< 0.05$ | $< 0.05$ |
| | | 20 | $< 0.05$ | $< 0.05$ | $< 0.05$ |
| | 90 | 10 | $< 0.05$ | $< 0.05$ | $< 0.05$ |
| | | 20 | $< 0.05$ | $< 0.05$ | $< 0.05$ |
| | 105 | 10 | $< 0.05$ | $< 0.05$ | $< 0.05$ |
| | | 20 | $< 0.05$ | $< 0.05$ | $< 0.05$ |

It appears as though there is a consistent effect due to subject, and often an effect due to session in variability in the EMG amplitudes. This does not conclusively state that the EMG data is repeatable across sessions, and further analysis is required.

## 4.3 Force Estimation

As described in Section 3.2, FOS estimation models were developed using the Hill-based FOS candidate functions for each trial of each data collection session. These models were evaluated using average evaluation %RMSE ($RMSE_{AVE}$). A summary of the $RMSE_{AVE}$ calculated for all models developed with data from each session is provided in Tables 4.3 and 4.4. Also provided for each subject are the minimum mean evaluation %RMSE ($RMSE_{MIN}$), the standard deviation ($SD_{AVE}$) of the %RMSE across all 8 models in one session and a normalized version of the standard deviation ($SD_{NORM}$), which is calculated as:

$$SD_{NORM} = \frac{SD_{AVE}}{RMSE_{AVE}} \times 100 \tag{4.2}$$

The normalized standard deviation term is intended to provide context for the $SD_{AVE}$ term. Results are organized based on whether a PMA relationship or a CMA ($MA_i = 1$) were used in the FOS candidate functions.

Table 4.3: Evaluation %RMSE (Average and Minimum) and SD for models developed using candidate functions with a PMA

| **Subject** | **Session** | **Evaluation %RMSE and SD** | | | |
|---|---|---|---|---|---|
| | | **Polynomial Moment Arm** | | | |
| | | $RMSE_{AVE}$ | $RMSE_{MIN}$ | $SD_{AVE}$ | $SD_{NORM}$ |
| M1 | 1 | 8.88 | 5.71 | 4.85 | 54.6% |
| | 2 | 9.49 | 7.66 | 4.21 | 44.4% |
| | 3 | 11.0 | 7.62 | 7.19 | 65.4% |
| M2 | 1 | 11.07 | 8.60 | 6.85 | 61.9% |
| | 2 | 11.05 | 9.36 | 6.05 | 54.8% |
| M3 | 1 | 8.91 | 7.56 | 5.00 | 56.1% |
| | 2 | 6.40 | 5.57 | 2.41 | 37.7% |
| | 3 | 8.08 | 6.54 | 4.06 | 50.2% |
| M4 | 1 | 10.51 | 9.35 | 4.34 | 41.3% |
| | 2 | 20.58 | 18.22 | 11.30 | 54.9% |
| F1 | 1 | 11.34 | 8.54 | 5.20 | 45.9% |
| | 2 | 11.35 | 8.88 | 6.87 | 60.5% |
| F2 | 1 | 14.88 | 12.00 | 9.15 | 61.5% |
| | 2 | 10.62 | 8.56 | 6.47 | 60.9% |
| F3 | 1 | 7.33 | 6.18 | 2.91 | 39.7% |
| | 2 | 9.20 | 8.29 | 4.28 | 46.5% |
| | 3 | 14.86 | 13.93 | 6.24 | 42.0% |
| F4 | 1 | 12.15 | 9.00 | 7.65 | 63.0% |
| | 2 | 11.79 | 8.47 | 7.85 | 66.6% |
| | 3 | 8.62 | 7.16 | 4.69 | 54.4% |
| F5 | 1 | 10.33 | 7.53 | 8.11 | 78.5% |
| | 2 | 4.40 | 3.74 | 1.55 | 35.2% |
| | 3 | 5.56 | 4.86 | 2.15 | 38.7% |
| F6 | 1 | 9.87 | 7.27 | 6.64 | 67.3% |
| | 2 | 9.33 | 7.32 | 6.20 | 66.5% |
| | 3 | 8.77 | 6.69 | 4.45 | 50.7% |
| **Average** | | **10.25** | **8.25** | **5.64** | **53.8%** |

Table 4.4: Evaluation %RMSE (Average and Minimum) and SD for models developed using candidate functions with a CMA

| **Subject** | **Session** | **Evaluation %RMSE and SD** | | | |
|---|---|---|---|---|---|
| | | **Constant Moment Arm** | | | |
| | | $RMSE_{AVE}$ | $RMSE_{MIN}$ | $SD_{AVE}$ | $SD_{NORM}$ |
| M1 | 1 | 9.48 | 5.77 | 5.32 | 56.1% |
| | 2 | 9.04 | 8.38 | 3.91 | 43.3% |
| | 3 | 10.54 | 7.55 | 6.66 | 63.2% |
| M2 | 1 | 10.89 | 8.50 | 6.99 | 64.2% |
| | 2 | 12.18 | 9.63 | 7.04 | 57.8% |
| M3 | 1 | 8.05 | 6.99 | 4.51 | 56.0% |
| | 2 | 6.13 | 5.27 | 2.40 | 39.2% |
| | 3 | 8.91 | 7.11 | 4.36 | 48.9% |
| M4 | 1 | 9.91 | 8.79 | 4.20 | 42.4% |
| | 2 | 19.62 | 17.14 | 11.48 | 58.5% |
| F1 | 1 | 11.29 | 8.15 | 5.47 | 48.4% |
| | 2 | 10.68 | 8.80 | 6.10 | 57.1% |
| F2 | 1 | 16.21 | 13.04 | 9.69 | 59.8% |
| | 2 | 9.76 | 8.08 | 5.99 | 61.4% |
| F3 | 1 | 6.78 | 6.22 | 2.29 | 33.8% |
| | 2 | 8.47 | 7.67 | 3.99 | 47.1% |
| | 3 | 14.13 | 12.38 | 6.45 | 45.6% |
| F4 | 1 | 12.22 | 8.96 | 7.69 | 62.9% |
| | 2 | 11.85 | 8.17 | 7.86 | 66.3% |
| | 3 | 8.60 | 7.81 | 4.57 | 53.1% |
| F5 | 1 | 10.35 | 7.53 | 8.15 | 78.7% |
| | 2 | 4.61 | 3.79 | 1.69 | 36.7% |
| | 3 | 5.71 | 4.78 | 2.23 | 39.1% |
| F6 | 1 | 9.99 | 6.91 | 6.90 | 69.1% |
| | 2 | 9.54 | 7.20 | 6.51 | 68.2% |
| | 3 | 9.21 | 7.14 | 5.31 | 57.7% |
| **Average** | | **10.16** | **8.14** | **5.68** | **54.4%** |

The ability of the Hill-based FOS models to predict wrist force was consistent across subjects and sessions, with average %RMSE ranging between 4-21%. It appears that the PMA and CMA methods are equivalent, with slightly lower evaluation error found for models using a CMA. The standard deviations are quite high with respect to the mean values, as the normalized standard deviations ranged from 35-79% of the mean for the PMA method and from 34-79% of the mean for the CMA method.

### 4.3.1 Comparison of Muscle-Model-Based Candidate Functions using PMA and CMA

A number of factors may significantly affect the %RMSE results. In order to determine if the type of moment arm calculation is significant, a series of paired t-tests were run on individual subject data. Specifically, the evaluation %RMSE calculated for each model (one model for each data set) were compared when models were generated with a PMA and a CMA in the candidate functions. That means, for 1 subject who participated in 3 sessions of data collection, 24 models will be generated using each moment arm calculation method, and 24 paired comparisons will be performed between the evaluaion %RMSE values. The only stipulation with this method is that the data used must resemble a normal distribution and the variance of the two samples must be the same. Only one case revealed that the constant moment arm method generated significantly lower error ($p<0.05$). Results are summarized in Table 4.5.

Table 4.5: Results for paired t-test performed on %RMSE for each moment arm calculation method

| Subject | Normal Distribution | Equal Variance | p |
|---|---|---|---|
| M1 | no | – | – |
| M2 | yes | yes | 0.185 |
| M3 | yes | yes | 0.662 |
| M4 | yes | yes | 0.162 |
| F1 | yes | yes | 0.251 |
| F2 | yes | yes | 0.679 |
| F3 | yes | yes | <0.05 |
| F4 | yes | yes | 0.793 |
| F5 | no | – | – |
| F6 | yes | yes | 0.094 |

The %RMSE calculated for each subject using the PMA and CMA candidate functions was not significantly lower for one method over the other. Both methods

Table 4.6: Evaluation %RMSE (Average and Minimum) and SD for models developed using candidate functions presented in Mobasser *et al.* (2007) [70] with isometric data

| **Subject** | **Session** | **Evaluation %RMSE and SD** | | | |
|---|---|---|---|---|---|
| | | **Mobasser *et al.* Functions** | | | |
| | | $RMSE_{AVE}$ | $RMSE_{MIN}$ | $SD_{AVE}$ | $SD_{NORM}$ |
| M1 | 1 | 13.64 | 6.12 | 10.30 | 75.5% |
| | 2 | 11.80 | 8.25 | 7.63 | 64.7% |
| | 3 | 11.30 | 5.48 | 7.83 | 69.3% |
| M2 | 1 | 17.78 | 8.03 | 23.82 | 134.0% |
| | 2 | 13.90 | 6.03 | 10.72 | 77.1% |
| M3 | 1 | 8.27 | 7.03 | 4.74 | 57.3% |
| | 2 | 5.64 | 4.12 | 2.28 | 40.4% |
| | 3 | 7.99 | 6.11 | 3.69 | 46.2% |
| M4 | 1 | 8.74 | 7.76 | 2.92 | 33.4% |
| | 2 | 16.23 | 14.44 | 8.02 | 49.4% |
| F1 | 1 | 11.98 | 8.28 | 6.72 | 56.1% |
| | 2 | 14.93 | 7.26 | 12.38 | 82.9% |
| F2 | 1 | 15.78 | 14.32 | 10.86 | 68.8% |
| | 2 | 14.86 | 5.46 | 11.24 | 75.6% |
| F3 | 1 | 5.81 | 4.85 | 1.75 | 30.1% |
| | 2 | 7.41 | 4.90 | 3.27 | 44.1% |
| | 3 | 12.50 | 11.20 | 6.75 | 54.0% |
| F4 | 1 | 12.69 | 4.72 | 9.05 | 71.3% |
| | 2 | 23.60 | 4.07 | 22.25 | 94.3% |
| | 3 | 6.34 | 4.37 | 3.44 | 54.3% |
| F5 | 1 | 12.19 | 8.61 | 10.53 | 86.4% |
| | 2 | 5.17 | 3.52 | 1.94 | 37.5% |
| | 3 | 5.96 | 4.99 | 2.21 | 37.1% |
| F6 | 1 | 10.02 | 4.53 | 6.87 | 68.6% |
| | 2 | 7.09 | 5.41 | 4.14 | 58.4% |
| | 3 | 7.25 | 4.91 | 3.63 | 50.1% |
| **Average** | | **11.11** | **6.72** | **7.65** | **62.19%** |

were able to estimate wrist force with similar accuracy, even though the low standard deviations observed for the CMA method suggested that using a constant moment arm resulted in less variance in the results.

### 4.3.2 Comparison to Model Development using Non-Muscle-Model-Based Candidate Functions

FOS models with a size of $M = 7$ were developed using the non-muscle-model-based candidate functions of Mobasser *et al.* [70] for the isometric data collected in this

study from 10 subjects. The average and minimum %RMSE and standard deviation are presented in Table 4.6.

The evaluation %RMSE found for FOS models generated using the non-muscle-model-based candidate functions for isometric data ranged from 5-24%. The average standard deviation ranged from 2-22 and the normalized standard deviation ranged from 30-134%. To compare these results with evaluation results using the Hill-model-based functions, the difference in error between the methods was calculated for each dataset and each subject. Figure 4.6 presents the change in error between each Hill-based-method (PMA and CMA) and the non-model based method. Negative values indicate that the Hill-based method produced lower evaluation error than the non-muscle-based-model, while positive values indicate that the candidate functions from Mobasser *et al.* generate lower evaluation error. The percentage difference in error ($\%D$) is calculated with respect to the non-model-based error according to:

$$\%D_{PMA-Mobasser} = \frac{\%RMSE_{AVE_{PMA}} - \%RMSE_{AVE_{mobasser}}}{\%RMSE_{AVE_{mobasser}}} \tag{4.3}$$

$$\%D_{CMA-Mobasser} = \frac{\%RMSE_{AVE_{CMA}} - \%RMSE_{AVE_{mobasser}}}{\%RMSE_{AVE_{mobasser}}} \tag{4.4}$$

Details of the calculated values for %D are provided in Table F.1 in Appendix F. The average values for %D in error indicate that both Hill-based-muscle-models track the force more accurately than the non-muscle-based-models. Overall %RMSE was marginally lower for the Hill-based models over the non-muscle-based FOS models. This was true for both the PMA and CMA methods as shown in Figure 4.6.

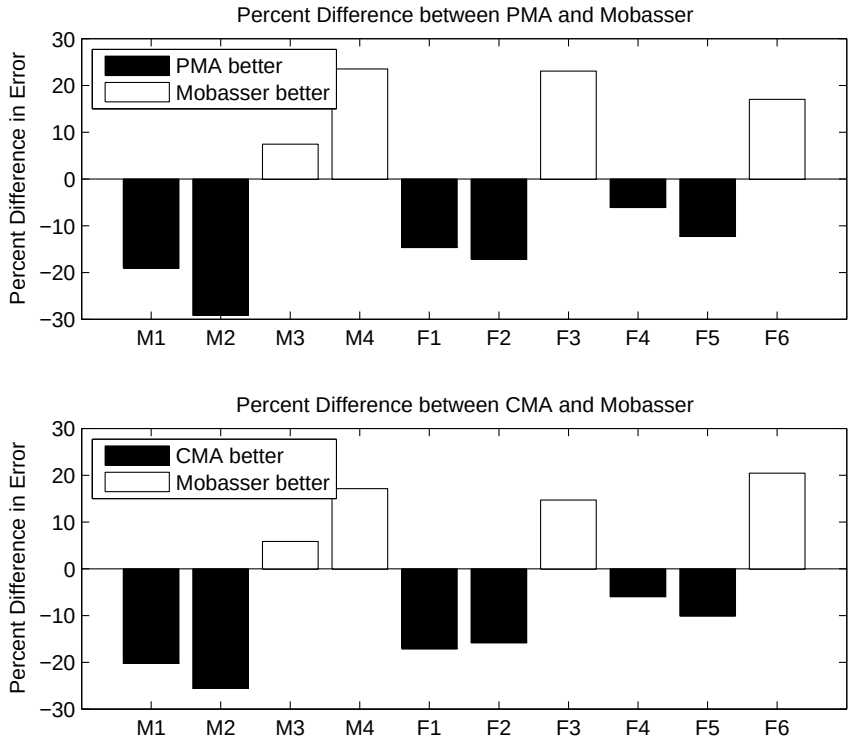


Figure 4.6: Percentage difference in model error between PMA and Mobasser et al. functions (Top) and between CMA and Mobasser *et al.* functions (Bottom). Results for each subject are given as averages across sessions.

## 4.4 Estimating Subject-Specific Hill Model Parameters

### 4.4.1 Frequency Analysis to Determine Optimal Joint Angle

It was observed in early model analysis that often the same candidate functions were repeatedly chosen in FOS models for the same subject. The decision to limit the optimal joint angles within the pool of candidate functions ($p_m$) to a range of $\pm 10^\circ$ from the $\theta_{0i}$ represented in the first candidate function selected for a muscle, where $i$ represents the biceps brachii, brachioradialis and triceps brachii, aimed to tailor models to better represent the natural optimal joint angle for the individual subject. Using the $\theta_{0i}$ represented in the candidate functions selected for all models developed for a particular subject, a frequency analysis was performed to assess the number of times a $\theta_{0i}$ was selected for each subject. A summary of the frequency of $\theta_{0i}$ selected for each muscle and each subject are provided in terms of percentage of the total number of functions chosen. This analysis was performed using models developed using the PMA and CMA methods and are provided in Figures 4.7 and 4.8, respectively.

A clear trend was observed in the functions selected for the triceps brachii. Using PMA, the majority of FOS models included $F^{CE}$ functions with $\theta_0$ ranging from $100^\circ$ to $120^\circ$ while this trend shifting to a range between $80^\circ$ and $100^\circ$ with CMA. Results for the biceps brachii were slightly more variable between subjects using PMA, but were quite consistent in the range of $60^\circ$ to $90^\circ$ with CMA. Similarly with the brachioradialis, there was greater variability between subjects in terms of $\theta_0$ for functions selected with PMA compared to CMA.

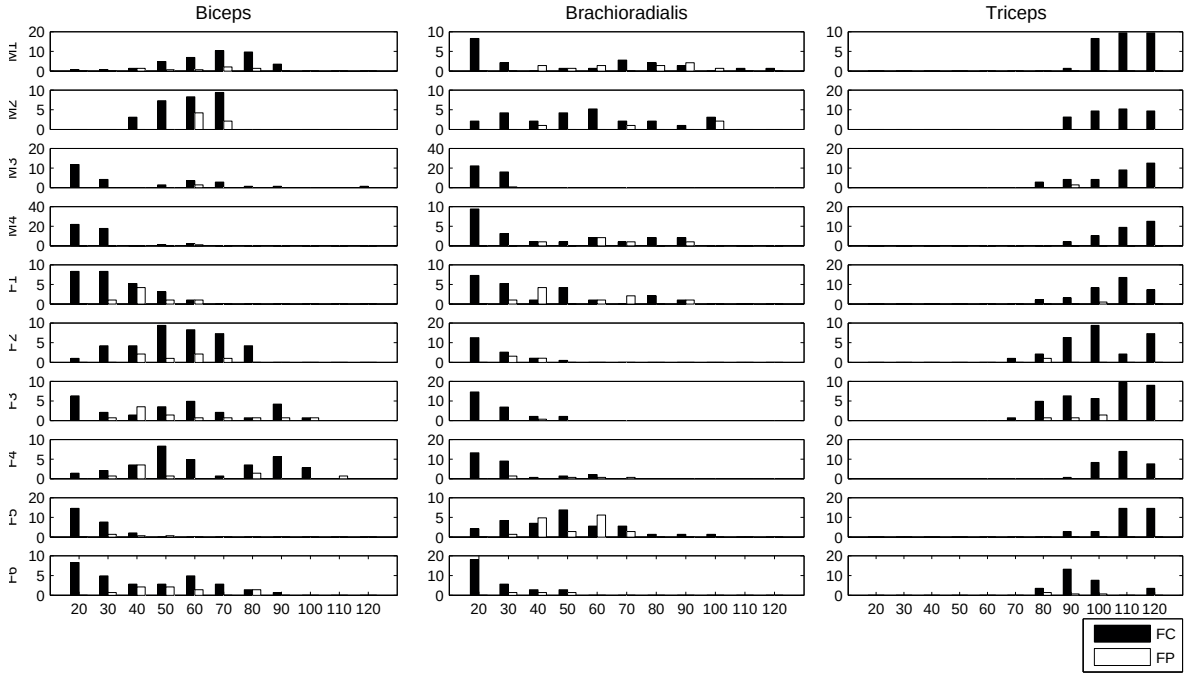


Figure 4.7: Frequency analysis of optimal joint angles selected in FOS models for all subjects via using a PMA in the candidate function calculations, given as a percentage of total functions chosen. note: scale is not consistent

Out of the 96-144 candidate functions that composed the 16-24 models for each subject (6 functions for each model), a weighted average ($\theta_{0wi}$) of the optimal joint angles identified in the functions was calculated, where $i$ represents the biceps brachii, brachioradialis and triceps brachii, to take into account the number of times particular $\theta_{0i}$ were included in the FOS models. The ($\theta_{0w}$) was calculated for each muscle for each subject to determine a value that will likely be more representative of the subject's true optimal joint angle. Statistical values including $\theta_{0w}$ and the standard deviation (SD) of $\theta_{0w}$ are included in Tables 4.7 and 4.8 for models incorporating a PMA and a CMA respectively.

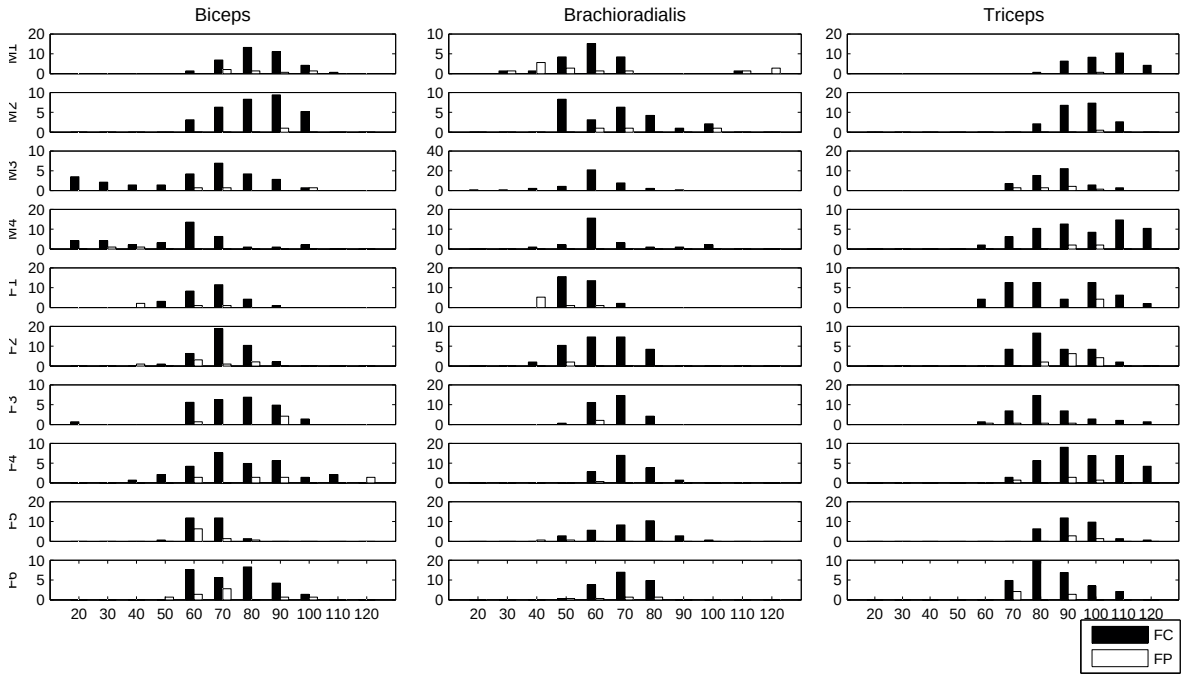


Figure 4.8: Frequency analysis of optimal joint angles selected in FOS models for all subjects via using a CMA in the candidate function calculations, given as a percentage of total functions chosen. note: scale is not consistent

### 4.4.2 Comparison of PMA and CMA Weighted Optimal Joint Angle

The weighted optimal joint angles provided in Tables 4.7 and 4.8 suggest a wide disparity between the joint angle functions selected in the PMA and CMA methods. The Mann-Whitney test was selected as an appropriate comparison of means rather than a paired t-test, because the distributions of joint angles for each subject was not normal, especially for the PMA method [42]. Table 4.9 illustrates the results of a Mann-Whitney test for independent samples, comparing the weighted optimal joint angle calculated using PMA and CMA. Looking at the results in Table 4.9, it is clear that there exists a significant difference in the $\theta_{0w}$ identified using the PMA and

Table 4.7: Weighted optimal joint angle $\theta_{0w}$ of biceps brachii, brachioradialis and triceps brachii from candidate functions using a PMA

| **Subject** | **Optimal Joint Angle (deg) (±SD)** | | |
|---|---|---|---|
| | **PMA** | | |
| | **Biceps** | **Brachioradialis** | **Triceps** |
| M1 | 66.6°(±15.4) | 55.1°(±31.9) | 110.0°(±8.7) |
| M2 | 59.4°(±9.7) | 60.0°(±25.6) | 106.5°(±10.7) |
| M3 | 41.3°(±25.4) | 24.3°(±5.0) | 106.7°(±15.4) |
| M4 | 27.6°(±11.0) | 46.5°(±25.4) | 111.1°(±9.5) |
| F1 | 34.7°(±11.9) | 44.0°(±22.1) | 105.9°(±11.0) |
| F2 | 54.9°(±15.3) | 27.6°(±8.8) | 100.4°(±14.5) |
| F3 | 53.6°(±24.5) | 27.1°(±9.6) | 102.0°(±14.4) |
| F4 | 61.2°(±23.5) | 30.9°(±14.1) | 109.3°(±7.9) |
| F5 | 26.2°(±7.8) | 50.2°(±16.9) | 111.8°(±9.0) |
| F6 | 45.0°(±20.3) | 28.3°(±10.8) | 94.5°(±11.3) |
| **Average** | 47.1°(±16.5) | 39.4°(±17.0) | 105.8°(±11.2) |

CMA methods for each muscle. Most comparisons between optimal joint angles for each subject and each muscle calculated using the PMA and CMA were significantly different, with only 4 cases out of 30 resulting in a p-value greater than 0.05.

Table 4.8: Weighted optimal joint angle $\theta_{0w}$ of biceps brachii, brachioradialis and triceps brachii from candidate functions using a CMA

| **Subject** | **Optimal Joint Angle (deg) (±SD)** | | |
|---|---|---|---|
| | **CMA** | | |
| | **Biceps** | **Brachioradialis** | **Triceps** |
| M1 | 83.1°(±11.0) | 61.3°(±21.9) | 103.6°(±10.4) |
| M2 | 82.5°(±12.2) | 68.1°(±16.4) | 95.7°(±8.7) |
| M3 | 61.9°(±23.1) | 60.2°(±11.7) | 86.1°(±10.2) |
| M4 | 54.5°(±21.0) | 64.8°(±14.2) | 96.1°(±17.2) |
| F1 | 65.2°(±11.5) | 53.5°(±7.9) | 87.5°(±16.7) |
| F2 | 70.5°(±9.9) | 62.8°(±11.4) | 86.7°(±11.1) |
| F3 | 75.4°(±15.0) | 66.8°(±7.3) | 83.4°(±13.7) |
| F4 | 78.2°(±18.3) | 71.4°(±8.1) | 96.6°(±14.1) |
| F5 | 64.9°(±6.5) | 71.1°(±13.0) | 92.9°(±8.9) |
| F6 | 74.2°(±12.7) | 70.0°(±8.4) | 84.8°(±11.7) |
| **Average** | 71.4°(±14.1) | 65.0°(±12.0) | 91.3°(±12.3) |

Table 4.9: Results for Mann-Whitney test for independent samples between weighted optimal joint angles calculated for each subject using PMA and CMA

| | **p-value** | | |
|---|---|---|---|
| **Subject** | **Biceps** | **Brachioradialis** | **Triceps** |
| M1 | <0.05 | 0.4085 | <0.05 |
| M2 | <0.05 | 0.1585 | <0.05 |
| M3 | <0.05 | <0.05 | <0.05 |
| M4 | <0.05 | <0.05 | 0.0864 |
| F1 | <0.05 | <0.05 | <0.05 |
| F2 | <0.05 | <0.05 | <0.05 |
| F3 | 0.1750 | <0.05 | <0.05 |
| F4 | <0.05 | <0.05 | <0.05 |
| F5 | <0.05 | <0.05 | <0.05 |
| F6 | <0.05 | <0.05 | <0.05 |

### 4.4.3 New FOS Model Development using PMA and CMA Weighted Optimal Joint Angle

Following the calculation of $\theta_{0w}$ for each muscle for each subject, a new pool of candidate functions for $F^{CE}$ and $F^{PE}$ using the new weighted value for optimal joint angle were generated using the methods outlined previously. Since the choice of optimal joint angle for each muscle was restricted to $\theta_{0w}$, additional options for the $F^{CE}$ functions were added to represent more variety in the shape of the force-length curve. Rather than using three values of the Gaussian fit parameter $\varphi_v$ as in previous function generation, two additional values of $\varphi_v = 0.15$, 0.25 were added to generate a total of 5 $F^{CE}$ functions for each muscle. The resulting five force-length curves for subject M3 are shown in Figure 4.9. Values of $\varphi_{vT}$, the fit parameter for force-angle curves, were calculated for for each weighted optimal joint angle and each subject, corresponding to values of $\varphi_v = 0.1$, 0.15, 0.2, 0.25 and 0.3 are provided in Table 4.10.

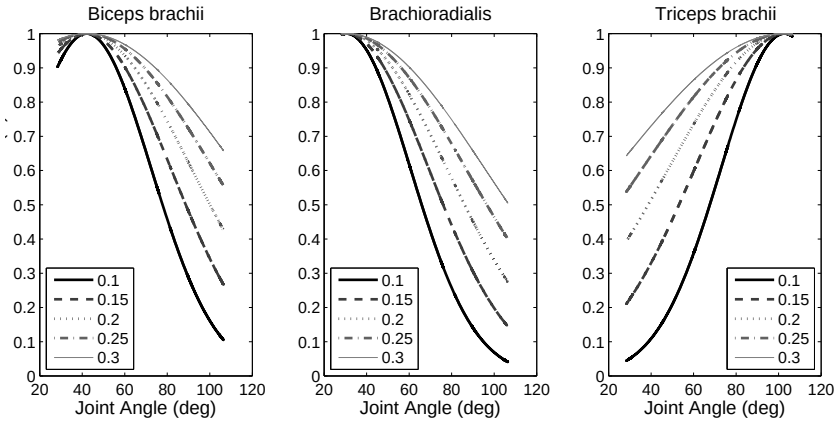


Figure 4.9: Example of varying shapes of force-length curves for each muscle using values of $\varphi_v = 0.1, 0.15, 0.2, 0.25$ and 0.3

Therefore, by using the 5 new $F^{CE}$ and 1 new $F^{PE}$ functions corresponding to $\theta_{0w}$ for each muscle, the total number of candidate functions ($N$) available in the candidate

Table 4.10: Values for $\varphi_{vT}$ for each subject calculated to estimate force-length curves as a function of weighted optimal joint angle to correspond with values of $\varphi_v = 0.1, 0.15, 0.2, 0.25$ and 0.3 for the biceps brachii, brachioradialis and triceps brachii

| **Muscle** | $\varphi_v$ | $\varphi_{vT}$ | | | | | | | | | |
|---|---|---|---|---|---|---|---|---|---|---|---|
| | | **Subject** | | | | | | | | | |
| | | M1 | M2 | M3 | M4 | F1 | F2 | F3 | F4 | F5 | F6 |
| Biceps | 0.1 | 0.34 | 0.43 | 0.74 | 1.14 | 0.89 | 0.50 | 0.52 | 0.40 | 1.21 | 0.67 |
| | 0.15 | 0.53 | 0.63 | 0.96 | 1.52 | 1.17 | 0.70 | 0.72 | 0.61 | 1.62 | 0.88 |
| | 0.2 | 0.70 | 0.81 | 1.19 | 1.92 | 1.46 | 0.88 | 0.90 | 0.78 | 2.05 | 1.09 |
| | 0.25 | 0.87 | 0.98 | 1.44 | 2.34 | 1.78 | 1.06 | 1.08 | 0.95 | 2.50 | 1.31 |
| | 0.3 | 1.04 | 1.15 | 1.71 | 2.79 | 2.11 | 1.24 | 1.27 | 1.12 | 2.94 | 1.55 |
| Brachioradialis | 0.1 | 0.45 | 0.38 | 1.26 | 0.60 | 0.64 | 1.10 | 1.11 | 0.96 | 0.53 | 1.06 |
| | 0.15 | 0.64 | 0.56 | 1.66 | 0.78 | 0.84 | 1.43 | 1.46 | 1.25 | 0.72 | 1.39 |
| | 0.2 | 0.77 | 0.70 | 2.05 | 0.94 | 1.00 | 1.75 | 1.79 | 1.53 | 0.86 | 1.70 |
| | 0.25 | 0.91 | 0.83 | 2.44 | 1.10 | 1.17 | 2.09 | 2.13 | 1.80 | 1.00 | 2.01 |
| | 0.3 | 1.04 | 0.96 | 2.81 | 1.27 | 1.35 | 2.41 | 2.47 | 2.10 | 1.16 | 2.34 |
| Triceps | 0.1 | 0.28 | 0.28 | 0.28 | 0.28 | 0.28 | 0.29 | 0.29 | 0.28 | 0.28 | 0.30 |
| | 0.15 | 0.40 | 0.40 | 0.40 | 0.39 | 0.40 | 0.42 | 0.41 | 0.40 | 0.39 | 0.43 |
| | 0.2 | 0.51 | 0.52 | 0.52 | 0.51 | 0.52 | 0.53 | 0.53 | 0.51 | 0.51 | 0.55 |
| | 0.25 | 0.63 | 0.64 | 0.64 | 0.62 | 0.64 | 0.65 | 0.65 | 0.63 | 0.62 | 0.68 |
| | 0.3 | 0.74 | 0.76 | 0.76 | 0.74 | 0.76 | 0.78 | 0.77 | 0.75 | 0.74 | 0.80 |

pool to be used for FOS model selection was equal to $N = 18$ for each subject. A summary of all candidate functions included in this pool of $N = 18$ functions is provided in Table C.2 in Appendix C. A summary of the average evaluation %RMSE ($RMSE_{AVE}$) over all models developed with data from each session and using a PMA and CMA is provided in Tables 4.11 and 4.12, respectively. Also provided are the minimum evaluation %RMSE ($RMSE_{MIN}$) and the standard deviation ($SD_{AVE}$) of the %RMSE across all 8 models from one session, for each subject. No appreciable improvement was observed in the evaluation %RMSE for FOS models developed using the $\theta_{0w}$-based candidate functions compared to the initial FOS model generation with the pool of candidate functions representing a range of $\theta_0$.

Using the functions selected in the FOS models when 5 choices of $\varphi_v$ were provided,

Table 4.11: Evaluation %RMSE (Average and Minimum) and SD for models developed using $\theta_{0w}$ for each muscle and each subject and using a PMA

| **Subject** | **Session** | **Evaluation %RMSE and SD** | | |
|---|---|---|---|---|
| | | **PMA** | | |
| | | $RMSE_{AVE}$ | $RMSE_{MIN}$ | $SD_{AVE}$ |
| M1 | 1 | 11.42 | 8.10 | 5.93 |
| | 2 | 11.01 | 9.05 | 4.83 |
| | 3 | 10.28 | 7.51 | 6.55 |
| M2 | 1 | 10.92 | 8.70 | 6.42 |
| | 2 | 11.52 | 9.20 | 6.26 |
| M3 | 1 | 8.80 | 7.06 | 5.31 |
| | 2 | 6.25 | 5.26 | 2.75 |
| | 3 | 7.83 | 6.93 | 3.04 |
| M4 | 1 | 10.44 | 9.26 | 3.13 |
| | 2 | 19.74 | 17.26 | 9.31 |
| F1 | 1 | 10.59 | 8.99 | 4.81 |
| | 2 | 10.63 | 9.59 | 6.07 |
| F2 | 1 | 15.44 | 12.55 | 9.29 |
| | 2 | 12.66 | 9.50 | 8.40 |
| F3 | 1 | 7.67 | 6.50 | 2.51 |
| | 2 | 8.71 | 7.47 | 3.73 |
| | 3 | 15.54 | 13.33 | 6.68 |
| F4 | 1 | 12.52 | 9.18 | 8.08 |
| | 2 | 11.53 | 8.84 | 7.57 |
| | 3 | 7.89 | 6.98 | 3.66 |
| F5 | 1 | 10.28 | 7.61 | 8.14 |
| | 2 | 4.33 | 3.85 | 1.58 |
| | 3 | 5.65 | 4.71 | 2.26 |
| F6 | 1 | 10.40 | 9.06 | 7.01 |
| | 2 | 9.56 | 8.58 | 6.06 |
| | 3 | 8.77 | 6.54 | 4.24 |
| **Average** | | **10.40** | **8.52** | **5.52** |

a weighted average value of $\varphi_v$ was calculated using a similar method described to calculate $RMSE_{MIN}$ and the standard deviation ($SD_{AVE}$) of the %RMSE across all 8 models in one session, for each subject. Using the functions selected in the FOS models when 5 choices of $\varphi_v$ were provided, a weighted average value of $\varphi_v$ was calculated using a similar method described to calculate $\theta_{0w}$. Table 4.13 provides these subject-specific Hill-model parameter values for each subject and each muscle.

The average evaluation error across all subjects for models developed using $\theta_{0w}$ in the $N = 18$ candidate functions increases slightly compared to the results for the $N = 132$ candidate functions, however, the average standard deviation is marginally

Table 4.12: Evaluation %RMSE (Average and Minimum) and SD for models developed using $\theta_{0w}$ for each muscle and each subject and using a CMA

| **Subject** | **Session** | **Evaluation %RMSE and SD** | | |
|---|---|---|---|---|
| | | **CMA** | | |
| | | $RMSE_{AVE}$ | $RMSE_{MIN}$ | $SD_{AVE}$ |
| M1 | 1 | 13.30 | 10.35 | 6.72 |
| | 2 | 13.26 | 10.56 | 5.38 |
| | 3 | 13.74 | 9.63 | 9.27 |
| M2 | 1 | 15.75 | 12.80 | 9.27 |
| | 2 | 13.77 | 11.59 | 7.04 |
| M3 | 1 | 8.25 | 7.02 | 4.87 |
| | 2 | 5.82 | 4.77 | 2.52 |
| | 3 | 7.80 | 6.85 | 3.49 |
| M4 | 1 | 9.86 | 8.92 | 3.78 |
| | 2 | 17.96 | 17.13 | 9.60 |
| F1 | 1 | 11.91 | 8.84 | 5.97 |
| | 2 | 10.69 | 9.40 | 6.18 |
| F2 | 1 | 16.16 | 13.62 | 9.43 |
| | 2 | 15.80 | 12.53 | 10.35 |
| F3 | 1 | 7.38 | 6.63 | 2.51 |
| | 2 | 8.31 | 7.71 | 3.52 |
| | 3 | 14.31 | 12.23 | 6.32 |
| F4 | 1 | 13.07 | 9.37 | 8.54 |
| | 2 | 12.83 | 9.24 | 8.83 |
| | 3 | 10.36 | 8.12 | 5.69 |
| F5 | 1 | 10.78 | 8.49 | 8.30 |
| | 2 | 4.78 | 4.09 | 1.62 |
| | 3 | 5.68 | 4.90 | 2.07 |
| F6 | 1 | 12.32 | 10.97 | 9.03 |
| | 2 | 11.89 | 10.37 | 8.68 |
| | 3 | 9.12 | 6.82 | 5.04 |
| **Average** | | **11.34** | **9.34** | **6.31** |

smaller. The fact that the FOS method can still develop models that can estimate wrist force with a similar accuracy when the pool of candidate functions is reduced to optimal values is promising. Perhaps the FOS method still requires some flexibility in terms of candidate function selection, in order to generate more accurate force estimation models.

Table 4.13: Weighted average values for $\varphi_{vT}$ calculated from the expanded force-length FOS models generated using PMA

| | $\varphi_{vT}$ | | |
|---|---|---|---|
| **Subject** | **Biceps** | **Brachioradialis** | **Triceps** |
| M1 | 0.72 | 0.78 | 0.50 |
| M2 | 0.92 | 0.82 | 0.64 |
| M3 | 1.17 | 2.45 | 0.60 |
| M4 | 2.06 | 1.06 | 0.49 |
| F1 | 1.78 | 1.08 | 0.60 |
| F2 | 0.85 | 1.95 | 0.59 |
| F3 | 0.91 | 1.89 | 0.57 |
| F4 | 0.76 | 1.76 | 0.50 |
| F5 | 2.35 | 0.91 | 0.59 |
| F6 | 1.24 | 1.87 | 0.60 |

## 4.5 Model and Parameter Evaluation

### 4.5.1 Inter-Session Reliability

Inter-session validation was performed by taking FOS models generated with data collected in Session 1 and evaluating the model with data collected in Session 2 (and Session 3 if applicable), and vice-versa. Visual inspection of the model accuracy suggests that using models and data from different sessions provides good wrist force estimation. An example illustrating the model generated from data collected from subject M3 in Session 2-Trial 4 evaluated with data collected in Session 3-Trial 5 is presented in Figure 4.10. It is clear that the model successfully tracks the sustained force during the isometric contractions as well as the low force intervals between isometric contractions. Similar results were observed for Session 3 models evaluated using data collected in Session 2. Table 4.14 provides a summary of the evaluation %RMSE and SD for models developed with data from subject M3 in Session 2 and evaluated with data from Session 3, and also %RMSE and SD for models trained with

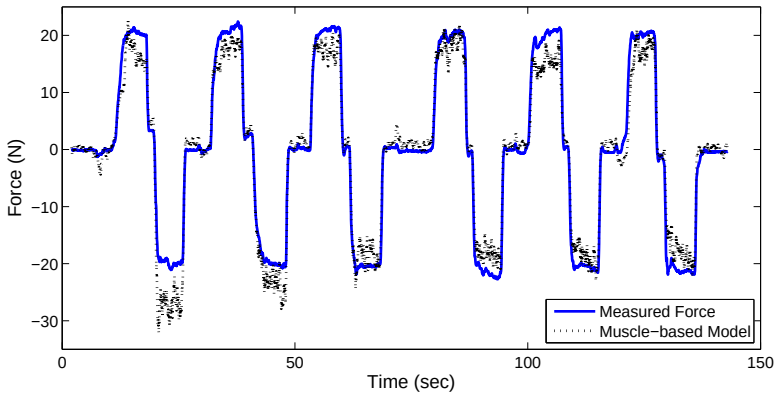


Figure 4.10: Example of inter-session validation for subject M3 using a FOS model generated and evaluated using data from different sessions

data from Session 3 and evaluated with data from Session 2. The evaluation %RMSE is consistent with the error observed when models were trained and evaluated with data collected in the same session (Table 4.7)

Table 4.14: Evaluation %RMSE (Average) and SD for PMA models developed using data collected from subject M3 in session 2 and evaluated with data collected in session 3, and vice versa

| **Model Training and Evaluation Condition** | | | |
|---|---|---|---|
| **Trained with S2, Evaluation with S3** | | **Trained with S3, Evaluation with S2** | |
| **Training Trial** | **%RMSE (SD)** | **Training Trial** | **%RMSE (SD)** |
| 1 | 11.00 (5.09) | 1 | 9.51 (2.80) |
| 2 | 10.09 (4.23) | 2 | 12.44 (5.10) |
| 3 | 8.39 (3.49) | 3 | 9.02 (2.69) |
| 4 | 10.28 (3.67) | 4 | 7.33 (1.78) |
| 5 | 12.12 (5.46) | 5 | 5.95 (1.72) |
| 6 | 9.66 (5.11) | 6 | 5.79 (2.23) |
| 7 | 9.42 (5.85) | 7 | 10.74 (4.50) |
| 8 | 8.82 (5.15) | 8 | 7.24 (2.66) |
| **Average** | **9.97 (4.76)** | **Average** | **8.50(2.93)** |

### 4.5.2 Evaluation of Triceps Optimal Joint Angle

In order to assess the weighted optimal joint angle identified for each subject, if the force or torque generated by an individual muscle at varying joint angles can be isolated, then a force-angle or torque-angle relationship for that muscle can be obtained. From such a relationship, a peak force or torque at a specific angle would suggest an optimal joint angle. It is difficult to isolate the activity of elbow flexors, because multiple muscles are involved in generating the net elbow flexion torque, however it is reasonable to assume that the triceps brachii is the major elbow extensor and activity in this muscle generates elbow extension torque.

In a separate data collection session, two subjects (M2 and M3) were asked to contract their triceps brachii to a target EMG level at each of the six angles used during the isometric testing (45°, 60°, 75°, 90° and 105°). The EMG level was identified during the normalization procedure, as the approximate magnitude observed in the 10N ramp force. The subject was provided with visual feedback of EMG magnitude to help him/her achieve a constant EMG level. The end of the QARM bar was restrained by the experimenter as the subject contracted his/her triceps brachii, and the resulting wrist force was measured. This procedure was repeated three times. The force measured during the experimental validation procedure for the triceps brachii as well as the normalized EMG level for the triceps brachii, biceps brachii and brachioradialis across the five joint angles for both subjects is provided in Figure 4.11.

The magnitude of the force measured at each joint angle increased slightly as the arm was placed in more flexed positions. This may suggest that the muscles are able to generate higher forces at higher joint angles because they are near the optimal joint angle on the force-angle curve, or this may be due to the effect of stretch in the

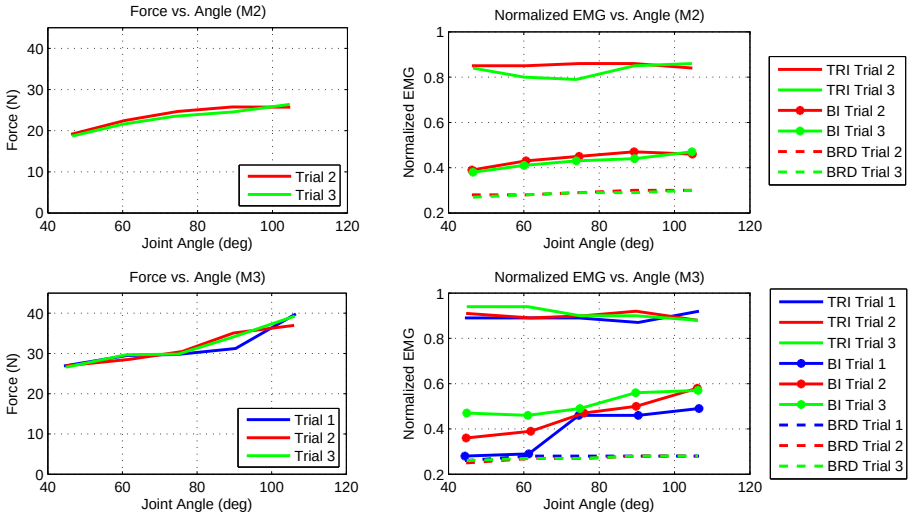


Figure 4.11: Triceps optimal joint angle validation results for subjects M2 and M3. Left: Force measured at varying joint angles for constant EMG signal. Right: Measured EMG signals for triceps brachii, biceps brachii and brachioradialis

parallel elastic components of the triceps brachii. A traditional force-length curve was not observed over this joint angle range, and it is difficult to validate the optimal joint angles predicted by the FOS models for these two subjects, which was approximately 106° for both subjects.

The subjects were instructed to contract only the triceps brachii, and keep the biceps brachii and brachioradialis relaxed during each trial. EMG activity from all three muscles were recorded to ensure that triceps activity remained constant through the various joint angles, and to assess how well the subjects were able to keep their elbow flexors relaxed. While the EMG level for the triceps brachii remained constant at each of the 5 joint angles, it is clear that co-contraction of the biceps brachii was present. It does not appear that this method is able to validate the weighted optimal joint angles identified for each subject.

# Chapter 5

# Discussion

## 5.1 Success of Hill-based Muscle Model in Predicting Wrist Force

Using the Hill-based candidate functions, FOS models were able to generate estimates of force at the wrist due to activity in the upper arm muscles with good accuracy. Average %RMSE ranged between 4-20% using the weighted optimal joint angles determined for each subject and demonstrated consistency across subjects and data collection sessions. This was a slight improvement over the non-muscle-model-based candidate functions proposed by Mobasser *et al.* in [70], which resulted in average %RMSE ranging from 5-24% for the same data sets across all 10 subjects.

The force estimation results obtained using the FOS models compare well to results presented in the literature. Koo and Mak [47] in their EMG driven musculoskeletal model reported root mean square (RMS) error between predicted and measured joint trajectories ranging from 10° to 35° which, for a joint range of 140° represents

error of 7-25%. Cavallaro *et al.* [8] reported average RMS errors in elbow torque estimation of $4.2Nm$ and $3.4Nm$ in elbow flexion and extension respectively. Assuming that the range of torque generated in their experiments was $20Nm$ (estimated from Figure 8a in [8]) this represents a range of 17-21% error. Liu *et al.* [63] using their neural network model to predict muscle force reported RMS errors ranging from 10-21% which they considered excellent.

The resulting FOS models were able to predict force at the wrist and demonstrated equivalent estimation error to models generated with EMG driven musculoskeletal models as well as multi-layer perceptron neural networks.

## 5.2 Simplifying Assumptions in Hill Muscle Model

Many assumptions were made in order to simplify the Hill-based muscle model candidate functions used in this study. These assumptions involve the types of equations used, physiological parameter values, the muscle length/joint angle relationships, and the range of parameter values (resolution) between the candidate functions. The candidate functions used in the FOS models were chosen from a finite pool of functions that included a wide range of optimal joint angles to represent variability in subject physiology. This is in contrast to other models that use optimization methods or other algorithms to fine tune parameter values to minimize model error [8, 48]. Some studies have shown that Hill-based models are sensitive to certain parameter values used in the models [78, 86]. In this work, while the range of choices of optimal joint angles and force-length curve shapes in the pool of FOS candidate functions is quite large, other parameters such as the maximal musculotendon length, tendon slack length and optimal muscle length used in the derivation of the muscle length/joint angle

relationship were estimated from literature values. As well, the joint angle/muscle moment arm relationship was based on one source, and may not directly take into account differences in subject size. Therefore, some error will be introduced by the simplifications and assumptions made in the development of Hill-based muscle model candidate functions, and will be discussed below.

### 5.2.1 Neglecting the Series Elastic Component

The force generated by the series elastic component ($F^{SE}$) was neglected in this study. As with the other components of Hill muscle models, the SE is not intended to directly represent physiological structures of muscle, however many researchers still refer to the SE as a representation of the elasticity of the muscle tissue and tendon. Zajac [100] suggests that the SE can be separated into elastic contribution of muscle ($SE_m$) and tendon ($SE_t$). The $SE_m$ is primarily attributed to the cross-bridge linkages in muscle, and is highly dependant on contraction dynamics of muscle, while the $SE_t$ can be considered to behave as an undamped spring [22]. Zajac suggests that energy stored in muscle cross-bridges is small compared to the energy that is stored in tendon, therefore, it is possible to neglect the contribution of the $SE_m$ [100]. It has been shown that for the muscles of the upper arm (biceps brachii, triceps brachii and brachialis) the stretch in the tendon is small, in the physiological operating range of these muscles, ranging between 4-10% of the optimal muscle length [28]. Therefore the tendon can be assumed to be infinitely stiff [80] and the SE unit can be neglected.

### 5.2.2 Effect of using a Symmetric Force-Length Curve

Traditional illustrations of the force-length relationship for individual muscle fibres rather than whole muscles, present a shape that is not symmetrical about the maximal isometric force. As shown in Figure 2.6, the slope of the ascending part of the curve is steeper than the descending part of the curve. A reduction in force at shorter sarcomere lengths is caused by a reduced overlap surface for actin and myosin filaments, however additional factors such as deformation of the myosin filaments and increased fluid and osmotic pressures may also hinder sarcomere force generation [84]. In the present work, the force-length curve was approximated using a Gaussian function, which is symmetrical about the optimal muscle length. Once the function was expressed as a function of joint angle rather than muscle length, the shape of the curve was no longer symmetric due to the non-linear relationship between muscle length and joint angle [57]. However, the original model that was approximated was based on a symmetric Gaussian function [8]. Many other researchers have used symmetric force-length relationships of Gaussian [36, 77] or parabolic [86, 98] shapes and it is assumed that the approximated shape of the force-length relationship is adequate for the purposes of this research.

### 5.2.3 Number of Muscles Included in FOS Candidate Functions

The decision to use only the biceps brachii and brachioradialis to describe elbow flexion in the FOS models, and not include muscle activation signals from the brachialis was necessary due to limitations in the data collection. Data collection was performed using surface EMG electrodes, and due to the position of the brachialis in the arm

it is difficult to isolate brachialis EMG signals without contaminating the signal with cross-talk from the biceps brachii. Typically, the brachialis is measured using needle electrodes rather than surface electrodes [25]. However, the goal of this research initially was to develop a model describing elbow motion, that could be implemented in a prosthetic limb, where surface EMG is the only realistic method for obtaining muscle activation.

### 5.2.4 Number of EMG Signals Used for Each Muscle

Two EMG sensors were positioned side-by-side over the belly of each muscle of interest in this study. The average of the processed EMG signals were used as input signals to the FOS model for the biceps brachii and the triceps brachii, however it was determined that the two EMG signals collected for the brachioradialis were not consistent. The brachioradialis functions as an elbow flexor, therefore it is expected that there should be higher activation in this muscle during elbow flexion. However observation of the brachioradialis signal from the lateral EMG sensor revealed a high level of signal recorded during elbow extension. Figure 5.1 illustrates this observation for subject M1.

It is apparent that there is not a large enough area on the skin surface on which two EMG sensors can be placed and obtain clean recordings from the brachioradialis. The forearm has many narrow muscles confined in a small space, and it is possible that the lateral EMG sensor that was meant to measure EMG signals from the brachioradialis, was accidentally picking up cross-talk from the extensor carpi radialis longus. Figure 5.2 shows the proximity of these two muscles.

### 5.2.5 Effect of Removing Force-Velocity Equation from the Isometric Model

The force-velocity component of $F^{CE}$ was set equal to 1 in the FOS model generation using isometric data. This was meant to simplify the calculations, however may not be entirely accurate as each subject was required to move their arm through intervals of approximately 15° to the correct position for each isometric contraction. A slight spike in arm angular velocity is visible in data sets such as in Figure 4.4 in between each isometric contraction. It was assumed that any contribution to force by the force-velocity component would be small and could be reasonably neglected in this work.

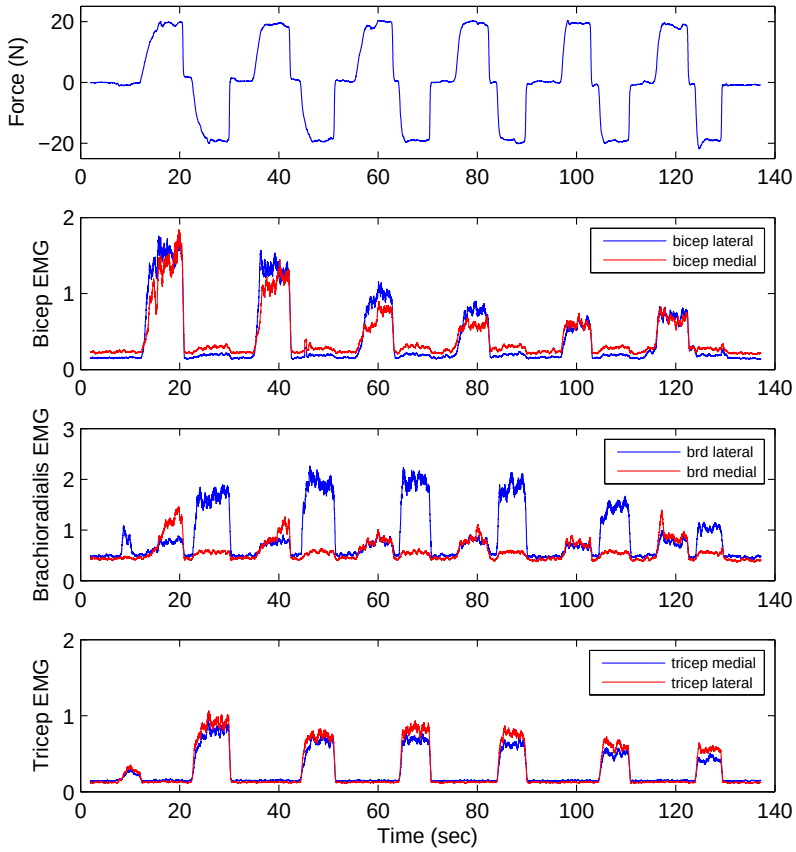


Figure 5.1: Example data for subject M1 illustrating discrepancies in the normalized EMG signal for both sensors measuring the brachioradialis activity. Recall positive force indicates a contraction in flexion while negative force indicates an extension contraction.

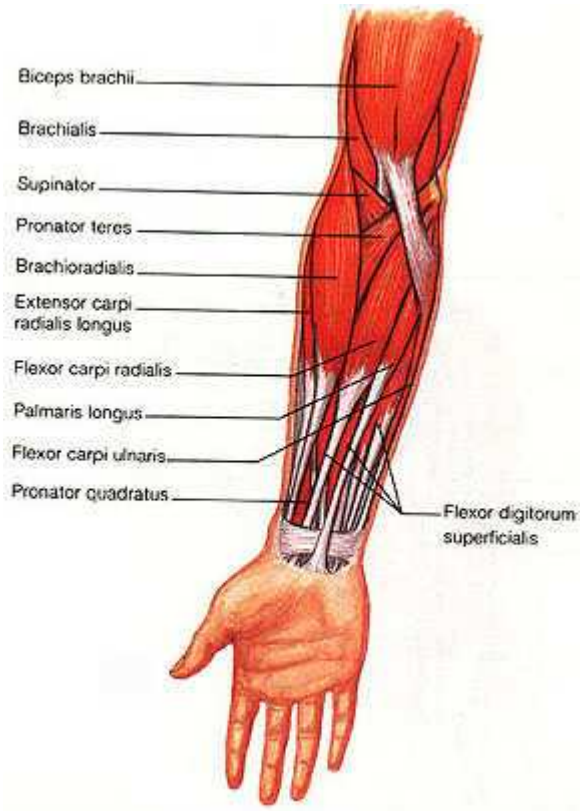


Figure 5.2: Illustration of the proximity of the brachioradialis to the extensor carpi radialis in the forearm [82]

## 5.3 Suggestions for Improvement to FOS Model Development

### 5.3.1 Optimal Model Size

The optimal model size of 7 candidate functions was chosen based on findings reported in [70] as well as preliminary studies suggesting that 7 functions was a good compromise between error reduction and over training of the model. Analysis of the isometric data collected in this study indicates that for some subjects, optimal FOS model size is shifted towards 9 or 10 candidate functions. In the future, it would be beneficial to determine the optimal FOS model size for each individual subject to further reduce %RMSE. Averaging the minimum %RMSE values in Table 4.1 results in an average value of 8.36%. Compared to the average error for a model size of 7 functions (8.79) selecting the optimal model size for each subject could offer an improvement in %RMSE of 5%. However, maintaining a constant model size for all subjects simplifies model generation and allows for comparison between subjects and data sets.

### 5.3.2 Modifications to QARM Equipment Set-up

Two important observations with respect to the QARM testbed were made during the data collection sessions. During isometric contractions, subjects aligned the aluminum forearm bar with marked angles and the experimenter held the end of the bar while the subject contracted in either flexion or extension. The subjects were given visual feedback of their force levels, therefore they adjusted their contractions to achieve the target force ($10N$ or $20N$). During these adjustments, the experimenter had to

accommodate for any slight changes in force by the subject and keep the end of the aluminum bar at a constant angle. This was very difficult, and some variability can be observed in the angle data for the isometric contractions. This situation may also have encouraged muscle co-activation of the subject's arm muscles, to increase stability of the arm during the isometric contractions. Therefore, it is suggested that a modification be made to the QARM testbed such that the forearm bar can be locked in position by a passive barrier during isometric contractions at various angles. One suggestion would be to drill holes in the platform so that pins could be inserted into the platform to hold the aluminum bar in place at a number of joint angles.

The second observation is that there was a relatively high level of noise in the sEMG data. The commercial sEMG sensors that were used in this study were part of the Myosens (Invenium Technologies) portable sEMG collection system. However, in this study, the sEMG sensors were integrated into the existing QARM data aquisition and processing system, so that collection of EMG signals and joint kinematic data was simultaneous. Therefore, two small test boxes were constructed. The sEMG sensors were plugged into the box which routed the EMG signals to a data acquisition board in the computer used for data collection. However, because the EMG cables were short in length, the test boxes were located in close proximity to a power supply, and some noise was introduced into the signal. If an additional shelf or platform were constructed to house the test boxes, sufficiently far away from the power supply, this would likely improve signal quality.

### 5.3.3 Datasets Used for FOS Model Training

In this study, datasets collected in each individual trial were used to train separate FOS models for each subject. This means that variability in candidate function selection between models is likely a direct result of small changes from one dataset to the next. This is especially true for models developed for the target force level of $10N$ compared to the target force level of $20N$. It is therefore suggested that alternate methods be used to generate FOS models that represent a wider selection of data collected from one subject. Two proposed methods are briefly outlined.

#### Data Segmentation

Data segmentation is a proposed method of combining small segments from each dataset collected in each trial, and arranging them together to form new training sets. As shown in Figure 5.3, data collected in each trial (Data 1, Data 2... Data 8) can be cropped into equal blocks and used to form new multi-trial training sets for the FOS method. Segments can be combined in order as in the figure, or the segments could be randomized, as long as only one segment is used from each data collection trial.

#### Data Concatenation

Data summation is a proposed method of combining entire datasets collected during each trial into one large training set. In this case, it will be necessary to down-sample the data due to the large number of data points collected in each trial. Currently, an average data set contains 140,000 to 180,000 data points. Prior to model development, the data is downsampled by 20, resulting in approximately 7000-9000 data points. By

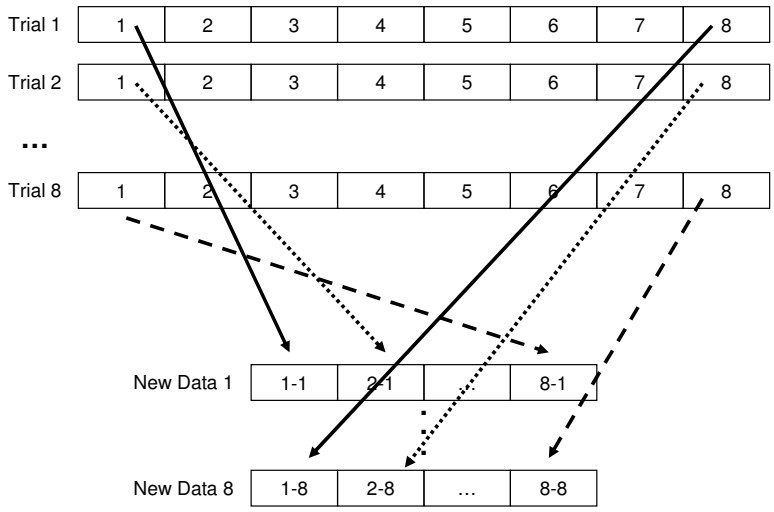


Figure 5.3: Proposed segmentation of data to create new FOS training sets

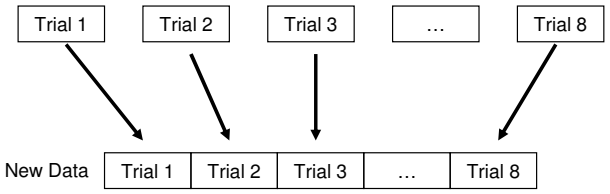


Figure 5.4: Proposed summation of data to create new FOS training sets

incorporating either segments of data from different trials, or entire datasets collected from different trials, in the FOS training dataset, the models which are generated may provide a more accurate and robust mapping between joint kinematic data, muscle activity, and resulting wrist force.

### 5.3.4 Incorporating Dynamic Motion

Previous work by Mobasser *et al.* [70] had good success using dynamic datasets to train FOS models to predict wrist force during dynamic flexion and extension of the

elbow. In the current work, only isometric data was used to develop FOS models. It is therefore suggested that Hill-based candidate functions be used in FOS models to predict dynamic motion.

### 5.3.5 Investigating the Movement of Muscle Bulk under Skin Surface over Range of Joint Angles

It was suggested that some of the change in EMG magnitude that was observed in isometric contractions at different joint angles, results from the muscle bulk shifting under the skin (and hence beneath the sEMG electrodes) rather than being a function solely of the force-length properties of the muscle. One method which can be adopted in the future to assess the effect of muscle movement under the skin during elbow flexion would be to utilize a linear array of sensors rather than individual sEMG sensors [69]. As the muscle bulk moves beneath the skin surface, the sEMG signal can be measured from various electrodes to ensure that an optimal signal is obtained.

It may also be helpful to normalize the data at each joint angle using EMG data collected during a normalization contraction (either motor-applied torque or a maximum voluntary contraction) for each joint angle. This may help to reduce the effects of the muscle bulk moving beneath the skin, and the location of the EMG sensors with respect to the innervation zone as the muscle moves.

### 5.3.6 Submaximal Activation of Muscle During Experiments

It has been reported that the traditional force-length relationship for muscle is applicable for maximal isometric contractions only, and that submaximal contractions demonstrate a force-length curve that is shifted towards longer muscle lengths. In

other words, a traditional force-length curve created using maximum voluntary contractions may demonstrate a peak force at 90°, while a force-length curve generated using submaximal contractions may suggest a peak force generation ranging from 45-75° [35, 84]. The isometric studies performed in this work were at $10N$ and $20N$ of wrist force, therefore it may be true that optimal joint angles identified for data collected at the different force levels may be different and it would be beneficial to identify optimal joint angles for each subject at a variety of activation levels. Further investigation may be warranted to assess if there is a difference in optimal joint angles identified using data with isometric contractions in excess of $20N$.

## 5.4 Validation of Optimal Joint Angle

### 5.4.1 Preliminary Validation for the Triceps Brachii

Experimental methods were used to try and validate the optimal joint angle identified for the triceps brachii muscle for 2 subjects. As described previously, subjects contracted their triceps muscles to a target EMG level and the resulting force at the wrist was measured and plotted (see Figure 4.11). It is expected that since the triceps brachii is the primary elbow extensor, the contribution of this muscle to the net extension torque about the elbow should be close to 100%. Therefore, recalling the traditional force-length curve it is expected that the plot of extension force vs. joint angle should peak near to the estimated optimal joint angle for each subject ($\sim 106°$ for PMA models and $\sim 90°$ for CMA models for both subject M2 and M3). The plots in Figure 4.11 do reveal an increasing force measurement with joint angle, however due to the limitations in the range of motion of the device (subjects find it difficult

to flex their arms much beyond 110°) it is unknown whether the curve would begin to fall at higher joint angles, or the extent that $F^{PE}$ of the triceps brachii may be contributing to wrist force.

It is important to note that the measured wrist force may not directly represent the full extension torque about the elbow in this experiment, as there is some activity observed in the biceps brachii, particularly for subject M2 at angles greater than 75°. This activity suggests that co-contraction of the muscles about the elbow may be occurring to increase stability of the arm. Any flexion torque about the elbow due to contraction of the biceps brachii will reduce the net extension torque, and thus reduce the force measured at the wrist.

### 5.4.2 Literature Data

The weighted optimal joint angles found for each subject can be compared to values from the literature summarized in Table 2.1. Figure 5.5 illustrates the range of optimal joint angles for the biceps brachii, brachioradialis and triceps brachii from the literature as well as the calculated weighted optimal joint angles using both the PMA and CMA methods.

For the biceps brachii and brachioradialis, the calculated weighted optimal joint angle values lie within the range of the literature values, as the published optimal joint angles for the elbow flexors have a wide range. The calculated weighted optimal joint angles for the triceps brachii are slightly higher than literature values, however the average value from the CMA method is more similar to the average literature value.

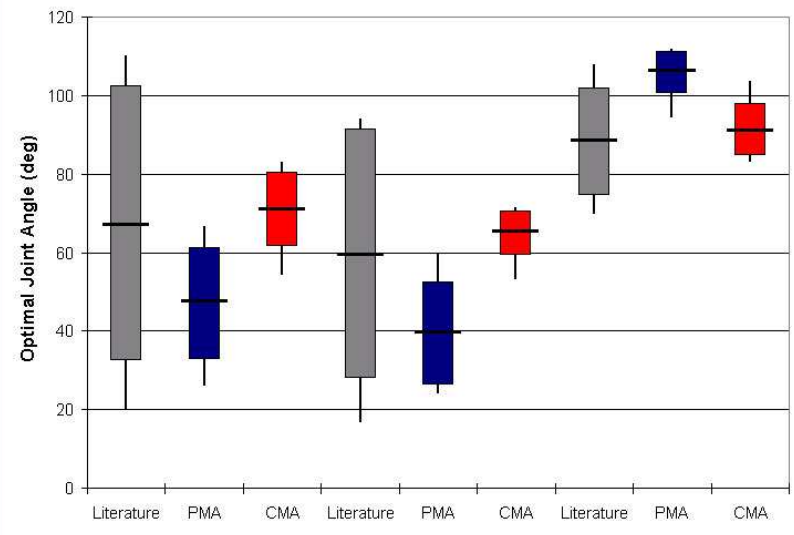


Figure 5.5: Summary of optimal joint angles for the biceps brachii, brachioradialis and triceps brachii provided in literature and calculated using the PMA and CMA FOS models. The horizontal black line is the mean value, the grey bar represents one standard deviation from the mean, and the vertical black lines show the minimum and maximum values

### 5.4.3 Imaging Methods

Optimal joint angle values could be validated for each subject using imaging methods. Using an equation from [26], Li *et al.* [58] estimated the optimal muscle fascicle length of the biceps brachii and brachioradialis using two ultrasound images (one on the anterior part of the upper arm, $2cm$ proximal to the elbow joint, and the second on the lateral part of the forearm, $1cm$ distal to the elbow), respectively, taken at multiple joint angle positions. The following equation was used to estimate the optimal muscle fibre length $\hat{L}_{0i}$:

$$\hat{L}_{0i} = L_f + \frac{MT_1}{sin\alpha} + \frac{MT_2}{sin\alpha} \tag{5.1}$$

where $L_f$ is the visible part of the muscle fascicle in the ultrasound image, $MT_1$

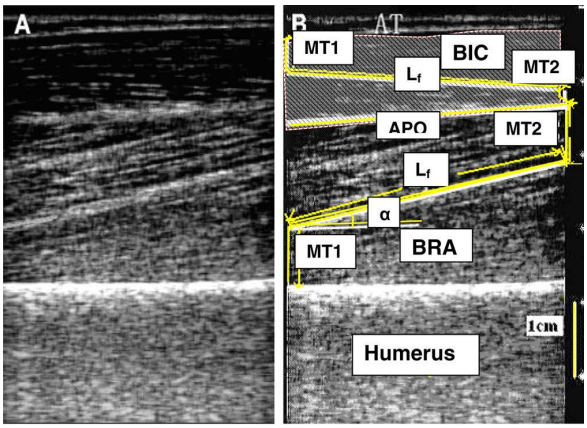


Figure 5.6: A) Original ultrasound image of the biceps and brachialis from [58]. B) Image with appropriate labels for equation 5.1. The upper shaded area (BIC) is the biceps while the lower area (BRA) is the brachialis; these two muscles are separated by an aponeurosis (APO); $L_f$ is the visible part of the muscle fascicle that can be measured; $MT_1$ is the distance of the fibre distal end point to the superficial aponerurosis; $MT_2$ is the distance of the fibre proximal end to the bone; $\alpha$ is the pennation angle

is the distance from fibre distal end point to the superficial aponeurosis, $MT_2$ is distance from the fibre proximal end to the bone and $\alpha$ is the pennation angle of the muscle [26]. Figure 5.6 provides an example ultrasound image from the anterior upper arm, and shows the measurements which can be incorporated into equation 5.1 [58]. The resulting $\hat{L}_{0i}$ can then be converted back into joint angle. Li *et al.* used the ultrasound method to estimate the optimal muscle length for arm flexors, using optimal joint angles published in [48]. They then used these estimated muscle length values in the biomechanical model in [48] to solve for musculotendon length and muscle moment arm. It is interesting to note that Li *et al.* commented that the trigonometric approximation provided in Equation 5.1 might not be accurate for the elbow flexors at joint angles $> 80°$ because the muscle fascicles become curved when the muscle is contracted to this degree.

## 5.5 Benefits of Using a Physiologically Relevant Model

While many methods exist for the estimation of muscle forces or joint torques using EMG data (a brief summary was provided in Section 2.6), few provide an opportunity to tailor the model to take into account subject size or physiology.

### 5.5.1 Subject Specific Muscle Parameters

It has been shown that muscle physiological parameters measured from cadaver specimens may not reflect true physiological parameters of the individual's live tissue, due to the effects of rigor mortis and chemicals used to preserve specimens [66]. As well, while imaging methods are a proposed option for estimating muscle physiological parameters of a living person, access to such equipment may be hindered by high expense, or by availability of the equipment and individuals trained to operate the equipment and interpret results. Finally, while EMG-driven models can identify subject-specific parameters using an optimization procedure, the proposed FOS method offers a more computationally efficient method of estimating these parameters. The ability of the FOS method to identify subject-specific Hill-muscle parameters has a wide range of applications in neuromuscular modelling. Modifications to the candidate functions used in the FOS method or further analysis of the coefficient values may provide information about additional physiological parameters. While the values estimated in this study (optimal joint angle and $\varphi_{vT}$) need to be validated, the results of this preliminary work suggest that this method could be useful for elucidating *in vivo* muscle characteristics.

### 5.5.2 Use of a Constant Muscle Moment Arm vs. Polynomial Relationship

Force generation in upper arm muscles and their contribution to joint torque about the elbow is dependant on the length of the muscle moment arm, and the length of the moment arm changes as a function of joint angle. The use of the PMA relationship from Lemay and Crago [57] in the Hill-based FOS candidate functions attempted to reflect this fact. It was assumed that the coefficient generation within the FOS method would adjust for any deviation from this polynomial relationship for individual subjects. When a constant value is substituted for this polynomial moment arm relationship, the ability of the FOS method to accurately predict force at the wrist does not change significantly. Therefore, it was assumed that the coefficient values in the FOS method can adequately account for an average moment arm value, and the error associated with neglecting the change in moment arm with joint angle is overcome by the ability to tailor the average moment arm to each subject.

The two different moment arm methods did have an impact on the candidate functions which were chosen in the FOS models, and in turn the values calculated for the weighted optimal joint angle for each subject. Weighted optimal joint angles calculated for the biceps brachii and brachioradialis are on average, 25° lower when the PMA method is used in the FOS candidate functions. For the triceps brachii, use of the PMA results in weighted optimal joint angles that are higher by approximately 15° compared to model development using the CMA. Figure 5.7 shows the force-length curves for the three muscles for a single subject over a range of joint angles. The curves have been multiplied by the polynomial moment arm relationship or simply

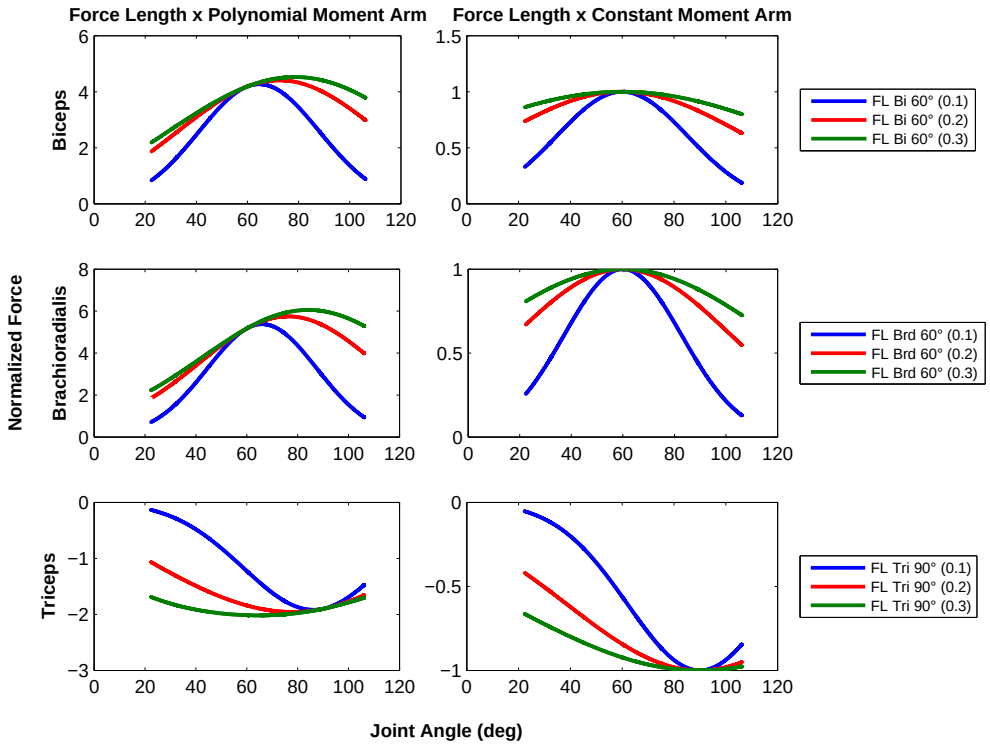


Figure 5.7: Effect of multiplying the force-length curves for the biceps brachii, brachioradialis and triceps brachiias by polynomial moment arm and constant moment arm. Curves are shown for subject F5 for $\varphi_v = [0.1 - 0.3]$

multiplied by a factor of $\pm 1$ (representing the CMA). It is especially evident for force-length curves with a wider shape ($\varphi_v = 0.2, 0.3$) that the peak of the curve is shifted towards higher angles for the biceps brachii and brachioradialis, and lower angles for the triceps brachii when multiplied by the PMA. In addition, the part of the curve that represents longer muscle lengths (smaller angles for the elbow flexors and higher angles for the extensor) is lower in magnitude.

It is difficult to determine with certainty which method should be used, as both methods resulted in models with equivalent accuracy in terms of force estimation. Observations of the frequency distribution of the selected candidate functions using

both moment arm methods (Figures 4.7 and 4.8) suggest that the function selection using the CMA method is more consistent, especially for the biceps brachii and brachioradialis. As shown in Tables 4.7 and 4.8, average standard deviations for the optimal joint angle across all 10 subjects for the biceps brachii and brachioradialis were 14.1 and 12.0 respectively using the CMA method. This value increased to 16.5 and 17.0 for the two muscles using the PMA method. The observed reduction in variability in optimal joint angles found using the CMA method compared to the PMA method is also apparent in Figure 5.5.

More analysis on the FOS coefficient values will need to be performed to assess their ability to account for the muscle moment arm, and warrant the negation of a well known physiological relationship between muscle moment arm and joint angle.

# Chapter 6

# Conclusions and Future Work

## 6.1 Summary and Conclusions

The aim of this project was to develop a novel method of identifying *in vivo* subject-specific physiological parameters (such as $\theta_0$ and $\varphi_{vT}$) of the upper arm using Fast Orthogonal Search. This was accomplished within a framework of a force estimation model for elbow flexion and extension. The results presented here provide evidence that the FOS method used with physiologically-based basis functions can provide a good estimate of force at the wrist due to flexion and extension torque about the elbow.

Focusing on the contribution of the biceps brachii, brachioradialis and triceps brachii to elbow torque, a Hill-based muscle model was used to develop a wide range of candidate functions for the FOS method. FOS models were generated to predict the force at the wrist from flexion and extension torque at the elbow. Two methods were used to incorporate the muscle moment arm into the Hill-based candidate functions (PMA and CMA). The evaluation %RMSE of both the PMA and CMA Hill-based

FOS models were compared to results of FOS models constructed using non-muscle-model-based candidate functions as suggested by [70]. Average evaluation error was lower than non-muscle-model-based results by 1.7% and 2.6% when the PMA and CMA methods were used in the Hill-based FOS models respectively.

A frequency analysis of the Hill-based candidate functions selected by the FOS models revealed trends in the $F^{CE}$ and $F^{PE}$ functions chosen for the triceps brachii, and to a lesser extent the biceps brachii and brachioradialis. Weighted optimal joint angles ($\theta_{0w}$) were calculated for each subject based on FOS model development using a large pool of candidate functions ($N = 132$). These $\theta_{0w}$ were incorporated into a new pool of candidate functions ($N = 18$) to identify subject-specific force-length curve shape parameters ($\varphi_{vT}$). Use of the $\theta_{0w}$ values in FOS candidate functions yielded $RMSE_{AVE}$ ranging from 4.3-19.7%, suggesting that the $\theta_{0w}$ is a good approximation of the subject's true physiology.

Comparing the results of the two Hill-based methods, some reduction in %RMSE was observed for the CMA models, however this was not statistically significant. Perhaps a more interesting observation was that estimates for optimal joint angles suggested by CMA models were less variable than those found using the PMA models. Multiplying a Gaussian function by a polynomial expression as in the PMA method appears to shift the peak of the force curve quite dramatically toward higher joint angles for elbow flexors and lower joint angles for elbow extensors (as shown in Figure 5.7). This may explain the variability in optimal joint angle selection in the PMA method. Perhaps modelling the force-angle curve as a Gaussian function implicitly accounts for the effect of a muscle moment arm that changes with respect to joint angle, therefore maintaining a constant factor for the moment arm contributes to a

more accurate estimation of muscle force.

Therefore, in addition to generating a more accurate estimation of force at the wrist resulting from elbow flexion and extension torque, the Hill-based candidate functions can implicitly provide information about physiological parameters of the upper arm.

## 6.2 Future Work

Expanding on the utility of this method will require a larger subject pool with data recorded during isometric contractions as well as dynamic motion. The force-velocity component of the $F^{CE}$ functions is not excited with the isometric data; performing isotonic (constant force) and isokinetic (constant velocity) contractions will introduce the effects of muscle contraction velocity into the $F^{CE}$ functions. Introducing force-varying isometric contractions may also activate the muscles over a wider range than the two force levels of $10N$ and $20N$ used in this study.

Data collection trials and sessions may also be re-structured. The length and number of trials that can be performed in one session is limited by the onset of muscle fatigue, especially for contractions at or above $20N$ of target wrist force. Obtaining more repetitions of isometric contractions at specific angles may limit the number of joint angles that can be included in one trial. Increasing the number of data collection sessions will also increase the quality and quantity of data. In addition, for the purpose of assessing subject position and the ability to maintain a constant shoulder and wrist position, it would be beneficial to monitor sEMG activity from muscles in the shoulder such as the deltoid, and muscles in the forearm that are associated with wrist flexion and extension. Often, subjects needed to be reminded

not to clench their fist or move their hand during the isometric contractions, and it is unknown whether these extra movements may have artificially inflated sEMG signals from the brachioradialis (*i.e.* cross-talk), or contributed to any inconsistencies in measured force between trials.

Expanding the size of the pool of candidate functions which are available to the model such as including more variation in force-length curves or narrower resolution of optimal joint angles (*i.e.* 5° rather than every 10°) may reduce the variance observed in the weighted optimal joint angle calculations. In terms of candidate functions, perhaps it would be possible to include FOS candidate functions for the brachialis muscle, that take into account the physiology of this muscle and its contribution to elbow torque. The sEMG signals from this muscle can be recorded, however the signal will be heavily affected by cross-talk from the biceps brachii. Investigation into methods of removing the cross-talk signal will need to be performed.

Re-arranging the way in which datasets are used as training sets for FOS model development is another promising avenue for future work. Combining components of data collected from different subjects using the data segmentation or data concatenation procedures may result in more generalized models and more consistent physiological parameter selection.

In the current work, tendon behaviour is assumed to be infinitely stiff, therefore the entire SE unit is neglected. Some error will be introduced in the model by neglecting the tendon elasticity in the FOS model candidate functions, therefore future work may include modifying the Hill-based candidate functions to include an external $SE_t$ unit as in [48].

Finally, future work may also utilize imaging techniques such as ultrasound or

MRI to validate the optimal joint angles determined through the FOS method, as well as muscle moment arm relationships used in FOS model development.

# Bibliography

[1] A. A. Amis, D. Dowson, and W. Wright. Muscle strengths and musculo-skeletal geometry of the upper limb. *Engineering in Medicine*, 8:41–48, 1979.

[2] K. N. An, F. C. Hui, B. F. Morrey, R. L. Linscheid, and E. Y. Chao. Muscles across the elbow joint: A biomechanical analysis. *Journal of Biomechanics*, 14:659–669, 1981.

[3] K. N. An, K. Takahashi, T. P. Harrigan, and E. Y. Chao. Determination of muscle orientations and moment arms. *Journal of Biomechanical Engineering*, 106:280–282, 1984.

[4] J. V. Basmajian and C. J. De Luca. *Muscles Alive: Their functions revealed by Electromyography, 5th Edition.* Williams and Wilkins, 1985.

[5] S. Bouchard, D. Rancourt, and E. A. Clancy. Emg-to-torque dynamic relationship for elbow constant angle contractions. In *Proceedings of the joint BMES/EMBS Conference*, pages 573–573, October 1999.

[6] T. S. Buchanan. Evidence that maximum muscle stress is not a constant: differences in specific tension in elbow flexors and extensors. *Medical Engineering and Physics*, 17(7):529–536, 1995.

[7] T. S. Buchanan, D. G. Lloyd, K. Manal, and T. F. Besier. Neuromusculoskeletal modeling: estimation of muscle forces and joint moment and movements from measurements of neural command. *Journal of Applied Biomechanics*, 20:367–395, 2004.

[8] E. E. Cavallaro, J. Rosen, J. C. Perry, and S. Burns. Real-time myoprocessors for a neural controlled powered exoskeleton arm. *IEEE Transactions on Biomedical Engineering*, 53(11):2387–2396, November 2006.

[9] Y. W. Chang, F. C. Su, H. W. Wu, and K. N. An. Optimum length of muscle contraction. *Clinical Biomechanics*, 14:537–542, 1999.

[10] T. C. Chen, K. Nosaka, and P. Sacco. Intensity of eccentric exercise, shift of optimum angle, and the magnitude of repeated-bout effect. *Journal of Applied Physiology*, 102:992–999, 2007.

[11] J. Cholewicki, S. M. McGill, and R. W. Norman. Comparison of muscle forces and joint load from an optimization and emg assisted lumbar spine model: Towards development of a hybrid approach. *Journal of Biomechanics*, 48(6):622–629, 1995.

[12] K. H. Chon. Accurate identification of periodic oscillations burried in white or coloured noise using fast orthogonal search. *IEEE Transactions on Biomedical Engineering*, 28(3):537–542, 2001.

[13] E. A. Clancy, S. Bouchard, and D. Rancourt. Estimation and application of emg amplitude during dynamic contractions. *IEEE Engineering in Medicine and Biology Magazine*, 20(6):47–54, 2001.

[14] E. A. Clancy and N. Hogan. Relating agonist-antagonist electromyograms to joint torque during isometric quasi-isotonic, non-fatiguing contractions. *IEEE Transactions on Biomedical Engineering*, 44(10):1024–1028, 1997.

[15] E. A. Clancy, E. L. Morin, and R. Merletti. Sampling, noise-reduction and amplitude estimation issues in surface electromyography. *Journal of Electromyography and Kinesiology*, 12:1–16, 2002.

[16] C. J. De Luca. The use of surface electromyography in biomechanics. *Journal of Applied Biomechanics*, 13:135–163, 1997.

[17] S. L. Delp and J. P. Loan. A computational framework for simulating and analyzing human and animal movement. *IEEE Computing in Science and Engineering*, 2:46–55, 2000.

[18] J. J. Dowling, E. Konert, P. Ljucovic, and D. M. Andrews. Are humans able to voluntarily elicit maximum muscle force? *Neuroscience Letters*, 179:25–28, 1994.

[19] V. R. Edgerton, P. Apor, and R.R. Roy. Specific tension of human elbow flexor muscles. *Acta physiologica Hungarica*, 75(3):205–216, 1990.

[20] J. M. Eklund, M. J. Korenberg, and P. J. McLellan. Nonlinear system identification and control of chemical processes using fast orthogonal search. *Journal of Process Control*, 17:742–754, 2007.

[21] A. Erfanian, H. J. Chizeck, and R. M. Hashemi. Using evoked emg as a synthetic force sensor of isometric electrically stimulated muscle. *IEEE Transactions on Biomedical Engineering*, 45(2):188–202, 1998.

[22] G. J. C. Ettema and P. A. Huijing. *"Architecture and Elastic Properties of the Series Elastic Element of Muscle-Tendon Complex", Winters, J. M. and Woo, S. L. Y. (ed.), in Multiple Muscle Systems.* Springer-Verlag, 1990.

[23] D. Farina. *"Surface Electromyography (EMG) Signal Processing", Akay, M. (ed.), in Encyclopedia of Biomedical Engineering.* Wiley and Sons, 2006.

[24] J. A. Faulkner. Terminology for contractions of muscles during shortening, while isometric, and during lengthening. *Journal of Applied Physiology*, 95:455–459, 2003.

[25] C. J. Feng, A. F. T. Mak, and T. K. K. Koo. A surface emg driven musculoskeletal model of the elbow flexion-extension movement in normal subjects and in subjects with spasticity. *Journal of Musculoskeletal Research*, 3(2):109–123, 1999.

[26] T. Finni and P. V. Komi. Two methods for estimating tendinous tissue elongation during human movement. *Journal of Applied Biomechanics*, 18(11):180–188, 2002.

[27] C. Fleischer and G. Hommel. Calibration of an emg-based body model with six muscles to control a leg exoskeleton. In *Proceedings of the IEEE International Conference on Robotics and Automation*, pages 2514–2519, 2007.

[28] I. Flemming, J. Bauersachs, A. Schafer, D. Scholz, J. Aldershvile, and R. Busse. Isometric contraction induces the $ca^{2+}$-independent activation of the endothelial nitric oxide synthase. *Proceedings of the National Academy of Sciences of the USA*, 96:1123–1128, 1999.

[29] University of South Florida. Florida Center for Instructional Technology, College of Education. `http://etc.usf.edu/clipart/4100/4148/arm_2.htm`, 2003.

[30] B. A. Garner and M. G. Pandy. Musculoskeletal model of the upper limb based on the visible human male dataset. *Computer methods in biomechanics and biomedical engineering*, 4(2):93–126, 2001.

[31] B. A. Garner and M. G. Pandy. Estimation of musculotendon properties in the human upper limb. *Annals of Biomedical Engineering*, 31:207–220, 2003.

[32] R. V. Gonzalez, E. L. Hutchins, R. E. Barr, and L. D. Abraham. Development and evaluation of a musculoskeletal model of the elbow joint complex. *Journal of Biomechanical Engineering*, 118:32–40, February 1996.

[33] A. M. Gordon, A. F. Huxley, and F. J. Julian. The variation in isometric tension with sarcomere length in vertebrate muscle fibres. *Journal of Physiology*, 184:170–192, 1966.

[34] G. L. Gottlieb and G. C. Agarwal. Dynamic relationship between isometric muscle tension and the electromyogram in man. *Journal of Applied Physiology*, 30(3):345–351, 1971.

[35] E. A. Hansen, H. D. Lee, K. Barrett, and W. Herzog. The shape of the force-elbow angle relationship for maximal voluntary contractions and sub-maximal electrically induced contractions in human elbow flexors. *Journal of Biomechanics*, 36:1713–1718, 2003.

[36] H. Hatze. Estimation of myodynamic parameter values from observations on isometrically contracting muscle groups. *European Journal of Applied Physiology*, 46:325–338, 1981.

[37] highfive.me.uk. `http://www.highfive.me.uk/Resources/Anatomy/UpperArm/All.JPG`, 2008.

[38] A. V. Hill. The heat of shortening and the dynamic constants of muscle. *Proceedings of the Royal Society of London B*, 126:136–195, 1938.

[39] A. L. Hof and J. W. Van den Berg. Emg to force processing i: An electrical analogue of the hill muscle model. *Journal of Biomechanics*, 14(11):747–758, 1981.

[40] K. R. S. Holzbaur, W. M. Murray, and S. L. Delp. A model of the upper extremity for simulating musculoskeletal surgery and analyzing neuromuscular control. *Annals of Biomedical Engineering*, 33:829–840, 2005.

[41] K. R. S. Holzbaur, W. M. Murray, G. E. Gold, and S. L. Delp. Upper limb muscle volumes in adult subjects. *Journal of Biomechanics*, 40:742–749, 2007.

[42] D. C. Howell. *"Statistical Methods for Psychology, 6th Edition.* Thompson Wadsworth, 2007.

[43] M. G. Hoy, F. E. Zajac, and M. E. Gordon. A musculoskeletal model of the human lower extremity: The effect of muscle, tendon and moment arm on the moment-angle relationship of musculotendon actuators at the hip, knee and ankle. *Journal of Biomechanics*, 23(2):157–169, 1990.

[44] M. Ito, H. Akima, and T. Fukunaga. In vivo moment arm determination using b-mode ultrasonography. *Journal of Biomechanics*, 33:215–218, 2000.

[45] A. Jaskolska, K. Kisiel-Sajewicz, W. Brzenczek-Owczarzak, G. H. Yue, and A Jaskolski. Emg and mmg of agonist and antagonist muscles as a function of age and joint angle. *Journal of Electromyography and Kinesiology*, 16:89–102, 2006.

[46] Y. Kawakami, K. Nakazawa, T. Fujimoto, D. Nozaki, M. Miyashita, and T. Fukunaga. Specific tension of elbow flexor and extensor muscles based on magnetic resonance imaging. *European Journal of Applied Physiology*, 68:139–147, 1994.

[47] T. K. K. Koo and A. F. T. Mak. Feasibility of using emg driven neuromusculoskeletal model for prediction of dynamic movement of the elbow. *Journal of Electromyography and Kinesiology*, 15:12–26, 2005.

[48] T. K. K. Koo, A. F. T. Mak, and L. K. Hung. In vivo determination of subject-specific musculotendon parameters: applications to the prime elbow flexors in normal and hemiparetic subjects. *Clinical Biomechanics*, 17:390–399, 2002.

[49] M. J. Korenberg. Fast orthogonal identification of non-linear difference equation and function expansion models. In *Proceedings of the 28th Midwest Symposium on Circuits and Systems, Louisville, KY, August 1985*, volume 1, pages 270–276, August 1985.

[50] M. J. Korenberg. Identifying nonlinear difference equation and functional expansion representations: the fast orthogonal algorithm. *Annals of Biomedical Engineering*, 16:123–142, 1988.

[51] M. J. Korenberg. A robust orthogonal algorithm for system identification. *Biological Cybernetics*, 60:267–276, 1989.

[52] Hof A. L. Emg and muscle force: An introduction. *Human Movement Science*, 3:119–153, 1984.

[53] J. Langenderfer, S. A. Jerabek, V. B. Thangamani, J. E. Kuhn, and R. E. Hughes. Musculoskeletal parameters of muscles crossing the shoulder and elbow and the effect of sarcomere length sample size on estimation of optimal muscle length. *Computers in Biology and Medicine*, 35:25–39, 2005.

[54] J. Langenderfer, S. LaScalza, A. Mell, J. E. Carpenter, J. E. Kuhn, and R. E. Hughes. An emg-driven model of the upper extremity and estimation of long head biceps force. *Clinical Biomechanics*, 19:664–670, 2004.

[55] J. H. Lawrence and C. J. De Luca. Myoelectric signal versus force relationship in different human muscles. *Journal of Applied Physiology*, 54(6):1653–1659, 1983.

[56] J. S. Leedham and J. J. Dowling. Force-length, torque-angle and emg-joint angle relationships of the human in vivo biceps brachii. *European Journal of Applied Physiology*, 70:421–426, 1995.

[57] M. A. Lemay and P. E. Crago. A dynamic model for simulating movements of the elbow, forearm and wrist. *Journal of Biomechanics*, 29(10):1319–1330, 1996.

[58] L. Li, K. Tong, R. Song, and T. K. K. Koo. Is maximum isometric muscle stress the same among prime elbow flexors? *Clinical Biomechanics*, 22:874–883, 2007.

[59] R. L. Lieber. *Skeletal Muscle Structure, Function, and Plasticity: The Physiological Basis of Rehabilitation, 2nd Edition*. Lippincott Williams and Wilkins, 2002.

[60] R. L. Lieber, W. M. Murray, D. L. Clark, V. R. Hentz, and J. Friden. Biomechanical properties of the brachioradialis muscle: Implications for surgical tendon transfer. *The Journal of Hand Surgery*, 30A(2):273–282, March 2005.

[61] Dorling Kindersley Limited. `http://www.dkimages.com/discover/previews/740/60417.JPG`, 2008.

[62] Y. H. Lin and T. W. Lu. The influence of neuromuscular activation on the estimation of optimal muscle length. *Journal of Back and Musculoskeletal Rehabilitation*, 17:15–19, 2004.

[63] M. M. Liu, W. Herzog, and H. H. C. M. Savelberg. Dynamic muscle force predictions from emg: an artificial neural network approach. *Journal of Electromyography and Kinesiology*, 9:391–400, 1999.

[64] C. N. Maganaris. Force-length characteristics of in vivo human skeletal muscle. *Acta physiologica Scandinavica*, 172(4):279–285, 2001.

[65] C. N. Maganaris, V. Baltzopoulos, and A. J. Sargeant. Changes in the tibialis anterior tendon moment arm from rest to maximum isometric dorsifexion: in vivo observations in man. *Clinical Biomechanics*, 14:661–666, 1999.

[66] D. C. Martin, M. K. Medri, R. S. Chow, V. Oxorn, R. N. Leekam, A. M. Agur, and N. H. McKee. Comparing human skeletal muscle architectural parameters of cadavers with in vivo ultrasonographic measurements. *Journal of Anatomy*, 199:429–434, 2001.

[67] D. R. McGaughey, M. J. Korenberg, K. M. Adeney, S. D. Collins, and G. J. M. Aitken. Using the fast orthogonal search with first term reselection to find subharmonic terms in spectral analysis. *Annals of Biomedical Engineering*, 31:741–751, 2003.

[68] D. R. McGaughey, M. Tarbouchi, K. Nutt, and A. Chikhani. Speed sensorless estimation of ac induced motors using the fast orthogonal search algorithm. *IEEE Transactions on Energy Conversion*, 21(1), 2006.

[69] R. Merletti, D. Farina, and M. Gazzoni. The linear electrode array: a useful tool with many applications. *Journal of Electromyography and Kinesiology*, 13:37–47, 2003.

[70] F. Mobasser, J. M. Eklund, and K. Hashtrudi-Zaad. Estimation of elbow-induced wrist force with emg signals using fast orthogonal search. *IEEE Transactions on Biomedical Engineering*, 54:683–693, April 2007.

[71] M. Moradi, K. Hashtrudi-Zaad, K. Mountjoy, and E. Morin. An emg-based force control system for prosthetic arms. In *Proceedings of the Biomedical Symposium*

*of the IEEE Canadian Conference on Electrical and Computer Engineering*, pages 1737–1742, 2008.

[72] Maryam Moradi. Force control for prosthetic arms using an emg-based wrist force observer. Master's thesis, Bremen Universitat, July 2007.

[73] E. L. Morin. *"Myoelectric Signal Processing", Akay, M. (ed.), in Encyclopedia of Biomedical Engineering.* Wiley and Sons, 2006.

[74] W. M. Murray, T. S. Buchanan, and S. L. Delp. The isometric functional capacity of muscles that cross the elbow. *Journal of Biomechanics*, 33:943–952, 2000.

[75] W. M. Murray, T. S. Buchanan, and S. L. Delp. Scaling of peak moment arms of elbow muscles with upper extremity bone dimensions. *Journal of Biomechanics*, 35:19–26, 2002.

[76] W. M. Murray, S. L. Delp, and T. S. Buchanan. Variation of muscle moment arms with elbow and forearm position. *Journal of Biomechanics*, 28:513–525, 1995.

[77] E. Otten. A myocybernetic model of the jaw system of the rat. *Journal of Neuroscience Letters*, 21:287–302, 1987.

[78] L. Out, T. G. M. Vrijkotte, A. J. van Soest, and M. F. Bobbert. Influence of the parameters of a human triceps surae muscle model on the isometric torque-angle relationship. *Journal of Biomechanical Engineering*, 118:17–25, 1996.

[79] E. Pennestri, R. Stefanelli, P. P. Valentini, and L. Vita. Virtual musculo-skeletal model for the biomechanical analysis of the upper limb. *Journal of Biomechanics*, 40:1350–1361, 2007.

[80] Dinh K. Pham. Modeling flexion/extension in the human elbow using processed surface emg. Master's thesis, Queen's University, September 1995.

[81] A. Philippou, G. C. Bogdanis, A. M. Nevill, and M. Maridaki. Changes in the angle-force curve of human elbow flexors following eccentric and isometric exercise. *European Journal of Applied Physiology*, 93:237–244, 2004.

[82] PhysioWeb. `http://www.physioweb.org/IMAGES/forearm_front.jpg`, 2008.

[83] P. Pigeon, L. Yahia, and A. G. Feldman. Moment arms and lengths of human upper limb muscles as functions of joint angles. *Journal of Biomechanics*, 29(10):1365–1370, 1996.

[84] D. E. Rassier, B. R. MacIntosh, and W. Herzog. Length dependence of active force production in skeletal muscle. *Journal of Applied Physiology*, 86:1445–1457, 1999.

[85] J. Rosen, M. B. Fuchs, and M. Arcan. Performances of hill-type and neural network muscle models toward a myosignal-based exoskeleton. *Computers and Biomedical Research*, 32:415–439, 1999.

[86] C. Y. Scovil and J. L. Ronsky. Sensitivity of a hill-based muscle model to perturbations in model parameters. *Journal of Biomechanics*, 39:2055–2063, 2006.

[87] F. Sepulveda, D. M. Wells, and C. L. Vaughan. A neural network representation of electromyography and joint dynamics in human gait. *Journal of Biomechanics*, 26(2):101–109, 1993.

[88] Elize A. Shirdel. Predicting neutropenia in breast cancer patients undergoing chemotherapy using a 2-stage fos-3nn model trained on first cycle blood counts. Master's thesis, Queen's University, May 2005.

[89] V. Strojnik. Muscle activation level during maximal voluntary effort. *European Journal of Applied Physiology*, 72:144–149, 1995.

[90] E. J. Van Zuylen, A. Van Velzen, and J. J. Denier Van der Gon. A biomechanical model for flexion torques of human arm muscles as a function of elbow joint angle. *Journal of Biomechanics*, 21(3):183–191, 1988.

[91] H. E. J. Veeger, B. Yu, K. N. An, and R. H. Rozendal. Parameters for modeling the upper extremity. *Journal of Biomechanics*, 30(6):647–652, 1997.

[92] S. M. Walker and G. R. Schrodt. I segment lengths and thin filament periods in skeletal muscle fibers of the rhesus monkey and the human. *Anatomical Record*, 178:63–82, 1974.

[93] D. A. Winter. *Biomechanics and Motor Control of Human Movement, 3rd Edition*. Wiley and Sons, 2005.

[94] J. M. Winters. *"Hill-based muscle models: A systems engineering approach", Winters, J. M. and Woo, S. L. Y. (ed.), in Multiple Muscle Systems*. Springer-Verlag, 1990.

[95] J. M. Winters and L. Stark. Analysis of fundamental human movement patterns through the use of in-depth antagonistic muscle models. *IEEE Transactions on Biomedical Engineering*, 32(10):826–839, 1985.

[96] J. M. Winters and L. Stark. Muscle models: What is gained and what is lost by varying model complexity. *Biological Cybernetics*, 55:403–420, 1987.

[97] J. M. Winters and L. Stark. Estimated mechanical properties of synergistic muscles involved in movements of a variety of human joints. *Journal of Biomechanics*, 21(12):1027–1041, 1988.

[98] R. D. Woittiez, P. A. Huijing, H. B. K. Boom, and R. H. Rozendale. A three-dimensional muscle model: A quantified relation between form and function of skeletal muscles. *Journal of Morphology*, 182:95–113, 1984.

[99] J. J. Woods and B. Bigland-Ritchie. Linear and non-linear surface emg/force relationships in human muscles: An anatomical/functional argument for the existence of both. *American Journal of Physical Medicine*, 62(6):287–299, 1983.

[100] F. E. Zajac. Muscle and tendon: properties, models, scaling and application to biomechanics and motor control. *Critical Reviews in Biomedical Engineering*, 17(4):359–411, 1989.

# Appendix A

# Muscle Parameters from Literature

## A.1 Maximal Musculotendon Length

The maximum length of a musculotendon unit $L_{MTmax}$ is the sum of the length of the muscle and its tendon when the joint is in a position of full extension, i.e. the muscle and tendon cannot be stretched any farther by means of manipulating the joints associated with that muscle within the functional operating range [31]. Values for this parameter are not widely reported in the literature. Table A.1 provides an average calculation from two sources.

## A.2 Tendon Slack Length

Tendon slack length ($L_{Ts}$) is defined as the length of the tendon at which any further elongation will result in tension developing in the tendon [100]. The following values for $L_{Ts}$ were presented in the literature. The values were generally were obtained through measurement of cadaveric specimens.

Table A.1: Maximum musculotendon length ($cm$) of short and long heads of the biceps brachii (BSH and BLH), the brachioradialis (BRD) and lateral, long and medial heads of the triceps brachii (TLtH, TLgH and TMH) as reported in literature

| **Study** | **Study Size (N)** | **Muscle** | | | | | |
|---|---|---|---|---|---|---|---|
| | | **BSH** | **BLH** | **BRD** | **TLtH** | **TLgH** | **TMH** |
| Lemay and Crago (1996) | 6* | 37.80 | 37.20 | 27.60 | 31.50 | 17.70 | 13.50 |
| Cavallaro *et al.* (2006) | 1† | 40.46 | 41.94 | 35.35 | 40.29 | 28.22 | 18.95 |
| **Average ± SD** | | **39.35 ± 2.6** | | **31.48 ± 5.5** | **29.43 ± 6.8** | | |

*Lemay and Crago cited maximal musculotendon lengths from An *et al.*[2] which had a study size of 6 cadavers
†Cavallaro *et al.* did not state how many subjects were used in their study, therefore it is assumed to be 1 subject

Table A.2: Tendon slack length length of biceps brachii, brachioradialis and triceps brachii as reported in literature

| Study | **Study size (n)** | **Muscle** | | | | | |
|---|---|---|---|---|---|---|---|
| | | **Biceps Short Head** | **Biceps Long Head** | **Brachioradialis** | **Triceps Long Head** | **Triceps Lateral Head** | **Triceps Medial Head** |
| Gonzalez *et al.* (1996) [32] | 7 | 20 | 20 | 12 | - | - | - |
| Murray *et al.* (2000) [74] | 10 | 18.3 (2.5) | 22.9 (1.6) | 16.9 (1.7) | 21.7 (2.9) | 18.7 (1.8) | |
| Koo *et al.* (2002) [48] | 5 | 21.7 | 25.9 | 9.0 | - | - | - |
| Garner and Pandy (2003) [31] | 3 | 22.98 | | 6.04 | 19.05 | | |
| Langenderfer *et al.* (2004) [53] | 2 | 15.8 (0.9) | 18.3 (1.4) | 10.5 (0.5) | 20.0 (0.6) | 16.7 (0.7) | 1.8 (1.1) |
| Holzbaur *et al.* (2005) [40] | 1 | 19.2 | 27.2 | 13.3 | 14.3 | 9.8 | 9.8 |
| **Weighted Average ± SD** | | **21.11 ± 2.2** | | **12.50 ± 3.8** | **18.50 ± 3.1** | | |

## A.3 Optimal Muscle Length

Optimal muscle length ($L_0$) is defined as the length of the muscle fibres in between the tendons at which the muscle is able to generate its maximum isometric force $F_0$. Optimal muscle length drives the force-length relationship and is attributed to the amount of overlap between actin-myosin filaments within the sarcomeres. A summary of values provided in the literature is provided in Table A.3. The weighted averages have been calculated for the biceps brachii, brachioradialis and triceps brachii.

Table A.3: Optimal muscle length of biceps brachii, brachioradialis and triceps brachii as reported in literature

| Study | **Study size (n)** | **Muscle** | | | | | |
|---|---|---|---|---|---|---|---|
| | | **Biceps Short Head** | **Biceps Long Head** | **Brachioradialis** | **Triceps Long Head** | **Triceps Lateral Head** | **Triceps Medial Head** |
| Amis *et al.* (1979) [1] | 4 | 15.7 | 15 | 14.2 | 7.4 | 6.8 | 5.9 |
| An *et al.* (1981) [2] | 4 | 15 (3.4) | 13.6 (2.4) | 16.4 (2.9) | 10.2 (1.9) | 8.4 (1.0) | 6.3 (1.4) |
| Kawakami *et al.* (1994) [46] | 4 | 20 | | 12 | 8 | | |
| Gonzalez *et al.* (1996) [32] | 7 | 14 | | 14.4 | 10 | | |
| Murray *et al.* (2000) [74] | 10 | 14.5 (3.2) | 12.8 (3.2) | 17.7 (3.0) | 12.7 (2.1) | 9.3 (2.8) | |
| Koo *et al.* (2002) [48] | 5 | 14.5 | 11.3 | 23.8 | - | - | - |
| Garner and Pandy (2003) [31] | 3 | 14.22 | | 27.03 | 8.77 | | |
| Langenderfer *et al.* (2004) [53] | 2 | 18.1 (0.4) | 15.6 (0.3) | 17.5 (1.8) | 17.6 (1.1) | 10.3 (2.4) | 14.5 (0.9) |
| Holzbaur *et al.* (2005) [40] | 1 | 13.2 | 11.6 | 17.3 | 13.4 | 11.4 | 11.4 |
| **Weighted Average ± SD** | | **14.66 ± 2.17** | | **17.52 ± 4.26** | **9.67 ± 2.09** | | |

## A.4 Physiological Cross-Sectional Area (PCSA)

Maximum isometric force ($F_0$) can be assumed to be proportional to the physiological cross-sectional area (PCSA) of a muscle. PCSA is defined as the total area normal to the longitudinal axis of the muscle fibres and can be calculated as the ratio between muscle volume ($Vol$) and $L_0$:

$$PCSA = \frac{Vol}{L_0} = \frac{mass/density}{L_0} \tag{A.1}$$

Therefore a weighted average PCSA value was calculated from values reported in the literature as summarized in Table A.4.

Table A.4: Physiological Cross-sectional Area (PCSA) ($cm^2$) and (SD) for the biceps brachii, brachioradialis and triceps brachii as reported in literature

| Study | **Study size (n)** | **Muscle** | | | | | |
|---|---|---|---|---|---|---|---|
| | | **Biceps Short Head** | **Biceps Long Head** | **Brachioradialis** | **Triceps Long Head** | **Triceps Lateral Head** | **Triceps Medial Head** |
| Amis *et al.* (1979) [1] | 4 | 3.96 | 4.13 | 3.22 | 20.44 | 15.42 | 14.46 |
| An *et al.* (1981) [2] | 4 | 2.1 (0.5) | 2.5 (0.5) | 1.5 (0.5) | 6.7 (2.0) | 6.0 (1.2) | 6.1 (2.3) |
| Edgerton *et al.* (1990) [19] | 4 | 1.6 | 2.2 | 1.8 | 23.8 | | |
| Murray *et al.* (2000) [74] | 10 | 2.1 (0.6) | 2.5 (1.1) | 1.2 (0.6) | 4.3 (1.8) | 10.5 (5.2) | |
| Garner and Pandy (2003) [31]† | 3 | 25.90 | | 3.08 | 76.30 | | |
| Langenderfer *et al.* (2004) [53] | 2 | 1.75 (0.79) | 1.57 (0.13) | 1.15 (0.37) | 3.6 (1.35) | 4.13 (1.22) | 3.21 (0.71) |
| Holzbaur *et al.* (2005) [40] | 1 | 3.1 | 4.5 | 1.9 | 5.7 | 4.5 | 4.5 |
| Holzbaur *et al.* (2007) [41] | 10 | 8.2 (3.4) | | 3.9 (1.8) | 40.0 (15.4) | | |
| **Weighted Average** | | **4.14** | | **2.38** | **19.54** | | |

†The values presented by Garner and Pandy for the biceps brachii and triceps brachii were neglected in calculating the average PCSA

## A.5 Maximum Muscle Stress/Specific Tension ($N/cm^2$)

The maximum muscle stress is commonly referred to as specific muscle tension in the literature and is defined as the maximum force developed per unit of cross-sectional area [6]. Units for specific tension are often given as $N/cm^2$ which is equivalent to units of pressure Pa. Buchanan [6] computed specific tension ($\sigma$) for elbow flexors and extensors using the following equations for joint moment ($M$):

$$M_{elbow} = \sum MA_i \cdot F_{0i} \tag{A.2}$$

$$M_{elbow} = \sigma \sum MA_i \cdot PCSA_i \tag{A.3}$$

A summary of values for $\sigma$ provided in the literature is provided in Table A.5.

Table A.5: Specific tension $\sigma$ (kPa) for muscles about the elbow as presented in the literature

| Study | Specific Tension $\sigma$ (kPa) | | |
|---|---|---|---|
| | **All** | **Elbow Flexors** | **Elbow Extensors** |
| An *et al.*, 1981 [2] | 1000 | - | - |
| Winters and Stark 1988 [97] | 500 | - | - |
| Zajac 1989 [100] | 350 | - | - |
| Buchanan 1995 [6] | - | 990-1480 | 430-910 |
| Koo *et al.*, 2002 [48] | 1293.7 | - | - |
| Garner and Pandy 2003 [31] | 330 | - | - |
| Koo and Mak 2005 [47] | 1000 | - | - |
| Holzbaur *et al.*, 2005 [40] | 1400 | - | - |
| Pennestri *et al.*, 2007 [79] | 1400 | - | - |

## A.6 Maximum Isometric Force $F_0$ ($N$)

There are few papers that specify the peak isometric force generated by the muscles of the upper limb. However, $F_{0i}$ is often calculated by multiplying the specific tension

and PCSA of a muscle:

$$F_{0i} = \sigma_i \cdot PCSA_i \tag{A.4}$$

where $\sigma_i$ is the specific tension of muscle $i$ converted to units of Pa, and $PCSA_i$ is the physiological cross-sectional area of muscle $i$ converted to $m^2$. Therefore, the values in Table A.6 are compiled from: values published in the literature [31, 40]; and values calculated as the product of $PCSA_i$ and $\sigma_i$ published in the literature [2, 32]; and an average value calculated as the product of the average values of $\sigma_i$ and $PCSA_i$ found in Tables A.4 and A.5 respectively.

Table A.6: Peak isometric force $F_0$ $(N)$ for muscles about the elbow provided in literature or calculated using literature values

| Study | **Muscle** | | | | | |
|---|---|---|---|---|---|---|
| | **Biceps Short Head** | **Biceps Long Head** | **Brachioradialis** | **Triceps Long Head** | **Triceps Lateral Head** | **Triceps Medial Head** |
| An *et al.* (1981) [2] | 210 | 250 | 150 | 670 | 600 | 610 |
| Gonzalez *et al.* (1996) [32] | 670 | | 430 | 1750 | | |
| Garner and Pandy (2003) [31] | 849.29 | | 101.56 | 2332.92 | | |
| Holzbaur *et al.* (2005) [40] | 435.6 | 624.3 | 261.3 | 798.5 | 624.3 | 624.3 |
| Calculated from average values in Tables A.4 and A.5 | 616.9 | | 195.3 | 2363.0 | | |
| **Average** | **731.2** | | **227.6** | **2074.6** | | |

# Appendix B

# Fast Orthogonal Search (FOS)

The Fast Orthogonal Search (FOS) method [50, 51] is a nonlinear identification method that forms a sum of $M$ linear or nonlinear basis functions $p_m(n)$ and coefficient terms $a_m$ and aims to minimize the mean square error between the estimate and the system output. The FOS model takes the form:

$$y(n) = \sum_{m=1}^{M} a_m p_m(n) + e(n) \tag{B.1}$$

The FOS method is based on the principals of Gram-Schmidt orthogonal identification, whereby orthogonal basis functions $w_m(n)$ would be generated from the candidate basis functions $p_m(n)$ and coefficients found to minimize the MSE of the estimate, therefore taking the form

$$y(n) = \sum_{m=1}^{M} g_m w_m(n) + e(n) \tag{B.2}$$

where the $g_m$ terms are the coefficients of the orthogonal basis functions $w_m(n)$, which are orthogonal over the entire data record such that:

$$\overline{w_i(n)w_j(n)} = 0, i, j\epsilon[1, M], i \neq j \tag{B.3}$$

Here the overline represents the average over the entire data record. The orthogonal functions are found by subtracting from each $p_m(n)$ the components which are "parallel" to the previously found orthogonal function $w_j(n)$, where $j < m$.

$$\begin{aligned} w_1(n) &= p_1(n) = 1 \\ w_2(n) &= p_2(n) - \alpha_{21} w_1(n) \\ &\vdots \\ w_m(n) &= p_m(n) - \sum_{r=1}^{m-1} \alpha_{mr} w_r(n) \end{aligned} \tag{B.4}$$

where $\alpha_{mr}$ represents the projection of $w_r$ on $p_m$ as:

$$\alpha_{mr} = \frac{\overline{w_r(n) p_m(n)}}{\overline{w_r^2(n)}}, \quad \begin{matrix} m = 2, \ldots, M \\ r = 1, \ldots, m-1 \end{matrix} \tag{B.5}$$

Since the error can be represented as mean square error (MSE):

$$\overline{e^2(n)} = [\overline{y(n) - \widehat{y}(n)}]^2 \tag{B.6}$$

then,

$$\begin{aligned} \overline{e^2(n)} &= \overline{\left[ y(n) - \left( \sum_{i=1}^{M} g_i w_i(n) \right) \right]^2} \\ &= \overline{y^2(n)} - 2y(n) \sum_{i=1}^{M} g_i w_i(n) + \sum_{i=1}^{M} g_i^2 \overline{w_i^2(n)} \end{aligned}$$

Since the basis functions $w_i(n)$ are orthogonal, the error can be written as:

$$\overline{e^2(n)} = \overline{y^2(n)} - \sum_{i=1}^{M} g_i^2 \overline{w_i^2(n)} \tag{B.7}$$

The coefficients $g_i$ that minimize the MSE of the model estimate can be found as:

$$g_i = \frac{\overline{y(n) w_i(n)}}{\overline{w_i^2(n)}} \tag{B.8}$$

From equation B.7, the iterative reduction in error of the model estimate can be measured as a term $Q(m)$ as:

$$Q(m) = g_i^2 \overline{w_i^2(n)} \tag{B.9}$$

Therefore, the method can select the best candidate functions to include in the model, selecting iteratively, the one that maximizes the value of $Q(m)$. However, in order to calculate $Q(m)$, both the coefficient values $g_i$ and orthogonal basis functions $w_i(n)$ need to be found. Calculating the orthogonal functions can be time-consuming and computationally expensive.

The benefit of the Fast Orthogonal Search method is that there is a way in which to circumvent the calculation of the actual orthogonalized basis functions $w_i(n)$ using only a few variables, and simply find the coefficients of the orthogonalized basis functions $g_i$. To do this, a number of orthogonal expansion coefficients are given.

$$g_m = \frac{C(m)}{D(m,m)}, \text{ for } m = 0, \ldots, M \tag{B.10}$$

where

$$D(0,0) = 1 \tag{B.11}$$

$$D(m,0) = \overline{p_m(n)}, \text{ for } m = 1, \ldots, M \tag{B.12}$$

$$D(m,r) = \overline{p_m(n)p_r(n)} - \sum_{i=0}^{r-1} \alpha_{ri} D(m,i), \text{ for } m = 1, \ldots, M \text{ and } r = 0, \ldots, m-1 \tag{B.13}$$

$$\alpha_{mr} = \frac{D(m,r)}{D(r,r)}, \text{ for } m = 1, \ldots, M \text{ and } r = 0, \ldots, m-1 \tag{B.14}$$

$$C(0) = \overline{y(n)} \tag{B.15}$$

$$C(m) = \overline{y(n)p_m(n)} - \sum_{r=0}^{m-1} \alpha_{mr} C(r), \text{ for } m = 1, \ldots, M \tag{B.16}$$

The algorithm implemented in MATLAB to develop the FOS models was based on the following pseudocode [50, 51]. For more details on the MATLAB codes used to calculated the FOS models, refer to [72].

$D(0,0)$=1

for $m = 1, \ldots, M$

    Calculate $D(m,0)$ using equation B.12

for $m = 1, \ldots, M$

    for $r = 0, \ldots, M-1$

        Calculate $\alpha_{mr}$ using equation B.14

        Calculate $D(m,r+1)$ using equation B.13

Recall that the term $Q(m)$ in equation B.9 represents the iterative reduction in model error. This error reduction for the addition of the $m$-th candidate function $p_m(n)$ can be written as

$$Q(m) = g_m^2 D(m,m) = \frac{C^2(m)}{D(m,m)} \tag{B.17}$$

As the FOS model moves through its iterative process, selecting candidate functions $p_m(n)$ which produce a maximum $Q(m)$, the selected $p_m$ is removed from the pool of candidates so that it will not be selected again. The FOS method continues

to select $p_m$ terms until $m = M$. The model coefficient terms $a_m$ from equation B.1 can then be calculated using

$$a_m = \sum_{i=M}^{M} g_i v_i \tag{B.18}$$

where

$$v_m = 1 \tag{B.19}$$

$$v_i = -\sum_{r=m}^{i=1} \alpha_{ir} v_r \text{ for } i = m, \ldots, M \tag{B.20}$$

# Appendix C

# List of Hill-Based Candidate Functions

## C.1 Initial Model Development

Table C.1 provides a list of all Hill-based candidate functions ($p_m$) used in the FOS method to generate wrist force estimation models. Candidate functions represent the contribution to the elbow moment of particular muscles in the arm and are provided in groups based on which muscle they represent ($i$=*Bi, Brd and Tri*) and which angle is used as $\theta_0$ ($\theta_0 = 20°, 30°, \ldots, 110°, 120°$). Therefore, candidate functions are incorporated into the FOS algorithm in the form:

$$p_m = \begin{cases} F^{CE}(\theta_{0i}, \varphi_{vi}) \cdot \frac{MA_i}{MA_{forearm}} = f_{li}(\theta_{0i}, \varphi_{vTi}) \cdot f_{vi}(\theta_{0i}) \cdot u_i(t) \cdot MA_i \\ F^{PE}(\theta_{0i}) \cdot \frac{MA_i}{MA_{forearm}} = F^{PE}(\theta_{0i}) \cdot MA_i \end{cases} \tag{C.1}$$

where the moment arm of the muscle ($MA_i$) is given as a polynomial relationship

or set to 1 depending on the required analysis, the length of the subject's forearm ($MA_{forearm}$) is set equal to 1 and $u_i(t)$ is assumed to equal the processed EMG ($e_i(t)$). For candidate functions used with isometric data, $f_{vi}$ is set equal to 1.

The functions are labelled in the following tables using the format $F^{CE}_{i\theta_0(\varphi_v)}$ and $F^{PE}_{i\theta_0}$ where $i$ refers to the muscle, $\theta_0$ is the optimal joint angle used in calculations of the force-length curve, the force-velocity relationship and the parallel elastic curve, and $\varphi_v$ is the Gaussian shape parameter ($\varphi_v = 0.1, 0.2, 0.3$) of the modeled force-length curve. Recall that the actual Gaussian shape parameters used ($\varphi_{vT}$) are provided in Table 3.2 in Section 3.

## C.2 Expanded Model Development

Once the weighted optimal joint angles were calculated for each muscle for each subject, a new set of candidate functions was developed for each subject, incorporating the weighted optimal joint angle and also expanding the choices of Gaussian shape parameters from three values to five ($\varphi_v = 0.1, 0.15, 0.2, 0.25, 0.3$). The pool of candidate functions incorporated into the FOS method was thus given as the following 18 functions in Table C.2:

Table C.1: Pool of Muscle-Model-Based Candidate Functions for the Biceps Brachii (Bi), Brachioradialis (Brd) and Triceps Brachii (Tri) used for main model development ($N = 132$) for each subject

| **Group** | $F^{CE}_{i\theta_0(\varphi_v)}$ | | | $F^{PE}_{i\theta_0}$ |
|---|---|---|---|---|
| BI-1 | $F^{CE}_{Bi20°(0.1)} \cdot MA_{Bi}$ | $F^{CE}_{Bi20°(0.2)} \cdot MA_{Bi}$ | $F^{CE}_{Bi20°(0.3)} \cdot MA_{Bi}$ | $F^{PE}_{Bi20°} \cdot MA_{Bi}$ |
| BI-2 | $F^{CE}_{Bi30°(0.1)} \cdot MA_{Bi}$ | $F^{CE}_{Bi30°(0.2)} \cdot MA_{Bi}$ | $F^{CE}_{Bi30°(0.3)} \cdot MA_{Bi}$ | $F^{PE}_{Bi30°} \cdot MA_{Bi}$ |
| BI-3 | $F^{CE}_{Bi40°(0.1)} \cdot MA_{Bi}$ | $F^{CE}_{Bi40°(0.2)} \cdot MA_{Bi}$ | $F^{CE}_{Bi40°(0.3)} \cdot MA_{Bi}$ | $F^{PE}_{Bi40°} \cdot MA_{Bi}$ |
| BI-4 | $F^{CE}_{Bi50°(0.1)} \cdot MA_{Bi}$ | $F^{CE}_{Bi50°(0.2)} \cdot MA_{Bi}$ | $F^{CE}_{Bi50°(0.3)} \cdot MA_{Bi}$ | $F^{PE}_{Bi50°} \cdot MA_{Bi}$ |
| BI-5 | $F^{CE}_{Bi60°(0.1)} \cdot MA_{Bi}$ | $F^{CE}_{Bi60°(0.2)} \cdot MA_{Bi}$ | $F^{CE}_{Bi60°(0.3)} \cdot MA_{Bi}$ | $F^{PE}_{Bi60°} \cdot MA_{Bi}$ |
| BI-6 | $F^{CE}_{Bi70°(0.1)} \cdot MA_{Bi}$ | $F^{CE}_{Bi70°(0.2)} \cdot MA_{Bi}$ | $F^{CE}_{Bi70°(0.3)} \cdot MA_{Bi}$ | $F^{PE}_{Bi70°} \cdot MA_{Bi}$ |
| BI-7 | $F^{CE}_{Bi80°(0.1)} \cdot MA_{Bi}$ | $F^{CE}_{Bi80°(0.2)} \cdot MA_{Bi}$ | $F^{CE}_{Bi80°(0.3)} \cdot MA_{Bi}$ | $F^{PE}_{Bi80°} \cdot MA_{Bi}$ |
| BI-8 | $F^{CE}_{Bi90°(0.1)} \cdot MA_{Bi}$ | $F^{CE}_{Bi90°(0.2)} \cdot MA_{Bi}$ | $F^{CE}_{Bi90°(0.3)} \cdot MA_{Bi}$ | $F^{PE}_{Bi90°} \cdot MA_{Bi}$ |
| BI-9 | $F^{CE}_{Bi100°(0.1)} \cdot MA_{Bi}$ | $F^{CE}_{Bi100°(0.2)} \cdot MA_{Bi}$ | $F^{CE}_{Bi100°(0.3)} \cdot MA_{Bi}$ | $F^{PE}_{Bi100°} \cdot MA_{Bi}$ |
| BI-10 | $F^{CE}_{Bi110°(0.1)} \cdot MA_{Bi}$ | $F^{CE}_{Bi110°(0.2)} \cdot MA_{Bi}$ | $F^{CE}_{Bi110°(0.3)} \cdot MA_{Bi}$ | $F^{PE}_{Bi110°} \cdot MA_{Bi}$ |
| BI-11 | $F^{CE}_{Bi120°(0.1)} \cdot MA_{Bi}$ | $F^{CE}_{Bi120°(0.2)} \cdot MA_{Bi}$ | $F^{CE}_{Bi120°(0.3)} \cdot MA_{Bi}$ | $F^{PE}_{Bi120°} \cdot MA_{Bi}$ |
| BRD-1 | $F^{CE}_{Brd20°(0.1)} \cdot MA_{Brd}$ | $F^{CE}_{Brd20°(0.2)} \cdot MA_{Brd}$ | $F^{CE}_{Brd20°(0.3)} \cdot MA_{Brd}$ | $F^{PE}_{Brd20°} \cdot MA_{Brd}$ |
| BRD-2 | $F^{CE}_{Brd30°(0.1)} \cdot MA_{Brd}$ | $F^{CE}_{Brd30°(0.2)} \cdot MA_{Brd}$ | $F^{CE}_{Brd30°(0.3)} \cdot MA_{Brd}$ | $F^{PE}_{Brd30°} \cdot MA_{Brd}$ |
| BRD-3 | $F^{CE}_{Brd40°(0.1)} \cdot MA_{Brd}$ | $F^{CE}_{Brd40°(0.2)} \cdot MA_{Brd}$ | $F^{CE}_{Brd40°(0.3)} \cdot MA_{Brd}$ | $F^{PE}_{Brd40°} \cdot MA_{Brd}$ |
| BRD-4 | $F^{CE}_{Brd50°(0.1)} \cdot MA_{Brd}$ | $F^{CE}_{Brd50°(0.2)} \cdot MA_{Brd}$ | $F^{CE}_{Brd50°(0.3)} \cdot MA_{Brd}$ | $F^{PE}_{Brd50°} \cdot MA_{Brd}$ |
| BRD-5 | $F^{CE}_{Brd60°(0.1)} \cdot MA_{Brd}$ | $F^{CE}_{Brd60°(0.2)} \cdot MA_{Brd}$ | $F^{CE}_{Brd60°(0.3)} \cdot MA_{Brd}$ | $F^{PE}_{Brd60°} \cdot MA_{Brd}$ |
| BRD-6 | $F^{CE}_{Brd70°(0.1)} \cdot MA_{Brd}$ | $F^{CE}_{Brd70°(0.2)} \cdot MA_{Brd}$ | $F^{CE}_{Brd70°(0.3)} \cdot MA_{Brd}$ | $F^{PE}_{Brd70°} \cdot MA_{Brd}$ |
| BRD-7 | $F^{CE}_{Brd80°(0.1)} \cdot MA_{Brd}$ | $F^{CE}_{Brd80°(0.2)} \cdot MA_{Brd}$ | $F^{CE}_{Brd80°(0.3)} \cdot MA_{Brd}$ | $F^{PE}_{Brd80°} \cdot MA_{Brd}$ |
| BRD-8 | $F^{CE}_{Brd90°(0.1)} \cdot MA_{Brd}$ | $F^{CE}_{Brd90°(0.2)} \cdot MA_{Brd}$ | $F^{CE}_{Brd90°(0.3)} \cdot MA_{Brd}$ | $F^{PE}_{Brd90°} \cdot MA_{Brd}$ |
| BRD-9 | $F^{CE}_{Brd100°(0.1)} \cdot MA_{Brd}$ | $F^{CE}_{Brd100°(0.2)} \cdot MA_{Brd}$ | $F^{CE}_{Brd100°(0.3)} \cdot MA_{Brd}$ | $F^{PE}_{Brd100°} \cdot MA_{Brd}$ |
| BRD-10 | $F^{CE}_{Brd110°(0.1)} \cdot MA_{Brd}$ | $F^{CE}_{Brd110°(0.2)} \cdot MA_{Brd}$ | $F^{CE}_{Brd110°(0.3)} \cdot MA_{Brd}$ | $F^{PE}_{Brd110°} \cdot MA_{Brd}$ |
| BRD-11 | $F^{CE}_{Brd120°(0.1)} \cdot MA_{Brd}$ | $F^{CE}_{Brd120°(0.2)} \cdot MA_{Brd}$ | $F^{CE}_{Brd120°(0.3)} \cdot MA_{Brd}$ | $F^{PE}_{Brd120°} \cdot MA_{Brd}$ |
| TRI-1 | $F^{CE}_{Tri20°(0.1)} \cdot MA_{Tri}$ | $F^{CE}_{Tri20°(0.2)} \cdot MA_{Tri}$ | $F^{CE}_{Tri20°(0.3)} \cdot MA_{Tri}$ | $F^{PE}_{Tri20°} \cdot MA_{Tri}$ |
| TRI-2 | $F^{CE}_{Tri30°(0.1)} \cdot MA_{Tri}$ | $F^{CE}_{Tri30°(0.2)} \cdot MA_{Tri}$ | $F^{CE}_{Tri30°(0.3)} \cdot MA_{Tri}$ | $F^{PE}_{Tri30°} \cdot MA_{Tri}$ |
| TRI-3 | $F^{CE}_{Tri40°(0.1)} \cdot MA_{Tri}$ | $F^{CE}_{Tri40°(0.2)} \cdot MA_{Tri}$ | $F^{CE}_{Tri40°(0.3)} \cdot MA_{Tri}$ | $F^{PE}_{Tri40°} \cdot MA_{Tri}$ |
| TRI-4 | $F^{CE}_{Tri50°(0.1)} \cdot MA_{Tri}$ | $F^{CE}_{Tri50°(0.2)} \cdot MA_{Tri}$ | $F^{CE}_{Tri50°(0.3)} \cdot MA_{Tri}$ | $F^{PE}_{Tri50°} \cdot MA_{Tri}$ |
| TRI-5 | $F^{CE}_{Tri60°(0.1)} \cdot MA_{Tri}$ | $F^{CE}_{Tri60°(0.2)} \cdot MA_{Tri}$ | $F^{CE}_{Tri60°(0.3)} \cdot MA_{Tri}$ | $F^{PE}_{Tri60°} \cdot MA_{Tri}$ |
| TRI-6 | $F^{CE}_{Tri70°(0.1)} \cdot MA_{Tri}$ | $F^{CE}_{Tri70°(0.2)} \cdot MA_{Tri}$ | $F^{CE}_{Tri70°(0.3)} \cdot MA_{Tri}$ | $F^{PE}_{Tri70°} \cdot MA_{Tri}$ |
| TRI-7 | $F^{CE}_{Tri80°(0.1)} \cdot MA_{Tri}$ | $F^{CE}_{Tri80°(0.2)} \cdot MA_{Tri}$ | $F^{CE}_{Tri80°(0.3)} \cdot MA_{Tri}$ | $F^{PE}_{Tri80°} \cdot MA_{Tri}$ |
| TRI-8 | $F^{CE}_{Tri90°(0.1)} \cdot MA_{Tri}$ | $F^{CE}_{Tri90°(0.2)} \cdot MA_{Tri}$ | $F^{CE}_{Tri90°(0.3)} \cdot MA_{Tri}$ | $F^{PE}_{Tri90°} \cdot MA_{Tri}$ |
| TRI-9 | $F^{CE}_{Tri100°(0.1)} \cdot MA_{Tri}$ | $F^{CE}_{Tri100°(0.2)} \cdot MA_{Tri}$ | $F^{CE}_{Tri100°(0.3)} \cdot MA_{Tri}$ | $F^{PE}_{Tri100°} \cdot MA_{Tri}$ |
| TRI-10 | $F^{CE}_{Tri110°(0.1)} \cdot MA_{Tri}$ | $F^{CE}_{Tri110°(0.2)} \cdot MA_{Tri}$ | $F^{CE}_{Tri110°(0.3)} \cdot MA_{Tri}$ | $F^{PE}_{Tri110°} \cdot MA_{Tri}$ |
| TRI-11 | $F^{CE}_{Tri120°(0.1)} \cdot MA_{Tri}$ | $F^{CE}_{Tri120°(0.2)} \cdot MA_{Tri}$ | $F^{CE}_{Tri120°(0.3)} \cdot MA_{Tri}$ | $F^{PE}_{Tri120°} \cdot MA_{Tri}$ |

Table C.2: Pool of Muscle-Model-Based Candidate Functions for the Biceps Brachii (Bi), Brachioradialis (Brd) and Triceps Brachii (Tri) used for expanded model development ($N = 18$) for each subject

| **Group** | **Function** | | |
|---|---|---|---|
| BI-Subject | $F^{CE}_{Bi\theta_w(0.1)} \cdot MA_{Bi}$<br>$F^{CE}_{Bi\theta_w(0.25)} \cdot MA_{Bi}$<br>$F^{PE}_{Bi\theta_w} \cdot MA_{Bi}$ | $F^{CE}_{Bi\theta_w(0.15)} \cdot MA_{Bi}$<br>$F^{CE}_{Bi\theta_w(0.3)} \cdot MA_{Bi}$ | $F^{CE}_{Bi\theta_w(0.2)} \cdot MA_{Bi}$ |
| Brd-Subject | $F^{CE}_{Brd\theta_w(0.1)} \cdot MA_{Brd}$<br>$F^{CE}_{Brd\theta_w(0.25)} \cdot MA_{Brd}$<br>$F^{PE}_{Brd\theta_w} \cdot MA_{Brd}$ | $F^{CE}_{Brd\theta_w(0.15)} \cdot MA_{Brd}$<br>$F^{CE}_{Brd\theta_w(0.3)} \cdot MA_{Brd}$ | $F^{CE}_{Brd\theta_w(0.2)} \cdot MA_{Brd}$ |
| TRI-Subject | $F^{CE}_{Tri\theta_w(0.1)} \cdot MA_{Tri}$<br>$F^{CE}_{Tri\theta_w(0.25)} \cdot MA_{Tri}$<br>$F^{PE}_{Tri\theta_w} \cdot MA_{Tri}$ | $F^{CE}_{Tri\theta_w(0.15)} \cdot MA_{Tri}$<br>$F^{CE}_{Tri\theta_w(0.3)} \cdot MA_{Tri}$ | $F^{CE}_{Tri\theta_w(0.2)} \cdot MA_{Tri}$ |

# Appendix D

# Example FOS Model

The following Tables provide details about FOS models generated for data collected from Subject M3 during session 2. Table D.1 presents the FOS candidate functions and corresponding coefficients for models developed using the PMA method, while Table D.2 presents the equivalent for models developed using the CMA method.

Table D.1: FOS Candidate functions and coefficient values selected for models generated using data collected from subject M3 during session 2 with the PMA method

| Trial | Coefficient | Function | Evaluation %RMSE | Evaluation SD |
|---|---|---|---|---|
| 1 | 8.49 | 1 | 5.57 | 1.99 |
| | 1075.63 | $F^{CE}_{Tri120°(0.3)} \cdot MA_{Tri}$ | | |
| | -1551.75 | $F^{CE}_{Brd20°(0.2)} \cdot MA_{Brd}$ | | |
| | 894.55 | $F^{CE}_{Bi20°(0.2)} \cdot MA_{Bi}$ | | |
| | 2201.52 | $F^{CE}_{Tri110°(0.2)} \cdot MA_{Tri}$ | | |
| | 1839.97 | $F^{CE}_{Brd20°(0.3)} \cdot MA_{Brd}$ | | |
| | -495.90 | $F^{CE}_{Bi20°(0.3)} \cdot MA_{Bi}$ | | |
| 2 | 8.62 | 1 | 5.59 | 2.13 |
| | 989.75 | $F^{CE}_{Tri120°(0.3)} \cdot MA_{Tri}$ | | |
| | -1790.30 | $F^{CE}_{Brd20°(0.2)} \cdot MA_{Brd}$ | | |
| | -578.92 | $F^{CE}_{Bi20°(0.3)} \cdot MA_{Bi}$ | | |
| | 2358.13 | $F^{CE}_{Tri110°(0.2)} \cdot MA_{Tri}$ | | |
| | 2064.39 | $F^{CE}_{Brd20°(0.3)} \cdot MA_{Brd}$ | | |
| | 961.35 | $F^{CE}_{Bi20°(0.2)} \cdot MA_{Bi}$ | | |
| 3 | 10.00 | 1 | 7.17 | 2.38 |
| | 2734.50 | $F^{CE}_{Tri120°(0.3)} \cdot MA_{Tri}$ | | |
| | 2637.80 | $F^{CE}_{Brd20°(0.3)} \cdot MA_{Brd}$ | | |
| | 164.50 | $F^{PE}_{Bi60°} \cdot MA_{Bi}$ | | |
| | -2403.75 | $F^{CE}_{Brd30°(0.2)} \cdot MA_{Brd}$ | | |
| | 352.26 | $F^{CE}_{Bi50°(0.1)} \cdot MA_{Bi}$ | | |
| | 1749.01 | $F^{CE}_{Tri120°(0.1)} \cdot MA_{Tri}$ | | |
| 4 | 8.81 | 1 | 7.27 | 1.36 |
| | 3265.21 | $F^{CE}_{Tri120°(0.3)} \cdot MA_{Tri}$ | | |
| | 3455.74 | $F^{CE}_{Brd20°(0.3)} \cdot MA_{Brd}$ | | |
| | -2397.53 | $F^{CE}_{Brd30°(0.3)} \cdot MA_{Brd}$ | | |
| | 6627.19 | $F^{CE}_{Bi20°(0.3)} \cdot MA_{Bi}$ | | |
| | -6290.75 | $F^{CE}_{Bi30°(0.3)} \cdot MA_{Bi}$ | | |
| | -140.43 | $F^{CE}_{Brd30°(0.1)} \cdot MA_{Brd}$ | | |
| 5 | 7.81 | 1 | 7.54 | 3.42 |
| | 3073.89 | $F^{CE}_{Tri90°(0.2)} \cdot MA_{Tri}$ | | |
| | 2312.60 | $F^{CE}_{Brd20°(0.3)} \cdot MA_{Brd}$ | | |
| | -411.89 | $F^{CE}_{Bi20°(0.2)} \cdot MA_{Bi}$ | | |
| | -2058.08 | $F^{CE}_{Brd30°(0.2)} \cdot MA_{Brd}$ | | |
| | 969.49 | $F^{CE}_{Bi30°(0.1)} \cdot MA_{Bi}$ | | |
| | -482.22 | $F^{CE}_{Tri80°(0.1)} \cdot MA_{Tri}$ | | |
| 6 | 9.27 | 1 | 5.82 | 2.21 |
| | 3274.97 | $F^{CE}_{Tri90°(0.2)} \cdot MA_{Tri}$ | | |
| | 2190.19 | $F^{CE}_{Brd20°(0.3)} \cdot MA_{Brd}$ | | |
| | 1610.64 | $F^{CE}_{Bi20°(0.2)} \cdot MA_{Bi}$ | | |
| | -1987.96 | $F^{CE}_{Brd30°(0.2)} \cdot MA_{Brd}$ | | |
| | -1000.60 | $F^{CE}_{Bi20°(0.3)} \cdot MA_{Bi}$ | | |
| | -271.12 | $F^{CE}_{Tri80°(0.1)} \cdot MA_{Tri}$ | | |
| 7 | 9.51 | 1 | 5.84 | 2.91 |
| | 253.60 | $F^{CE}_{Tri90°(0.2)} \cdot MA_{Tri}$ | | |
| | 1142.86 | $F^{CE}_{Brd20°(0.3)} \cdot MA_{Brd}$ | | |
| | 460.86 | $F^{CE}_{Bi30°(0.2)} \cdot MA_{Bi}$ | | |
| | 3277.76 | $F^{CE}_{Tri100°(0.2)} \cdot MA_{Tri}$ | | |
| | -922.21 | $F^{CE}_{Brd20°(0.2)} \cdot MA_{Brd}$ | | |
| | 228.29 | $F^{PE}_{Tri90°} \cdot MA_{Tri}$ | | |
| 8 | 8.56 | 1 | 6.42 | 2.92 |
| | -958.46 | $F^{CE}_{Brd20°(0.2)} \cdot MA_{Brd}$ | | |
| | 987.88 | $F^{CE}_{Tri90°(0.2)} \cdot MA_{Tri}$ | | |
| | 3308.30 | $F^{CE}_{Bi60°(0.3)} \cdot MA_{Bi}$ | | |
| | 2401.06 | $F^{CE}_{Tri100°(0.2)} \cdot MA_{Tri}$ | | |
| | 1156.66 | $F^{CE}_{Brd20°(0.3)} \cdot MA_{Brd}$ | | |
| | -2933.81 | $F^{CE}_{Bi70°(0.3)} \cdot MA_{Bi}$ | | |
| **Average** | | | 6.40 | 2.41 |

Table D.2: FOS Candidate functions and coefficient values selected for models generated using data collected from subject M3 during session 2 with the CMA method

| Trial | Coefficient | Function | Evaluation %RMSE | Evaluation SD |
|---|---|---|---|---|
| 1 | 7.58 | 1 | 5.88 | 1.89 |
| | 54.55 | $F^{CE}_{Tri90°(0.3)} \cdot MA_{Tri}$ | | |
| | 171.23 | $F^{CE}_{Brd60°(0.3)} \cdot MA_{Brd}$ | | |
| | 7.35 | $F^{CE}_{Bi20°(0.3)} \cdot MA_{Bi}$ | | |
| | 32.37 | $F^{CE}_{Brd60°(0.1)} \cdot MA_{Brd}$ | | |
| | 59.61 | $F^{PE}_{Tri80°} \cdot MA_{Tri}$ | | |
| | -171.84 | $F^{CE}_{Brd60°(0.2)} \cdot MA_{Brd}$ | | |
| 2 | 7.28 | 1 | 6.05 | 2.39 |
| | 53.91 | $F^{CE}_{Tri90°(0.3)} \cdot MA_{Tri}$ | | |
| | 97.92 | $F^{CE}_{Brd60°(0.3)} \cdot MA_{Brd}$ | | |
| | -24.21 | $F^{CE}_{Bi20°(0.3)} \cdot MA_{Bi}$ | | |
| | -0.72 | $F^{CE}_{Brd60°(0.1)} \cdot MA_{Brd}$ | | |
| | 33.66 | $F^{CE}_{Bi30°(0.2)} \cdot MA_{Bi}$ | | |
| | -69.85 | $F^{CE}_{Brd50°(0.2)} \cdot MA_{Brd}$ | | |
| 3 | 9.21 | 1 | 8.40 | 3.78 |
| | 54.99 | $F^{CE}_{Tri90°(0.3)} \cdot MA_{Tri}$ | | |
| | 14.77 | $F^{CE}_{Brd80°(0.3)} \cdot MA_{Brd}$ | | |
| | 76.90 | $F^{CE}_{Bi20°(0.2)} \cdot MA_{Bi}$ | | |
| | -66.26 | $F^{CE}_{Bi30°(0.2)} \cdot MA_{Bi}$ | | |
| | 31.09 | $F^{CE}_{Brd90°(0.2)} \cdot MA_{Brd}$ | | |
| | 12.12 | $F^{CE}_{Tri100°(0.1)} \cdot MA_{Tri}$ | | |
| 4 | 8.97 | 1 | 5.66 | 1.26 |
| | 110.39 | $F^{CE}_{Tri80°(0.3)} \cdot MA_{Tri}$ | | |
| | 120.38 | $F^{CE}_{Brd60°(0.3)} \cdot MA_{Brd}$ | | |
| | -1.78 | $F^{CE}_{Bi20°(0.3)} \cdot MA_{Bi}$ | | |
| | -91.95 | $F^{CE}_{Brd60°(0.2)} \cdot MA_{Brd}$ | | |
| | -53.69 | $F^{CE}_{Tri70°(0.2)} \cdot MA_{Tri}$ | | |
| | 8.65 | $F^{CE}_{Bi30°(0.2)} \cdot MA_{Bi}$ | | |
| 5 | 7.12 | 1 | 6.27 | 2.66 |
| | 52.93 | $F^{CE}_{Tri90°(0.3)} \cdot MA_{Tri}$ | | |
| | 178.19 | $F^{CE}_{Brd70°(0.3)} \cdot MA_{Brd}$ | | |
| | -170.01 | $F^{CE}_{Brd70°(0.2)} \cdot MA_{Brd}$ | | |
| | 16.88 | $F^{CE}_{Bi60°(0.1)} \cdot MA_{Bi}$ | | |
| | 12.19 | $F^{CE}_{Brd80°(0.1)} \cdot MA_{Brd}$ | | |
| | -4.64 | $F^{CE}_{Bi70°(0.2)} \cdot MA_{Bi}$ | | |
| 6 | 9.10 | 1 | 5.41 | 2.22 |
| | 78.49 | $F^{CE}_{Tri80°(0.2)} \cdot MA_{Tri}$ | | |
| | 44.59 | $F^{CE}_{Brd70°(0.3)} \cdot MA_{Brd}$ | | |
| | 2.63 | $F^{CE}_{Bi60°(0.3)} \cdot MA_{Bi}$ | | |
| | -20.92 | $F^{CE}_{Tri70°(0.1)} \cdot MA_{Tri}$ | | |
| | -26.23 | $F^{CE}_{Brd70°(0.1)} \cdot MA_{Brd}$ | | |
| | 7.77 | $F^{CE}_{Bi70°(0.1)} \cdot MA_{Bi}$ | | |
| 7 | 9.28 | 1 | 5.27 | 2.10 |
| | 58.25 | $F^{CE}_{Tri90°(0.3)} \cdot MA_{Tri}$ | | |
| | 79.33 | $F^{CE}_{Brd70°(0.3)} \cdot MA_{Brd}$ | | |
| | 8.40 | $F^{CE}_{Bi40°(0.3)} \cdot MA_{Bi}$ | | |
| | -15.92 | $F^{CE}_{Brd70°(0.1)} \cdot MA_{Brd}$ | | |
| | 8.49 | $F^{PE}_{Tri90°} \cdot MA_{Tri}$ | | |
| | -42.77 | $F^{CE}_{Brd60°(0.3)} \cdot MA_{Brd}$ | | |
| 8 | 8.62 | 1 | 6.11 | 2.88 |
| | -108.64 | $F^{CE}_{Brd50°(0.3)} \cdot MA_{Brd}$ | | |
| | 32.68 | $F^{CE}_{Tri90°(0.3)} \cdot MA_{Tri}$ | | |
| | -76.47 | $F^{CE}_{Bi80°(0.3)} \cdot MA_{Bi}$ | | |
| | 30.97 | $F^{CE}_{Tri90°(0.2)} \cdot MA_{Tri}$ | | |
| | 123.86 | $F^{CE}_{Brd60°(0.3)} \cdot MA_{Brd}$ | | |
| | 88.69 | $F^{CE}_{Bi70°(0.3)} \cdot MA_{Bi}$ | | |
| **Average** | | | 6.13 | 2.40 |

# Appendix E

# Changes to Experimental Procedure

Table E.1: List of modifications made to experimental and analysis procedures

| | **Decision** | **Details** |
|---|---|---|
| Experimental Procedure | Measurement of EMG from the biceps brachii and brachioradialis, but not the brachialis muscle | Previous work with the experimental setup [70, 72] have stated the difficulties of measuring true signal from the brachialis muscle using surface EMG sensors. Due to the deep location of the brachialis muscle in the arm, surface EMG will be contaminated with cross-talk from the biceps brachii muscle. Therefore, it was decided to omit signals from this muscle for this study. |
| | Isometric contractions at varying angles | Previous studies using the QARM system and FOS models [70] utilized dynamic data, however since the FOS candidate functions were developed based on Hill-model principals that are true under isometric conditions, the majority of data used in this project was isometric. |
| | Isometric contractions at 6 joint angles | Originally, joint angles of 15°, 30°, 45°, 60°, 75° and 90° were chosen to cover a wide range of the functional range of motion of the subject while positioned in the QARM. However testing revealed that isometric contractions at 15° were very difficult for subjects, especially at higher target force levels, therefore the range was shifted to 30°, 45°, 60°, 75°, 90° and 105°. The maximum time for data collection in one trial (due to computational limitations) was 200 seconds, and 12 isometric contractions with a duration of 5 seconds each could comfortably be performed by subjects. |
| | Completing isometric contractions in a non-randomized pattern | Early data collection procedures required that subjects perform isometric contractions at joint angles that were randomized for each trial. However, the act of the subject moving their arm back and forth from angle to angle introduced more dynamic behaviour in the data set than desired, therefore contractions were performed in order from 30° through to 105° to minimize the amount of motion required by the subject to move from one angle to the next. |
| | Data collection sessions completed on same day or consecutive days and sensor location marked on subject's skin | It was decided that error due to sensor placement between sessions could be reduced by ensuring that the sensors were placed in the same location for each session. Therefore, sessions were performed on the same day or on consecutive days and the sensor location was marked on the subject's skin so it could easily be replicated in the next session. |
| Data Analysis | Using mean EMG signals for biceps brachii and triceps brachii, but medial signal for brachioradialis | Much variability was observed between the two adjacent EMG sensors located over the brachioradialis. It was assumed that the size of the brachioradialis is too narrow to accommodate two adjacent sensors, therefore only data collected from the medial of the two sensors was used in candidate functions. |
| | Including neighbouring angles in candidate function selection | Initial FOS model generation used the first $\theta_0$ that was selected in a candidate function for each muscle as the angle for all further selection of candidate functions. It was decided to widen this span to $\pm 10°$ to allow some flexibility and room for FOS to compensate for error in model functions. |
| | Range of optimal joint angles used in candidate functions | Initial FOS candidate functions were developed for $\theta_0 = 40° - 100°$. This range was expanded to $\theta_0 = 20° - 120°$ because it better represented the range of motion over which the data was collected. |

# Appendix F

# Model Comparisons

To compare these results with evaluation results using the Hill-model-based functions, the difference in error between the methods was calculated for each dataset and each subject. Negative values indicate that the Hill-based method produced lower evaluation error than the non-muscle-based-model, while positive values indicate that the candidate functions from Mobasser *et al.* generate lower evaluation error. The percentage difference in error ($\%D$) is calculated with respect to the non-model-based error according to

$$\%D_{PMA-Mobasser} = \frac{\%RMSE_{AVE_{PMA}} - \%RMSE_{AVE_{mobasser}}}{\%RMSE_{AVE_{mobasser}}} \tag{F.1}$$

$$\%D_{CMA-Mobasser} = \frac{\%RMSE_{AVE_{CMA}} - \%RMSE_{AVE_{mobasser}}}{\%RMSE_{AVE_{mobasser}}} \tag{F.2}$$

Table F.1 presents the calculated values for %D between the PMA and Mobasser models, and between the CMA and Mobasser models.

Table F.1: Evaluation %RMSE (Average), difference in error magnitude and percentage difference in error for models developed using Hill-model-based candidate functions (with PMA and CMA) and using non-muscle-model-based (Mobasser *et al.* [70]) candidate functions

| **Subject** | **Session** | **Evaluation %RMSE** | | | **%Difference Calculation** | | | |
|---|---|---|---|---|---|---|---|---|
| | | Polynomial MA | Constant MA | Mobasser et al. (2007) | Polynomial - Mobasser | | Constant - Mobasser | |
| | | | | | Magnitude | %Difference | Magnitude | %Difference |
| M1 | 1 | 8.88 | 9.48 | 13.64 | -4.76 | -34.9% | -4.16 | -30.5% |
| | 2 | 9.49 | 9.04 | 11.80 | -2.31 | -19.6% | -2.76 | -23.4% |
| | 3 | 11.0 | 10.54 | 11.30 | -0.30 | -2.7% | -0.76 | -6.7% |
| M2 | 1 | 11.07 | 10.89 | 17.78 | -6.71 | -37.7% | -6.89 | -38.8% |
| | 2 | 11.05 | 12.18 | 13.90 | -2.85 | -20.5% | -1.72 | -12.4% |
| M3 | 1 | 8.91 | 8.05 | 8.27 | +0.64 | +7.7% | -0.22 | -2.7% |
| | 2 | 6.40 | 6.13 | 5.64 | +0.76 | +13.5% | +0.49 | +8.7% |
| | 3 | 8.08 | 8.91 | 7.99 | +0.09 | +1.1% | +0.92 | +11.5% |
| M4 | 1 | 10.51 | 9.91 | 8.74 | +1.77 | +20.3% | +1.17 | +13.4% |
| | 2 | 20.58 | 19.62 | 16.23 | +4.35 | +26.8% | +3.39 | +20.9% |
| F1 | 1 | 11.34 | 11.29 | 11.98 | -0.64 | -5.3% | -0.69 | -5.8% |
| | 2 | 11.35 | 10.68 | 14.93 | -3.58 | -24.0% | -4.25 | -28.5% |
| F2 | 1 | 14.88 | 16.21 | 15.78 | -0.90 | -5.7% | +0.43 | +2.7% |
| | 2 | 10.62 | 9.76 | 14.86 | -4.24 | -28.5% | -5.10 | -34.3% |
| F3 | 1 | 7.33 | 6.78 | 5.81 | +1.52 | +26.16% | +0.97 | +16.7% |
| | 2 | 9.20 | 8.47 | 7.41 | +1.79 | +24.2% | +1.06 | +14.3% |
| | 3 | 14.86 | 14.13 | 12.50 | +2.36 | +18.9% | +1.63 | +13.0% |
| F4 | 1 | 12.15 | 12.22 | 12.69 | -0.54 | -4.3% | -0.47 | -3.7% |
| | 2 | 11.79 | 11.85 | 23.60 | -11.81 | -50.0% | -11.75 | -49.8% |
| | 3 | 8.62 | 8.60 | 6.34 | +2.28 | +36.0% | +2.26 | +35.7% |
| F5 | 1 | 10.33 | 10.35 | 12.19 | -1.86 | -15.3% | -1.84 | -15.1% |
| | 2 | 4.40 | 4.61 | 5.17 | -0.77 | -14.9% | -0.56 | -10.8% |
| | 3 | 5.56 | 5.71 | 5.96 | -0.40 | -6.7% | -0.25 | -4.2% |
| F6 | 1 | 9.87 | 9.99 | 10.02 | -0.15 | -1.5% | -0.03 | -0.3% |
| | 2 | 9.33 | 9.54 | 7.09 | +2.24 | +31.6% | +2.45 | +34.6% |
| | 3 | 8.77 | 9.21 | 7.25 | +1.52 | +21.0% | +1.96 | +27.0% |
| **Average** | | | | | **-0.87** | **-1.7%** | **-0.95** | **-2.6%** |

# Appendix G

# Consent Form

# Identification of Normal Human Subject Arm Dynamics and Its Use in Human Muscle Recruitment Analysis and Control of Robots and Telerobots

CONSENT FORM

Principal Investigator: Dr. Keyvan Hashtrudi-Zaad
Phone Number (613) 533-2991

---

You are being invited to participate in a research study directed by Dr. Keyvan Hashtrudi-Zaad to identify the mechanical dynamics of a human arm and to employ the dynamic mapping for the analysis of muscle recruitment and/or for the control of robots and telerobots. At this initial visit, Dr. Hashtrudi-Zaad or his graduate student working on this project will read through this consent form with you and describe procedures in detail and answer any questions you may have. This study is being sponsored by Natural Science and Engineering Research Council (NSERC) and Ontario Centres of Excellence (OCE).

## Details of the Study:

The purpose of this study is i) to identify human arm's mechanical dynamics (e.g. linear mapping such as mass, damping, and stiffness, or a nonlinear mapping) involving elbow joint motion in horizontal plane, and ii) to use the dynamic mapping to analyze muscle recruitment in humans and/or to control a simple robot or a telerobotic system. You will be considered for this study only if you have no neural or musculoskeletal disorders that may affect your ability to generate movements of your arm.

The experiments will be conducted at the same place (WLH-506) two days after this initial visit. You will be seated comfortably on a chair in front of a table. You will be asked to put your arm on an adjustable robotic linkage with a handle at its end-point. Your arm will then be secured to the linkage using covered arm braces. The robotic device allows you to move your limb in the horizontal plane. The motor attached to the linkage allows us to apply small mechanical loads to your arm. We will monitor i) the activity of elbow muscles during the tasks by attaching small surface Electromyogram (EMG) electrodes to the skin overlying each muscle, ii) the elbow joint angle by an optical encoder installed on the motor, and iii) the contact force between your arm wrist and the linkage handle which is measured by a force sensor installed on the device. The EMG electrodes do not obstruct normal movements and are not invasive. The signals from the electrodes will be amplified using electronic equipment rated for use with humans.

The experiments will be conducted to either identify the mechanical dynamics of your arm, or to study muscle recruitment in humans, or to assess the controllers designed for a robotic or a telerobotic experimental setup, part of which is the above-mentioned robotic linkage. To this end, small-moderate loads will be applied by the robotic linkage to your arm. The response of your arm, e.g. your elbow angle, muscle EMG signals, and wrist contact forces will be collected. You will be instructed to perform a number of motor tasks requiring you to maintain your hand at a spatial target with specific force, or to move your hand between spatial targets. These small-moderate loads are harmless, but you will have to learn to compensate for these loads in order to perform the task. The total duration of the experiment sessions is expected to be less than 2 hours. Should the experiments continue beyond 1 hour, light refreshments will be served.

**Identification of Normal Human Subject Arm Dynamics and Its Use in Human Muscle Recruitment Analysis and Control of Robots and Telerobots, Consent Form (cont.)**

## Risks:

There are minor risks involved in participating in this study. The robotic linkage that will be handled by you is capable of applying a safe maximum continuous force of 40 Newton at the wrist area. This maps to the weight of a 4 kg object. To protect subjects against peak forces, which may exceed 40 Newtons, the following precautions have been taken in to account:

- Metal barriers covered with soft spongy material have been installed to prevent the linkage from rotating further, should your elbow angle pass certain angle.
- A panic button will be provided for you to stop the operation immediately at any time you wish.
- An Immediate shutdown procedure will be executed at the software level when the measured wrist forces and or the linkage velocity pass certain limit.

**Note:** Your participation in this study is voluntary. You may withdraw from these experiments at any time.

## Benefits:

Although you may not benefit directly from this study, your participation will contribute to our basic knowledge of human mechanical dynamics, human muscle recruitment, and how to incorporate this knowledge into the design of prosthetic and telerobotic systems controllers.

## Confidentiality:

All information obtained during the course of this study is strictly confidential and will be stored in password-protected files. The data will be available only to Dr. Hashtrudi-Zaad and his research partner Dr. Evelyn Morin (Department of Electrical and Computer Engineering of Queen's University), and their joint students working in the robotics lab WLH-506 on this project. Your anonymity will be protected at all times by using alphanumeric codes when analyzing or presenting your experimental data.

## Payment:

You will receive an hourly stipend of $5.00 up to a maximum of $20.00 per experiment. Also, should the experiment continue beyond 1 hour, light refreshments will be served.

## Voluntary participation and Subject Statement:

I have read and understand the above information describing this study. I have had the purposes, procedures and technical language of this study explained to me. I have been given sufficient time to consider the above information and to seek advice if I chose to do so. I have had the opportunity to ask questions which have been answered to my satisfaction. I am voluntarily signing this form. I will receive a copy of this consent form for my information.

If at any time I have further questions, problems or adverse events, I can contact Dr. Keyvan Hashtrudi-Zaad, the principal investigator of the project, at (613) 533-2991, or Dr. Steven Blostein, the Head of the Department of Electrical and Computer Engineering, Queen's University at (613) 533-2947. If I have questions regarding my rights as a research subject, I can contact Dr. Albert Clark, Chair of Research Ethics Board at (613) 533-6081.

**Identification of Normal Human Subject Arm Dynamics and Its Use in Human Muscle Recruitment Analysis and Control of Robots and Telerobots, Consent Form (cont.)**

By signing this consent form, I am indicating that I agree to participate in this study.

_____

**Name of subject**, please print

_____

**Signature of subject** date

**********

**** Please do not answer any of the following questions, if you are not comfortable with. ****

Birth year: _____

Dominant hand: R L

Sex: M F

Weight: _____ lbs or kgs

Contact Information: _____ (email address or telephone#)

**********

To be entered by experimenter:

Upper arm length: _____mm

Forearm length: _____mm

Subject code: _____

**Statement of Investigator:**

I, or one of my graduate research assistants, have carefully explained to the subject the nature of the above research study. I certify that, to the best of my knowledge, the subject understands the nature of the study, and demands, benefits, and risks involved to participants in this study.

_____

**Signature of investigator** date

_____

**Name and signature of witness** date

*Form latest update: April 11, 2008*